Title

Diffusion to Densities: Using Diffusion-Weighted Imaging to Study Gray Matter Microstructure.

Permalink

https://escholarship.org/uc/item/20c1r2fk

Author

Radhakrishnan, Hamsanandini

Publication Date

2022

Peer reviewed|Thesis/dissertation

UNIVERSITY OF CALIFORNIA,
IRVINE

Diffusion to Densities:
Using Diffusion-Weighted Imaging to Study Gray Matter Microstructure.

DISSERTATION

submitted in partial satisfaction of the requirements
for the degree of

DOCTOR OF PHILOSOPHY

in Mathematical Computational and Systems Biology

by

Hamsanandini Radhakrishnan

Dissertation Committee:
Professor Craig Stark, Chair
Professor Michael Yassa
Professor Elizabeth Head

2022

TABLE OF CONTENTS

iii

LIST OF ABBREVIATIONS

AD	Axial Diffusivity
ADC	Apparent Diffusion Coefficient
CA1	Cornu Ammonis 1
CSF	Cerebrospinal Fluid
DG	Dentate Gyrus
DTI	Diffusion Tensor Imaging
DWI	Diffusion Weighted Imaging
EPI	Echo Planar Imaging
FA	Fractional Anisotropy
FC	Fiber Cross-section
FD	Fiber Density
FIRE	*fms*-intronic regulatory element
FISO	Fractional Isotropy
GM	Gray Matter
HARDI	High Angular Resolution Diffusion Imaging
LDI	Lure Discrimination Index
MD	Mean Diffusivity
MDT	Microstructure Diffusion Toolbox
MRI	Magnetic Resonance Imaging
MST	Mnemonic Similarity Task

NDI	Neurite Density Index
NODDI	Neurite Orientation Dispersion and Density Imaging
ODI	Orientation Dispersion Index
RAVLT	Rey Auditory Verbal Learning Task
RD	Radial Diffusivity
WM	White Matter
WT	Wild Type

LIST OF FIGURES

LIST OF TABLES

ACKNOWLEDGEMENTS

am also profoundly grateful to Jessica Noche for patiently listening to me go down endless scientific spirals, teaching me how to better validate my results, socially vetting all my emails, and for being one of my favorite people to talk science with. A huge thank you to Elena Dominguez who, along with Jess, has been my family here. Thank you for the constant love and laughter, for feeding me delicious food, being the best company and for making grad school such a warm and happy experience.

The research in this thesis would have been impossible without all the collaborators who trusted me with their data and gave so much scientific insight along the way. A big thank you to Dr. Ilana Bennett for all your diffusion weighted wisdom, and without whom Chapter 3 would not exist. Another big thank you to every scientist who was a part of the beagle study: Margo Ubele, Stephanie Krumholz, Kathy Boaz, Jennifer Mefford, Erin Jones, Beverly Meacham, Dr. Jeffrey Smiley, Dr. László Puskás, Dr. David Powell, Dr. Christopher Norris and Dr. Elizabeth Head, without whom Chapter 4 would not exist. I also thank Drs. Andre Obenaus, Kara Wendel, Thomas Tourdias and Bassem Hiba for all the rodent data and wisdom. Another huge thank you to Dr. Matthew Blurton Jones and Sepideh Kiani Shabestari for going on the fire mouse adventure with me- I learned so much from that project! I am so grateful to have had the opportunity to learn brain clearing from Dr. Sunil Gandhi and a big thank you to you and everyone in the Gandhi Lab for sharing your enthusiasm, knowledge and friendship. A huge thank you to Steve Granger for getting excited about data with me, and for being my diffusion sounding board.

I am indebted to Manuella Yassa and the CNLM Ambassador family for all the outreach adventures, conversations, and for making grad school so much more magical and rewarding. A big thank you to my middle school science teacher, Amy Mcghee Stischok, for believing in my ability to do science, and to my high school teachers Leela Padma and Indu Ajith for continuing to instill confidence in me. A very big thank you to the MCSB administrator, Karen Martin, who has always been there to help and has gotten me through so many bureaucratic issues.

Grad school would not have been possible without all the emotional support and welcomed distractions I received from friends. A big thank you to my MCSB cohort for the game nights, and for making classes so much more bearable. I am particularly

VITA

Education

PhD Candidate, Stark Lab   2017 – present
University of California, Irvine
PI: Dr. Craig Stark, Professor, Department of Neurobiology
and Behavior
Department: Mathematical, Computational and Systems
Biology
Thesis: Diffusion to densities: Using Diffusion-Weighted
Imaging to study gray matter microstructure

Biotechnology Engineering, BS   2013 – 2017
BMS College of Engineering, Bangalore, India
Thesis: Ground nutshell derived nano-carbons: Synthesis,
characterization and *in vitro* antibacterial activity

Publications

More than just a single shell game: Higher-order   2021
diffusion measures complement tensor metrics and
volume in gray matter when predicting age and
cognition.
Neuroimage (Under review)
Radhakrishnan, H., Bennett, I.J., Stark, C.E.L.

Tacrolimus protects against aging-associated   2021
microstructural changes in the beagle brain
Journal of Neuroscience
Radhakrishnan, H., Ubele, M., Krumholz, S., Boaz, K.,
Mefford, J., Denhart, E., Meacham, B., Smiley, J., Puskás, L.,
Powell, D., Norris, C., Stark, C.E.L., Head, E.

Microstructural Alterations in Hippocampal Subfields   2020
Mediate Age-Related Memory Decline in Humans
Frontiers in Aging Neuroscience
Radhakrishnan, H., Stark, S., Stark, C.E.L.

Natural Biowaste of Groundnut Shell Derived Nano Carbons: Synthesis, Characterization and Its In-Vitro Antibacterial Activity   2017

Nano-structures & Nano-objects (12), 84-90.
Yallappa, S., DR, D., Sammeta, Y., **Radhakrishnan, H.**, Chandraprasad, M., Kumar, A., Hegde, G.

Select Presentations

Estimating neuronal and glial counts non-invasively using diffusion-weighted imaging   2021

Global Connectome, SfN (Poster)

The structural and cognitive consequences of Calcineurin inhibition in a preclinical canine model of Alzheimer's Disease   2020

Annual Alzheimer's Association International Conference – Neuroscience Next (Poster)

Estimating neuronal and glial counts non-invasively using diffusion weighted imaging   2020

Neurobiology and Behavior Retreat, UC Irvine (Invited Talk)

Tacrolimus as a potential anti-Alzheimer's therapy in a preclinical canine model   2020

Neurobiology and Behavior Neuroblitz, UC Irvine (Talk)

Investigating Brain Microstructure in Humans Using Advanced Diffusion Weighted Imaging   2020

Biophysics and Systems Biology Seminar Series, UC Irvine (Talk)

Microstructural Alterations in DG/CA3 Mediate Age-Related Decline in Verbal Recall   2020

Winter Conference on Learning and Memory, Park City (Talk)

Mapping Long Range Connections in the Pig Brain Using Diffusion Weighted Imaging and Light Sheet Microscopy   2019

Neurobiology and Behavior Neuroblitz, UC Irvine (Talk)

Age-Related Changes in Gray and White Matter Neurite Density and Diffusion Within Hippocampal Subfields and the Medial Temporal Lobe Reflect Memory Performance   2019
Neuroscience, SfN, Chicago (Poster)

Unveiling the Role of ncRNAs in Autism Spectrum Disorders   2016
National Symposium for Next Generation Sequencing (Poster)

Awards and Honors

Gordon and Rose McAlpine Foundation Award   2021
Gordon and Rose McAlpine Foundation for Neuroscience Research
Paper on "Tacrolimus protects against aging-associated microstructural changes in the beagle brain"

Third Place Finalist   2021
UCI Grad Slam
Talk on "Diffusion Diagnosis: Using Water to Image the Brain"

Trainee Professional Development Award   2020
Society for Neuroscience

2nd Place, Project Presentation   2016
National Symposium for Next Generation Sequencing, India
Poster on "Unveiling the Role of ncRNAs in Autism Spectrum Disorders"

Relevant Skills

Neuroimaging (*Diffusion Weighted Imaging, Magnetic Resonance Spectroscopy, Arterial Spin Labelling, Traditional Structural MRI*)

MRI Analysis (*AFNI, ANTS, FSL, MRTrix3, MIRACL, NODDI, MDT, DSI Studio*)

Bash Scripting (*Automation, pipeline development*)

Python (*Image Processing, Machine Learning with Keras, Data Analysis*)

Other coding (*R, MATLAB, C++, JavaScript*)

Statistics (*Generalized linear models, Analysis of Variance, Hypothesis Testing, Parametric and Non-Parametric Methods, Data Distributions and Analytics, Data Visualization*)

Tissue Clearing (*iDISCO+*) • **Immunohistochemistry**

Stereotaxic Surgery (*Intracranial viral injections, mouse*)

Microscopy (*Light-sheet, Confocal, Brightfield*)

Teaching

Molecular Biology   2021
Teaching Assistant
This class explored DNA replication, transcription,
translation and epigenetics. I was responsible for grading,
leading discussions and holding office hours.

Human Neuroimaging Lab   2020
Teaching Assistant
This was a flipped lab course that was an introduction to
MRI analysis and taught students how to use software like
AFNI, ANTs, and FSL, along with some bash scripting. I was
responsible for holding office hours, as well as grading all
assignments and lab reports.

Transparent Brain   2019

Instructor

This was a lab course that went through the entire pipeline
of clearing brains through iDISCO+ and imaging them with
a light-sheet microscope. I was responsible for designing
the course, conducting the lab lectures.

UCI Brain Camp   2019

Instructor and Pedagogical Fellow

This was an immersive neuroscience camp that engaged
middle and high school students over a two-week
program. I was responsible for designing and presenting
lessons and hands-on demonstrations and labs, as well as
mentoring a group of students in designing their own
experiment.

Leadership, Mentoring and Outreach

Peer Review   2020 – present

*Assisted in peer review for the journals Neuroimage and
Neuroimage-Clinical*

NeuroScholars   2019 – present

Program Mentor

Mentored minority undergraduate students, and led a four
week summer laboratory course that taught them
experimental and computational skills to make them
competitive in the job market.

Brain Explorer Academy   2019 – present

Mentor

Weekly neuroscience pedagogy and mentoring for K-12
students in Orange County.

Irvine Brain Bee   2019

Mentor

Mentored high school students and led practice sessions to
compete in the Irvine Brain Bee, a spelling-bee like
competition on neuroscience facts.

Center for Neurobiology of Learning and Memory Ambassador Program 2018 – present
Chair, K-12 Outreach Committee
This program aims to advance public understanding of brain science through outreach and educational activities through the UCI Center for the Neurobiology of Learning and Memory (CNLM). I manage the committee that designs, executes, and evaluates neuroscience-related events for K-12 students, with a focus on those in Title I schools in Orange County and surrounding communities.

Undergraduate Research Mentoring 2017 – present
I have supervised and mentored 5 undergraduate research assistants on various laboratory skills including database management, experimental design, data analysis, tissue clearing, immunohistochemistry, microscopy, stereotaxic surgery and communication strategies.

Make a Difference, Bangalore 2015 – 2017
Education Support Lead
Make A Difference is a youth driven, non-profit organisation working to ensure equitable outcomes for children in orphanages and street shelters in India. I managed a group of over 50 volunteers and helped them design lesson plans and supported them in mentoring and teaching.

Literary and Debating Society, BMSCE 2015 – 2017
President
I managed a group of over 50 students, and also organized, designed and hosted frequent workshops, seminars and competitions to enhance the literary culture of the school.

Bullzeye, the BMSCE Magazine 2015 – 2017
Editor-in-Chief
Bullzeye is the official newsletter and magazine of BMS College. I set publishing guidelines, reviewed content, wrote editorials, and led the editorial team.

AIESEC Bangalore 2013 – 2015

Team Leader, Marketing and Information Management
Led a team of 10 people for marketing and public relations, wrote promotional blog articles, and analyzed data for the organization.

Prior Research Experience

Computational Biology Fellow 2016

Institute of Mathematical Sciences
Worked on gene duplication models involving the sub functionalization theory, using the yeast genome as a sample system. Headed the computational analysis of big data.

Researcher 2016

Hegde Lab, BMS College of Engineering
Optimized the synthesis of carbon nanoparticles from groundnut shells to be used for bioimaging and drug delivery purposes.

Researcher 2015

Sashi Lab, BMS College of Engineering
Isolated non-coding RNAs in the NLGN4Y region of the Y chromosome through the intergenic clustering method to explain the striking profusion of autistic traits in human males.

ABSTRACT

Title: Diffusion to Densities: Using Diffusion-Weighted Imaging to Study Gray Matter Microstructure.

Name: Hamsanandini Radhakrishnan

Degree: Doctor of Philosophy

University: University of California, Irvine

Year: 2022

Committee Chair: Dr. Craig Stark

The brain goes through a large set of structural changes at the onset of aging, resulting in sometimes devastating cognitive and behavioral consequences. Targeting these changes at an early stage is key to protecting against later cognitive decline or even pathology. However, studying tissue microstructure in the brain non-invasively is not trivial, especially in humans. Most of our non-invasive metrics derived from neuroimaging can detect only large-scale changes like gross atrophy or cortical thinning, which are usually only observable when it is too late to intervene. Diffusion imaging, popularized for studying white matter microstructure, has recently advanced to the stage that it might be sensitive to gray matter cytoarchitectural properties as well. However, these diffusion metrics, especially the newer ones derived from biophysical modelling techniques like Neurite Orientation Dispersion and Density Imaging (NODDI), have not been adequately evaluated, especially in the context of cognitive aging.

In this thesis, with a series of both human and animal studies, we aim to fill some of these gaps in knowledge, focusing mainly on cognitive aging in the hippocampus. We first identify a novel aging biomarker in the dentate gyrus, that might be partially mediating aging-related cognitive decline. We then show that a combination of diffusion metrics is far better than traditional MRI metrics in predicting age or cognition associated properties. We also demonstrate that these metrics can also be used as non-invasive probes to measure the efficiency of intervention studies designed to protect against aging-related structural changes! Finally, we establish a pipeline to estimate cellular properties non-invasively through the diffusion metrics alone. These results together not only shine light on the power of diffusion MRI to study gray matter changes in aging, but also present a framework to extend this method to other domains.

INTRODUCTION

Structure commands function. If you breed an oyster the size of a horse, it wouldn't take first place in the Kentucky Derby no matter who rode it.

-Matheson's Law.

With over a hundred billion cells, the human brain might be the most complex biological structure in the known universe. Its anatomy plays an extremely important role in regulating function, behavior, and cognition; and is often severely influenced by pathology and age. While advances in microscopy and histology have been essential in examining some of these structural properties, these approaches have traditionally been static and two-dimensional, and cannot be used in humans in vivo. Neuroimaging techniques, especially magnetic resonance imaging (MRI), have been extremely powerful in visualizing the brain non-invasively. But traditional MRI methods, like T1 and T2-weighted imaging, can only detect coarse macrostructural properties like cortical thickness and regional volume, and are rarely sensitive to more microstructural properties. Diffusion weighted imaging has a unique strength in its ability to probe water molecule displacement in the brain, in the range of microns, making it sensitive enough to capture detailed microstructural properties of different tissue types! However, until fairly recently, diffusion imaging studies have exclusively focused on examining white matter microstructure, mainly because earlier modeling algorithms could not accommodate the complexity of gray matter cytoarchitecture. Modern advances in diffusion imaging, especially High Angular Resolution Diffusion Imaging (HARDI), have opened the door for studying gray matter microstructure as well. Beyond microstructural

1

sensitivity, another advantage diffusion MRI may have over its sister modalities in studying gray matter is that it can pack a multitude of quantitative parameters at a sub-voxel level. Correspondingly, the diversity of diffusion MRI metrics remain unparalleled. Yet, the value of these metrics in studying gray matter microstructure has not been adequately explored, especially in clinically relevant fields.

One of the most universally dramatic set of changes in the brain is caused by the onset of aging, and it can have devastating consequences. General cognition starts to decline, memory deteriorates, and in many cases, may even result in pathologies like Alzheimer's disease. A popular hotspot for aging-associated structural changes is the medial temporal lobe, and more specifically, the hippocampus. Again, while traditional MRI has been able to detect general atrophy and reduction in hippocampal volume with aging, many of these gross macrostructural changes are only observable when it is already too late to intervene. Identifying aging-related structural biomarkers associated with cognition may be critical to understanding the mechanisms of cognitive hippocampal aging.

Can modern diffusion imaging techniques help bridge some of the gaps in the field of cognitive aging? This thesis covers four separate research projects designed to answer major questions around this idea. The chapters in this thesis are organized as follows:

Chapter 1: This chapter provides background describing the physics and history of diffusion imaging. It briefly discusses the evolution of various diffusion imaging techniques, with a focus on the two techniques emphasized in this thesis: diffusion tensor modelling and biophysical modelling with NODDI.

Are the newer diffusion metrics also sensitive and specific enough to detect aging-related structural changes, specifically in hippocampal gray matter, associated with cognition and memory performance?

Chapter 2: In this initial study, we observe that NODDI metrics are different between young and older adults and have the power to detect aging-related microstructural properties in hippocampal gray matter. We identify a novel aging biomarker in the dentate gyrus, the neurite density index or NDI. We not only find that the dentate NDI is increased in older adults, but also that this increase might be partially mediating aging-associated cognitive decline.

A version of this chapter was first published in Frontiers in Aging Neuroscience (2020, DOI). The paper has been edited for clarity and relevance to this thesis. Note that this publication also examines whether constrained spherical deconvolution can resolve white matter microstructural properties (fornix) associated with age and cognition. These methods are not elaborated here as it is not the focus of this dissertation.

How do NODDI metrics, tensor metrics and volume compare in predicting age and cognition?

Chapter 3: In this chapter, we build upon the previous chapter's study and first replicate these results in a larger study population, speaking to the robustness and reliability of these NODDI metrics. We then ask if the NODDI metrics possess any inherent advantage over tensor metrics or traditional structural metrics like volume in predicting age and cognition, to warrant the increased acquisition time multi-shell diffusion protocols

present. We find that a combination of NODDI and tensor metrics consistently result in much higher prediction accuracies for both age and different types of memory performance than any of these metrics by themselves. We use these results to encourage neuroimaging data collection efforts to include a multi-shell diffusion sequence in their protocols, as these metrics may be able to capture microstructural variance that might be missed by traditional approaches, even in gray matter studies.

This chapter is under review at Neuroimage.

Can diffusion metrics be used to assess the efficacy of longitudinal interventions designed to protect the brain against the effects of aging?

Chapter 4: In this chapter, we go beyond the cross-sectional studies detailed in the previous chapters and ask if these diffusion metrics can detect more subtle longitudinal changes in gray matter microstructure, using a calcineurin-inhibiting drug intervention study in a preclinical canine model. We find that diffusion metrics are indeed useful in determining the efficacy of longitudinal intervention studies non-invasively and show that controlling the expression of calcineurin before gross aging-related cognitive deficits are observable is able to protect against aging-related structural deterioration.

This chapter was first published in the Journal of Neuroscience (2021, [DOI](DOI)).

And finally, what do these diffusion metrics neurobiologically represent? Can they be used to estimate cellular properties not accessible non-invasively otherwise?

Chapter 5: In the final research chapter, we ask whether we can translate these diffusion metrics into more comprehensible neurobiological properties. We show that these diffusion metrics have unique relationships with the densities of different cells depending on the region studied. Using computational modelling and extra trees regression, we design a pipeline that can successfully estimate different cell counts non-invasively from diffusion metrics alone.

Chapter 6: Conclusions, scope and limitations.

CHAPTER 1:

DIFFUSION WEIGHTED IMAGING

Magnetic resonance imaging (MRI) has been extremely valuable for non-invasively probing the structural properties of the brain. Diffusion weighted MRI has been especially useful in studying structural connectivity and other white matter properties. Here, we will discuss the physics behind how diffusion imaging works, some computational models typically used to analyze the diffusion signal and some caveats of these models.

1.1 THE PHYSICS OF DIFFUSION IMAGING

Diffusion is the random Brownian motion of molecules, driven by thermal energy (Jacobs, 1935). Einstein's equation for diffusion states that the squared displacement of molecules in a given volume is directly proportional to the observation time, with the constant of proportionality being the diffusion coefficient (Einstein, n.d.). Einstein's equation assumes "free" diffusion, where the distribution of molecular displacements obeys Gaussian Law. Under those conditions, the self-diffusion coefficient of water is about 3.0 x 10^{-9} m² s⁻¹ at 37 °C (Johansen-Berg & Behrens, 2014). However, the observed diffusion coefficient of water in biological tissue is lower than what Einstein's equation would predict. The movement of water molecules in the brain, for example, is hindered and restricted by cell membranes, fibers and macromolecules thereby lowering the diffusion coefficient to the *apparent diffusion coefficient*. Water molecules in these environments only displace a few micrometers at a time, making this phenomenon perfectly suited to

study microstructure, considering how both axons and cell bodies are on the scale of a few micrometers too.

The most basic MR signal measures the number of hydrogen nuclei in free water, also called spins, within a given volume. While performing diffusion imaging, the MRI is programmed such that the random displacements of these spins attenuate the MR signal. The amount of signal attenuation in the direction θ depends on the apparent diffusion coefficient in that direction.

Suppose the signal generated from a voxel when no diffusion gradient is present is S_O. After applying these spatial gradients, the signal is attenuated by an amount that depends on the direction of the gradient, such that:

$$S(\theta, b) = S_0 \, e^{-b \, A(\theta)} \tag{1.1}$$

The variable b represents a set of physical constants and experimental parameters, including the strength (G) and duration (δ) of the magnetic field gradients and can be given by:

$$b = \gamma^2 \, \delta^2 G^2 (\Delta - \frac{\delta}{3}) \tag{1.2}$$

Here, γ is the gyromagnetic ratio of the hydrogen nucleus and Δ is the delay between gradient pulses.

Although traditionally only a single b value (also referred to as a shell) is used to acquire a diffusion image, modern diffusion techniques may use multiple b values to measure

different tissue properties. A major focus of this proposal will be on models and techniques that utilize multiple shells.

While the b-value described above is a convenient way to express the MR signal decay, it still assumes that the diffusion in the system is primarily Gaussian. However, protons in the brain can be highly hindered, or even restricted, in tissue compartments, causing deviations from Gaussian diffusion. In such a case, the "q-space" formalism may be a more appropriate way to describe the diffusion weighting of the experiment (Hecke et al., 2015). This is in direct analogy with "k-space" sampling employed in typical MR measurements when acquiring T1 and T2 weighted images. Here, the voxel-wise sampling of 3D proton displacements can be described by the parameter q in "q-space". Empirically, the b-value is directly proportional to the square of the q-value.

1.1.1 The biophysics of diffusion in the brain

Diffusion in the brain can be broadly categorized into diffusion in two distinct spaces: extracellular and intracellular. Due to the presence of cell soma and other macromolecules, diffusion in the extracellular matrix is considered to be "hindered": with a lower diffusion coefficient than that of free water, but still reasonably Gaussian (Syková & Nicholson, 2008). Diffusion inside the cells themselves, however, tend to be more restricted: the displacement of the water molecules is constrained by the cell's dimensions and structure (Shepherd et al., 2009). This property is especially useful in conjunction with the fact that the distance a molecule diffuses in one direction in space may or may not be the same as its displacement in other directions. In a sample where there are no true barriers, like in the cerebrospinal fluid of the brain, diffusion is the same in all

directions and can be called *isotropic* diffusion. However, the direction of diffusion in regions with a specific geometric structure, like that found in white matter fibers, depends on the orientation of the axons themselves, and is hence termed *anisotropic* diffusion. By tracking the movement of water molecules in these fibers, we can make inferences about their orientation: as diffusion is typically fast along the fibers, but considerably slower in directions perpendicular to them, hindered mainly by the myelin sheath and the axonal membrane (Beaulieu, 2002). This feature of diffusion direction specificity has been imperative to the success of diffusion weighted imaging in mapping brain connectivity.
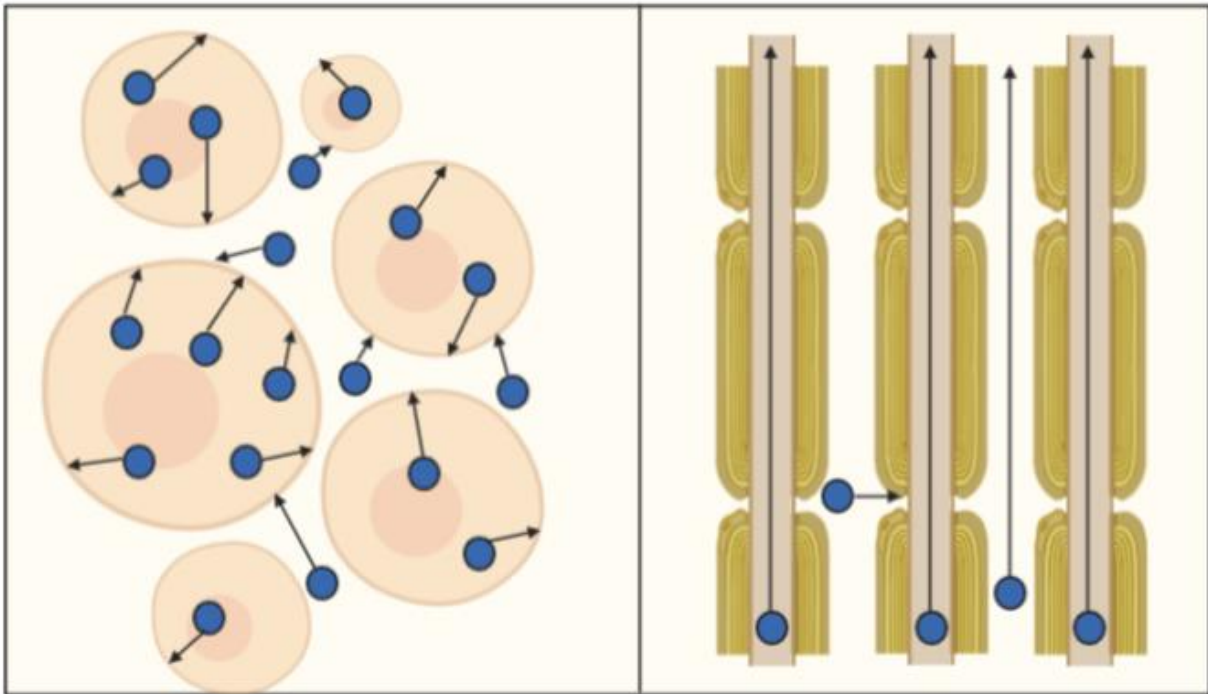
Figure 1.1: Diffusion in the extracellular matrix is hindered by the presence of cell bodies but is not biased towards any particular direction. Diffusion in neurites on the other hand, is anisotropic, and water molecules move faster along the neurite than across it.

1.2 MODELLING THE DIFFUSION SIGNAL

Unless we are interested in water itself, the diffusion signal is an indirect indicator of biological events in the brain. Many algorithms have been proposed to reconstruct the diffusion signal.

1.2.1 The diffusion tensor

The diffusion tensor is one of the most popular algorithms to model anisotropic diffusion. It characterizes Gaussian diffusion as a 3 x 3 symmetric matrix of numbers that represent diffusion displacements in 3D. It can be thought of as the 3D covariance matrix of displacements in a given time (Basser, Mattiello, & LeBihan, 1994; Basser, Mattiello, & Lebihan, 1994).

$$D = \begin{array}{ccc} D_{xx} & D_{xy} & D_{xz} \\ D_{yx} & D_{yy} & D_{yz} \\ D_{zx} & D_{zy} & D_{zz} \end{array} \qquad (1.3)$$

The diagonals of D correspond to the ADC along the three orthogonal axes, while the off-diagonal elements are the correlation between displacements along those orthogonal axes. Diagonalization of the diffusion tensor yield eigen values (λ_1, λ_2, and λ_3) and their vectors (v_1, v_2, v_3), which describe the directions and apparent diffusivities along the axes of principal diffusion. The tensor can be graphically represented as an ellipsoid. The principal axes of the ellipsoid are given by the eigen vectors of the tensor, and the lengths are defined by their corresponding eigen values.

From the tensor, different parameters can be derived that describe the nature of the voxel. For example, the principal axis of the tensor gives the primary orientation of the axonal bundles in that voxel. This concept has become the basis of several tractography algorithms. Moreover, the tensor can also shed light on some of the microstructural properties of the voxel. The mean of the eigen values of the tensor represents the mean diffusivity (MD) of the voxel. MD is sensitive to the overall density of structural membranes, making it an excellent biomarker for overall cellularity. As expected, the MD is the highest in CSF, considerably lower in gray matter (due to hindrance offered by cells and macromolecules) and the lowest in white matter (due to restriction of movement in the axons) (Alexander et al., 2007). Another important metric that can be derived from the tensor is the fractional anisotropy (FA).

$$FA = \sqrt{\frac{3}{2}} \frac{\sqrt{\left(\lambda_1 - \bar{\lambda}\right)^2 + \left(\lambda_2 - \bar{\lambda}\right)^2 + \left(\lambda_3 - \bar{\lambda}\right)^2}}{\lambda_1^2 + \lambda_2^2 + \lambda_3^2} \qquad (1.4)$$

Where $\bar{\lambda} = \frac{D_{xx} + D_{yy} + D_{zz}}{3}$

The FA ranges from 0 to 1, representing the directional bias of water in the given region, and is usually interpreted as a measure of axonal integrity. Unsurprisingly, FA is at its highest in white matter, and the lowest in CSF (Uddin et al., 2019).

Though the tensor is very useful, allowing the estimation of axonal fiber orientation and integrity, it suffers from many limitations. One of its primary problems stems from the fact that it can only recover a single fiber orientation at each voxel and fails at fiber

crossings. More specifically, when there are two or more fiber bundles contributing to the MR signal in a given voxel, the tensor often provides incorrect estimates of fiber orientation and integrity metrics, ultimately leading to anatomically inaccurate tractography (Jones & Cercignani, 2010)(Figure 1.2). Until recently, the tensor was not sophisticated enough to capture the cytoarchitectural complexities of gray matter.
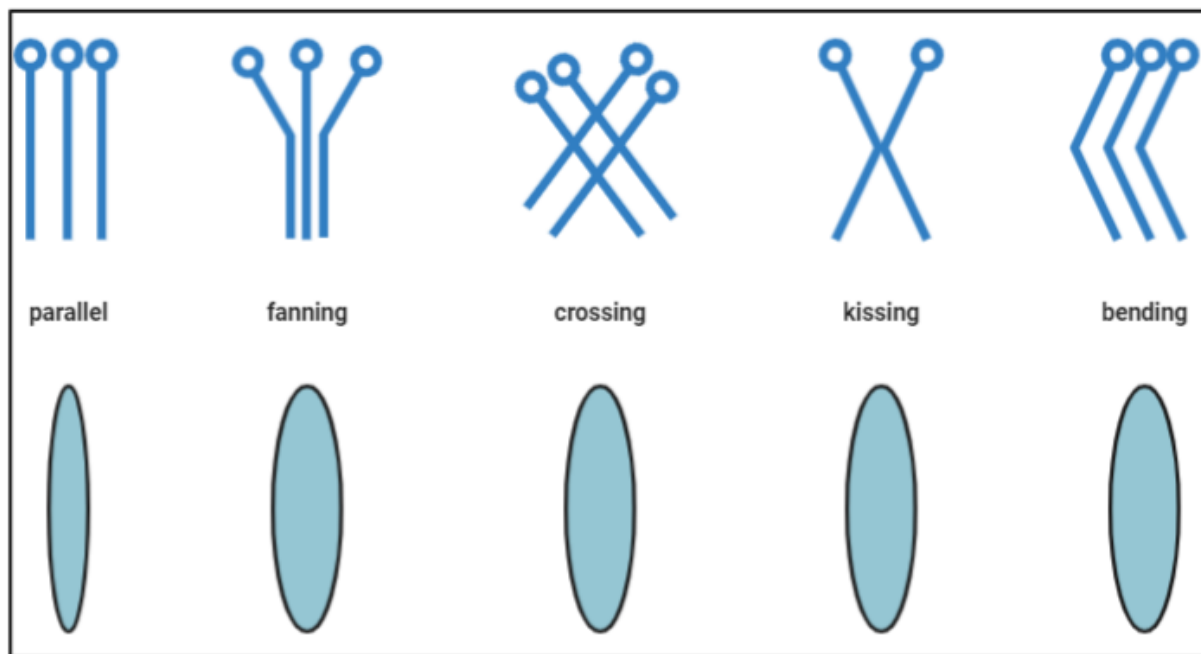
Figure 1.2: The tensor does not have the power to distinguish between complex fiber architecture, often resulting in inaccurate tractography.

1.2.2 High Angular Resolution Diffusion Imaging (HARDI) based models

The HARDI acquisition protocol involves measuring the diffusion signal using a large number of uniformly distributed diffusion weighted gradient directions, so as to capture the higher angular frequency features of the diffusion signal that are not adequately modelled by a single diffusion tensor (A. Anderson & Ding, n.d.; A. W. Anderson, 2005).

A number of different strategies have been proposed, for not only how to sample the range of directions used in acquisition, but also for how to estimate the diffusion orientation distribution function. Note that I will be discussing most of these techniques only briefly: the mathematical origins of these algorithms are beyond the scope of this thesis. This section is only to acknowledge the strides made in the field and the significance of the models used in this dissertation.

1.2.2.1 Diffusion Spectrum Imaging (DSI)

Here, the directions are sampled as a Cartesian grid in q-space, and a simple Fourier transform is performed on the data to calculate the diffusion propagator. The resolution of the propagator is determined by the range of the q-space sampled. Higher q values (and consequently higher b values) allow for characterizing smaller displacements and larger deviations from Gaussian behavior, and consequently offering better angular contrast (Wedeen et al., 2005).

While DSI offers a comprehensive picture of diffusion in a given MR voxel, the large set of sampling required results in very long scan times, rendering it impractical for routine use. Moreover, high q-values can only be achieved using long echo times, resulting in less than favorable SNR and resolution.

1.2.2.2 QBall Imaging (QBI)

In contrast to the Cartesian grid acquisition scheme used by DSI, QBI estimates orientation distribution functions using a spherical acquisition scheme, making its requirements more efficient than DSI (Descoteaux et al., 2007; Tuch, 2004). The propagator is reconstructed using the Funk-Radon transform. A Radon transform finds

the projection of an object over multiple angles. QBI was one of the first methods proposed to resolve the crossing fiber problem. More recently, variations of this technique have been proposed like incorporating the Laplace-Beltrami regularization to permit better denoising. Another related method is called the Diffusion Orientation Transform (DOT) which uses a slightly different function over a sphere and approximates a single contour of the diffusion propagator at a fixed displacement radius (Ozarslan et al., 2006).

1.2.2.3 Spherical Deconvolution

While the methods described in 3.2.1 and 3.2.2 focus on how the space is sampled during acquisition, spherical deconvolution focuses on the analysis of the signal acquired instead. This method is one of the first to recover the fiber orientation distribution function directly. The signal in a given voxel is considered to be the sum of the signals we would get from each fiber population with each orientation, weighted by the percentage of fibers in that orientation. The fiber orientation distribution (FOD) is then just the fraction of fibers aligned in each direction and can be calculated by the deconvolution of the response function of a single fiber population with the signal. The response function is usually estimated by considering only those voxels with the highest anisotropy- assuming that those voxels would probably only contain bundles in a single direction. The signal and the response are usually represented as spherical harmonic coefficients- in turn converting the deconvolution into a simple matrix inversion problem that yields the FODs, also represented as a spherical harmonic coefficient (Tournier et al., 2004, 2007).

This technique is often implemented with a non-negativity constraint on the iterative deconvolution process, thereby preserving the angular resolution while remaining robust

to noise. MRTrix3 uses constrained spherical deconvolution to estimate the FODs in white matter, and perform tractography (Tournier et al., 2012).

1.2.2.4 Biophysical Models

The HARDI based models described in the previous section have been extremely insightful and have helped deal with the crossing fiber problems that traditional tensor models faced. However, they are not specific enough to extract explicit features from the microstructural environment. Moreover, none of the models described above were designed to resolve complex cellular layers, like those found in gray matter. Biophysical models solve this problem by modelling the diffusion signal arising from different compartments in unique ways (Assaf et al., 2008; Assaf & Basser, 2005; Szafer et al., 1995). The two compartments most commonly used are the intracellular and extracellular spaces. White matter is usually modelled as a stack of cylinders or sticks- with the space inside and outside the sticks representing intra and extra-axonal compartments. The parameters used to define these sticks can be varied to quantify white matter architecture in terms of axon diameters, fiber densities, myelin thickness, etc.

Neurite Orientation Dispersion and Density Imaging or NODDI is one of the models most often mentioned in this thesis. NODDI also uses a HARDI based acquisition scheme, with multiple shells. Diffusion in extracellular space defined by the cellular membranes of somas or glial cells is hindered, with a Gaussian displacement pattern (Zhang et al., 2012). Diffusion in intra-cellular space, bounded by axonal or dendritic membranes, is non-Gaussian and restricted. NODDI uses sticks, an anisotropic tensor, and an isotropic compartment to model intracellular, extracellular and CSF compartments. The

orientation distribution of sticks can range from highly parallel to highly dispersed, thereby modelling the full spectrum of neurite orientation patterns found in brain tissue from the highly aligned corpus callosum to the intensely dendritic subcortical gray matter. The anisotropic tensor parameters used to describe the extracellular compartment is influenced by the "neurite" density as well as the orientation dispersion of the neurites. A major advantage of NODDI is that it doesn't discriminate a voxel based on its primary tissue type like some of its ancestors did, and is agnostic to its makeup (Colgan et al., 2016; Sato et al., 2017).
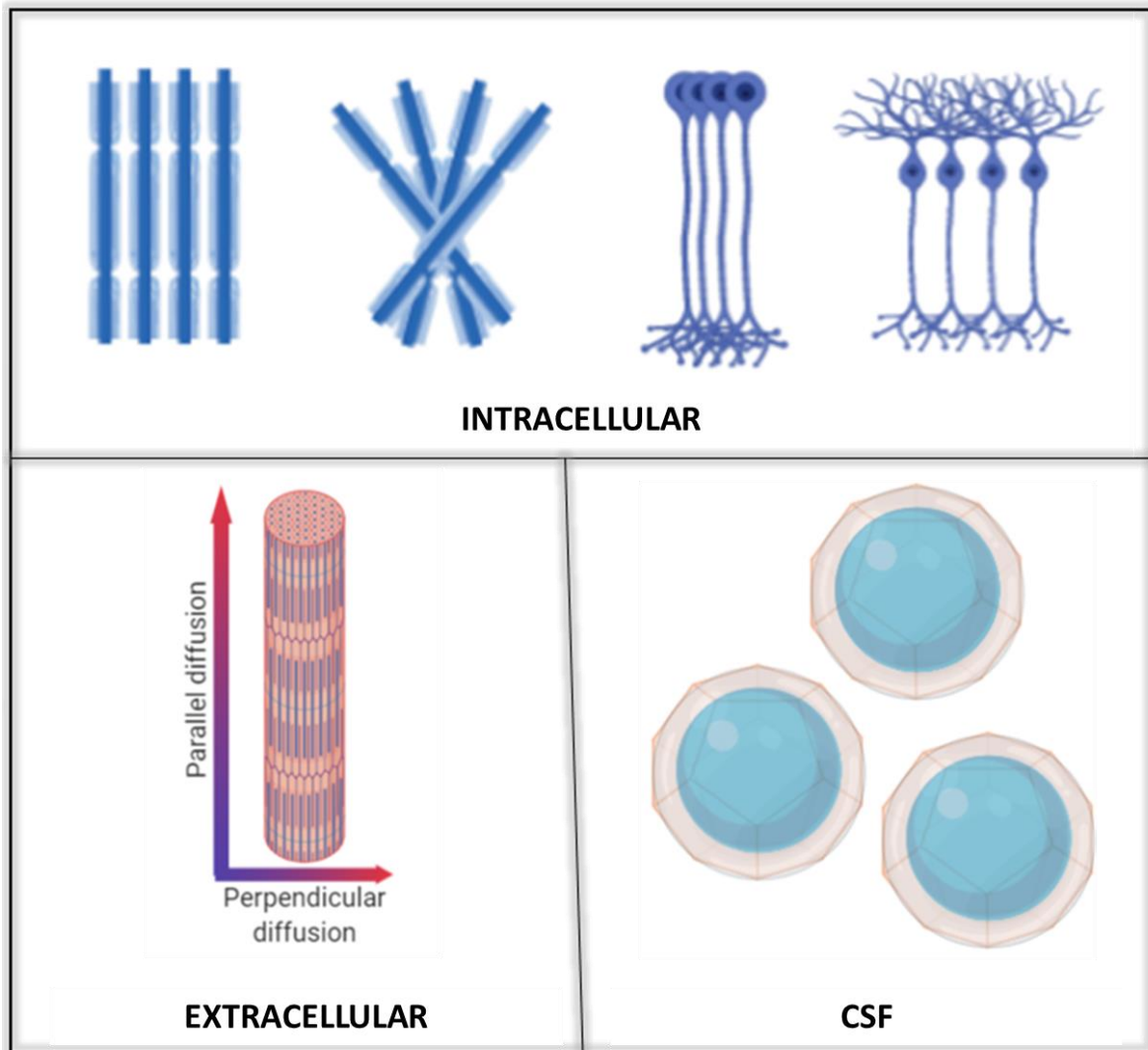
Figure 1.3: NODDI models diffusion in the brain as being either intracellular, extracellular or in CSF. It is agnostic to tissue type, allowing us to characterize the microstructure of even gray matter.

A major limitation of NODDI, and the other HARDI-based models described is the lack of histological validation or comprehensive understanding of what the metrics derived from these methods may neurobiologically mean.

1.4 DIFFUSION IMAGING IN GRAY MATTER

While diffusion-weighted imaging has been most often used to study white matter properties, recent advances especially in biophysical modelling, promise sensitivity to gray matter microstructure as well. Despite this, and the fact that there is currently no other non-invasive method to image gray matter microstructure, relatively few studies are published every year using diffusion imaging to study gray matter (Figure 1.4).

Papers with diffusion imaging as the primary method
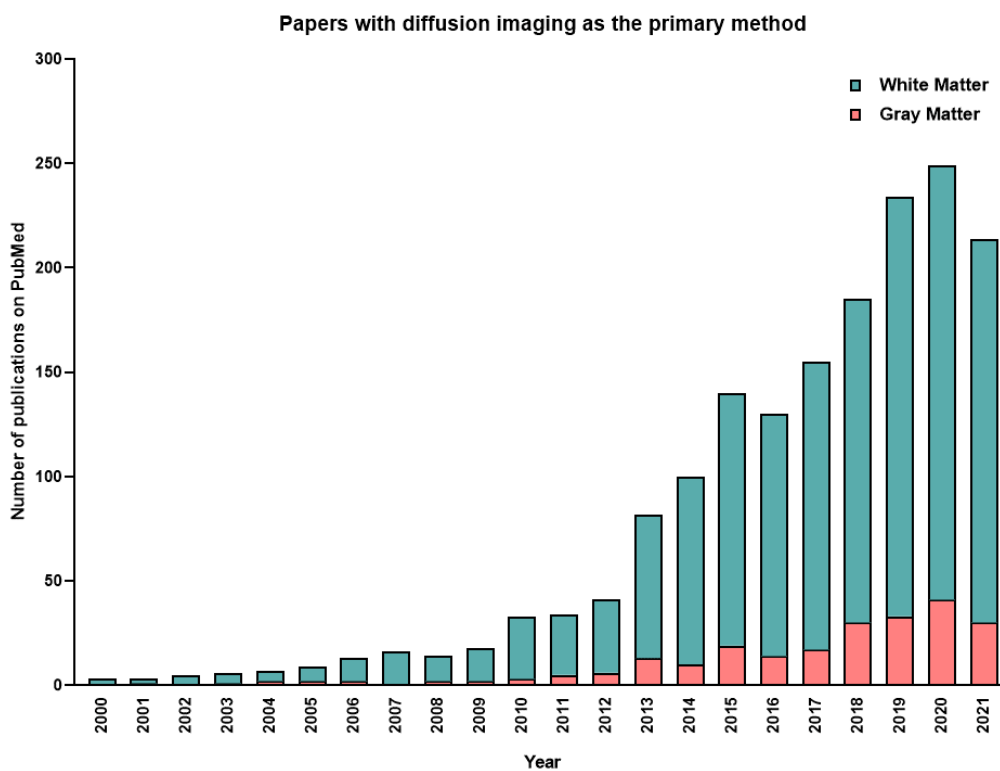
Figure 1.4: A PubMed search comparing titles/abstracts of papers with "diffusion MRI" and "White Matter" vs "diffusion MRI" and "Gray Matter" reveals that diffusion studies focused on white matter are published 5x more than diffusion studies on gray matter.

Most diffusion imaging methods effective at examining gray matter rely on multi-shelled scan sequences, which are often time consuming. Moreover, the value of these diffusion measures over conventional MRI measures like volume or cortical thickness is not yet

well understood. Interestingly, even the most basic tensor measures can provide meaningful information about the microstructural properties of gray matter (Aggarwal et al., 2015; Budde et al., 2011; Cloutman & Lambon Ralph, 2012; Jespersen et al., 2012; Leuze et al., 2014; McNab et al., 2013; Truong et al., 2014). The difference in these diffusion measures and their corresponding neurobiological implications between gray and white matter still leaves plenty to be explored. In the rest of this dissertation, we discuss in detail the implications of diffusion metrics in gray matter- especially in the context of cognitive hippocampal aging.

References

Aggarwal, M., Nauen, D. W., Troncoso, J. C., & Mori, S. (2015). Probing region-specific microstructure of human cortical areas using high angular and spatial resolution diffusion MRI. *NeuroImage*, *105*, 198–207. https://doi.org/10.1016/j.neuroimage.2014.10.053

Alexander, A. L., Lee, J. E., Lazar, M., & Field, A. S. (2007). Diffusion Tensor Imaging of the Brain. *Neurotherapeutics : The Journal of the American Society for Experimental NeuroTherapeutics*, *4*(3), 316–329. https://doi.org/10.1016/j.nurt.2007.05.011

Anderson, A., & Ding, Z. (n.d.). *Sub-voxel Measurement of Fiber Orientation using High Angular Resolution Diffusion Tensor Imaging*. 1.

Anderson, A. W. (2005). Measurement of fiber orientation distributions using high angular resolution diffusion imaging. *Magnetic Resonance in Medicine*, *54*(5), 1194–1206. https://doi.org/10.1002/mrm.20667

Assaf, Y., & Basser, P. J. (2005). Composite hindered and restricted model of diffusion (CHARMED) MR imaging of the human brain. *NeuroImage*, *27*(1), 48–58. https://doi.org/10.1016/j.neuroimage.2005.03.042

Assaf, Y., Blumenfeld-Katzir, T., Yovel, Y., & Basser, P. J. (2008). AxCaliber: A method for measuring axon diameter distribution from diffusion MRI. *Magnetic Resonance in Medicine*, *59*(6), 1347–1354. https://doi.org/10.1002/mrm.21577

Basser, P. J., Mattiello, J., & LeBihan, D. (1994). MR diffusion tensor spectroscopy and imaging. *Biophysical Journal*, *66*(1), 259–267. https://doi.org/10.1016/S0006-3495(94)80775-1

Basser, P. J., Mattiello, J., & Lebihan, D. (1994). Estimation of the Effective Self-Diffusion Tensor from the NMR Spin Echo. *Journal of Magnetic Resonance, Series B*, *103*(3), 247–254. https://doi.org/10.1006/jmrb.1994.1037

Beaulieu, C. (2002). The basis of anisotropic water diffusion in the nervous system—A technical review. *NMR in Biomedicine*, *15*(7–8), 435–455. https://doi.org/10.1002/nbm.782

Budde, M. D., Janes, L., Gold, E., Turtzo, L. C., & Frank, J. A. (2011). The contribution of gliosis to diffusion tensor anisotropy and tractography following traumatic brain injury: Validation in the rat using Fourier analysis of stained tissue sections. *Brain*, *134*(8), 2248–2260. https://doi.org/10.1093/brain/awr161

Cloutman, L., & Lambon Ralph, M. (2012). Connectivity-based structural and functional parcellation of the human cortex using diffusion imaging and tractography. *Frontiers in Neuroanatomy*, *6*, 34. https://doi.org/10.3389/fnana.2012.00034

Colgan, N., Siow, B., O'Callaghan, J. M., Harrison, I. F., Wells, J. A., Holmes, H. E., Ismail, O., Richardson, S., Alexander, D. C., Collins, E. C., Fisher, E. M., Johnson, R., Schwarz, A. J., Ahmed, Z., O'Neill, M. J., Murray, T. K., Zhang, H., & Lythgoe, M. F. (2016). Application of neurite orientation dispersion and density imaging (NODDI) to a tau pathology model of Alzheimer's disease. *NeuroImage*, *125*, 739–744. https://doi.org/10.1016/j.neuroimage.2015.10.043

Descoteaux, M., Angelino, E., Fitzgibbons, S., & Deriche, R. (2007). Regularized, fast, and robust analytical Q-ball imaging. *Magn Reson Med*, *58*, 497–510. https://doi.org/10.1002/mrm.21277

Einstein, A. (n.d.). *On the Motion of Small Particles Suspended in Liquids at Rest Required by the Molecular-Kinetic Theory of Heat*. 7.

Hecke, W. V., Emsell, L., & Sunaert, S. (2015). *Diffusion Tensor Imaging: A Practical Handbook*. Springer.

Jacobs, M. H. (1935). Diffusion Processes. In M. H. Jacobs (Ed.), *Diffusion Processes* (pp. 1–145). Springer. https://doi.org/10.1007/978-3-642-86414-8_1

Jespersen, S. N., Leigland, L. A., Cornea, A., & Kroenke, C. D. (2012). Determination of Axonal and Dendritic Orientation Distributions Within the Developing Cerebral Cortex by Diffusion Tensor Imaging. *IEEE Transactions on Medical Imaging*, *31*(1), 16–32. https://doi.org/10.1109/TMI.2011.2162099

Johansen-Berg, H., & Behrens, T. E. J. (Eds.). (2014). *Diffusion MRI: From quantitative measurement to in-vivo neuroanatomy* (2nd ed). Elsevier/Academic Press.

Jones, D. K., & Cercignani, M. (2010). Twenty-five pitfalls in the analysis of diffusion MRI data. *NMR in Biomedicine*, *23*(7), 803–820. https://doi.org/10.1002/nbm.1543

Leuze, C. W. U., Anwander, A., Bazin, P.-L., Dhital, B., Stüber, C., Reimann, K., Geyer, S., & Turner, R. (2014). Layer-Specific Intracortical Connectivity Revealed with Diffusion MRI. *Cerebral Cortex*, *24*(2), 328–339. https://doi.org/10.1093/cercor/bhs311

McNab, J. A., Polimeni, J. R., Wang, R., Augustinack, J. C., Fujimoto, K., Stevens, A., Janssens, T., Farivar, R., Folkerth, R. D., Vanduffel, W., & Wald, L. L. (2013). Surface based analysis of

diffusion orientation for identifying architectonic domains in the in vivo human cortex. *NeuroImage*, *69*, 87–100. https://doi.org/10.1016/j.neuroimage.2012.11.065

Ozarslan, E., Shepherd, T. M., Vemuri, B. C., Blackband, S. J., & Mareci, T. H. (2006). Resolution of complex tissue microarchitecture using the diffusion orientation transform (DOT). *NeuroImage*, *31*(3), 1086–1103. https://doi.org/10.1016/j.neuroimage.2006.01.024

Sato, K., Kerever, A., Kamagata, K., Tsuruta, K., Irie, R., Tagawa, K., Okazawa, H., Arikawa-Hirasawa, E., Nitta, N., Aoki, I., & Aoki, S. (2017). Understanding microstructure of the brain by comparison of neurite orientation dispersion and density imaging (NODDI) with transparent mouse brain. *Acta Radiologica Open*, *6*(4). https://doi.org/10.1177/2058460117703816

Shepherd, T. M., Thelwall, P. E., Stanisz, G. J., & Blackband, S. J. (2009). Aldehyde Fixative Solutions Alter the Water Relaxation and Diffusion Properties of Nervous Tissue. *Magnetic Resonance in Medicine : Official Journal of the Society of Magnetic Resonance in Medicine / Society of Magnetic Resonance in Medicine*, *62*(1), 26–34. https://doi.org/10.1002/mrm.21977

Syková, E., & Nicholson, C. (2008). Diffusion in brain extracellular space. *Physiological Reviews*, *88*(4), 1277–1340. https://doi.org/10.1152/physrev.00027.2007

Szafer, A., Zhong, J., Anderson, A. W., & Gore, J. C. (1995). Diffusion-weighted imaging in tissues: Theoretical models. *NMR in Biomedicine*, *8*(7–8), 289–296. https://doi.org/10.1002/nbm.1940080704

Tournier, J.-D., Calamante, F., & Connelly, A. (2007). Robust determination of the fibre orientation distribution in diffusion MRI: Non-negativity constrained super-resolved spherical deconvolution. *NeuroImage*, *35*(4), 1459–1472. https://doi.org/10.1016/j.neuroimage.2007.02.016

Tournier, J.-D., Calamante, F., & Connelly, A. (2012). MRtrix: Diffusion tractography in crossing fiber regions. *International Journal of Imaging Systems and Technology*, *22*(1), 53–66. https://doi.org/10.1002/ima.22005

Tournier, J.-D., Calamante, F., Gadian, D. G., & Connelly, A. (2004). Direct estimation of the fiber orientation density function from diffusion-weighted MRI data using spherical deconvolution. *NeuroImage*, *23*(3), 1176–1185. https://doi.org/10.1016/j.neuroimage.2004.07.037

Truong, T.-K., Guidon, A., & Song, A. W. (2014). Cortical Depth Dependence of the Diffusion Anisotropy in the Human Cortical Gray Matter In Vivo. *PLOS ONE*, *9*(3), e91424. https://doi.org/10.1371/journal.pone.0091424

Tuch, D. S. (2004). Q-ball imaging. *Magnetic Resonance in Medicine*, *52*(6), 1358–1372. https://doi.org/10.1002/mrm.20279

Uddin, M. N., Figley, T. D., Solar, K. G., Shatil, A. S., & Figley, C. R. (2019). Comparisons between multi-component myelin water fraction, T1w/T2w ratio, and diffusion tensor imaging measures in healthy human brain structures. *Scientific Reports*, *9*(1), 1–17. https://doi.org/10.1038/s41598-019-39199-x

Wedeen, V. J., Hagmann, P., Tseng, W.-Y. I., Reese, T. G., & Weisskoff, R. M. (2005). Mapping complex tissue architecture with diffusion spectrum magnetic resonance imaging. *Magnetic Resonance in Medicine*, *54*(6), 1377–1386. https://doi.org/10.1002/mrm.20642

Zhang, H., Schneider, T., Wheeler-Kingshott, C. A., & Alexander, D. C. (2012). NODDI: Practical in vivo neurite orientation dispersion and density imaging of the human brain. *NeuroImage*, *61*(4), 1000–1016. https://doi.org/10.1016/j.neuroimage.2012.03.072

MICROSTRUCTURAL ALTERATIONS IN HIPPOCAMPAL SUBFIELDS MEDIATE AGE-RELATED MEMORY DECLINE IN HUMANS

Can modern diffusion analysis methods identify more specific microstructural changes associated with age in the human medial temporal lobe?

Before diving into more complex analysis, we first asked whether the diffusion metrics studied were even sensitive to aging-related microstructural changes in the hippocampal subfields of humans. While the relationship between age and tensor metrics has been previously examined in these regions, very few reports consider the effect of hippocampal aging on the NODDI metrics, especially in a subfield-specific manner. In this chapter, we establish that NODDI metrics are indeed sensitive to hippocampal cytoarchitectural properties associated with age and cognition. Using advanced diffusion imaging in a cross-sectional cohort of 15 young (20–38 years, 28.4 ± 4.6 years, eight females) and 23 older (59–84 years, 69.9 ± 5.3 years, 14 females) adults, we identified a novel aging biomarker: the neurite density index or NDI. The NDI was increased in the hippocampal subfields and parahippocampal cortex of older adults, and this increase in the DG/CA3 subfield alone correlated with memory performance on the Rey Auditory Verbal Learning Test (RAVLT), even after regressing out the effect of age. Structural equation modelling further

revealed that this increase in NDI could be partially mediating age-related decreases in verbal recall performance. These results provide a far more comprehensive view than previously determined on the possible system-wide processes that may be occurring because of healthy aging and demonstrate that advanced diffusion weighted imaging is evolving into a powerful tool to study more than just white matter properties.

NB: A version of this chapter was first published in Radhakrishnan et al., Frontiers in Aging Neuroscience, 2020.

2.1 INTRODUCTION

Decades of research have shown that, even outside of overt pathology or dementia, aging is associated with cognitive decline, such as decreases in processing speed, poorer divided attention, and episodic memory impairments (Eckert, 2011; Glisky, 2007; Johnson, 1997; Schacter et al., 1997). While there are a host of changes in the brain that have been tied to age-related cognitive decline, structural and functional alterations in the hippocampus and other regions of the medial temporal lobe likely mediate much of these alterations of memory (Morrison & Baxter, 2012; S. M. Stark & Stark, 2017a). Human imaging studies have shown that the hippocampal volume decreases after the age of 70 at a rate of approximately 1.5% a year (Jack et al., 1998; Raz et al., 2005). This reduction could be due to synaptic size reduction (Petralia et al., 2014), microglia decrease (Sharaf et al., 2013), demyelination (Kövari Enikö et al., 2004; Peters, 2002) and/or other changes in connectivity (Fjell et al., 2016). More subtle changes are also observed in individual

neurons, such as shrinkage in soma size (Ahmad & Spear, 1993) and a reduction or regression in dendritic branching (Scheibel et al., 1975). Aging also results in axonal degeneration of the fornix and other white matter pathways, due to loss of myelinated fibers and alterations in the myelin sheath (Peters et al., 2010; Salvadores et al., 2017). Studies of these underlying neurobiological changes associated with age have largely been performed in animal models as direct studies in humans are often infeasible. However, new neuroimaging techniques may prove to be valuable tools for investigating these age-related alterations *in vivo* in the human brain.

Diffusion tensor imaging (DTI) has enabled us to probe white matter changes using measures like fractional anisotropy (FA) and mean diffusivity (MD), providing some form of *in vivo* measure of microstructure and integrity (Table 2.1). In the fornix, FA is reduced and MD is increased as a consequence of aging, reflecting a reduction in white matter integrity (Bennett & Madden, 2014; Bennett & Stark, 2015; Gunning-Dixon et al., 2009; Kochunov et al., 2012; Madden et al., 2012). These measures are also correlated with cognitive performance in both humans and rodents (Charlton et al., 2007; Kantarci, 2014; Takahashi et al., 2000). Though DTI has been extremely useful for studying microarchitectural properties in white matter and its influence on behavior, it is inherently a nonspecific technique. A change in FA could be caused by changes in myelination, axon diameter, membrane permeability, or axon packing density (Sampaio-Baptista & Johansen-Berg, 2017). DTI is also incapable of capturing complex microstructural details within a given voxel, which is particularly important in regions of crossing, kissing, and fanning fibers (Jeurissen et al., 2013; Zhang et al., 2012).

Metric	Abbreviation	Description	Range
Fractional Anisotropy	FA	A measure of axonal organization or integrity based on the coherence of orientations of the bundles. Mainly used to study white matter, and generally decreases with age. Reductions in FA can mean neurodegeneration, a myelin sheath depletion or just general atrophy of fiber bundles. (Budde et al., 2007; Song et al., 2003)	0 [most isotropic] - 1 [least isotropic]
Mean Diffusivity	MD	Another measure of white matter bundle integrity calculated as the average amount of water diffusion inside the voxel. MD in most regions increases with age, also suggesting demyelination or axonal degradation. (Abe et al., 2002; Grieve et al., 2007; Hsu et al., 2008)	Continuous (directly proportional to the amount of diffusion.)
Fiber Density	FD	Calculated as the integral of a given fixel's FOD. Directly proportional to the intra axonal volume of the fiber population aligned with the given fixel. (D. Raffelt et al., 2012)	0 [Least dense] - 1 [Most dense]
Fiber Cross Section	FC	Captures individual differences in the diameters of distinct fiber bundles. Computed as the amount of distortion necessary to warp a given FOD to the same FOD in template space. (D. A. Raffelt et al., 2017)	0 [least diameter] - 1 [most diameter]
Fiber Density	FDC	A joint metric of FD and FC calculated as their product. Captures both microstructural	0 - 1

and Cross Section		properties as well as more large-scale changes within bundles.	
Neurite Density Index	NDI	Calculated as the proportion of the voxel expressing unhindered diffusion along a given set of sticks, and also restricted diffusion perpendicular to the same set of sticks. Might be able to pick up on the number of neurites or the complexity of their dendrites. (Billiet et al., 2015)	0 [most extracellular] - 1 [most intracellular]
Orientation Dispersion Index	ODI	Measure of tortuosity coupling an intracellular and extracellular space. Gives the variability of neurite orientations, and might be able to pick up on the dispersion of axons and neurons within a voxel. (Billiet et al., 2015)	0 [Least dispersed] - 1 [Most dispersed]
Fractional Isotropy	FISO	Measure of the amount of isotropic free volume within a voxel- and is usually proportional to the amount of cerebrospinal fluid in a voxel. Might also pick up on other free water entities like dead cells. (Billiet et al., 2015)	0 [Least CSF] - 1 [Most CSF]

Table 2.1: A description of the diffusion metrics used.

Recent advances in diffusion imaging like multiple tensor models to Q-Ball and Q-space imaging (King et al., 1994; Tournier et al., 2004; Tuch, 2004) have attempted to address problems of complex fiber architecture, but these methods are still not fiber specific or easily assignable to segmented white matter pathways. Moreover, as we will show, voxel-

based analysis of these metrics may yield false positive differences between groups as multiple pathways can pass through a voxel, further confounding how we interpret "pathway-specific" metrics. To address this issue, fixel-based analysis (D. A. Raffelt et al., 2017) is one of the first techniques that enables tract-specific statistical analysis. Here, a "fixel" refers to a particular fiber population inside a voxel (D. A. Raffelt et al., 2015). Using constrained spherical deconvolution, this method can estimate the total intra-axonal volume of white matter axons in any direction, enabling the detection of tract-specific degeneration. This technique can estimate microstructural changes (fiber density), macrostructural changes (fiber cross section), and the differences arising from a combination of both classes of degeneration (see Table 2.1) (D. A. Raffelt et al., 2017). These metrics have proven to be more sensitive to microarchitectural alterations and more useful in revealing minute but clinically relevant disease-associated differences, as compared to traditional tensor-based analysis (Mito et al., 2018). However, very few studies have explored such changes associated with healthy aging and none (to our knowledge) have looked at age-related fixel-based decline in the fornix and its impact on cognitive performance.

In addition to problems with specificity, DTI was not *designed* to study gray matter architecture, and while one can derive tensor metrics in gray matter regions, the implications of these metrics are often hard to interpret. Neurite Orientation Dispersion and Density Imaging (NODDI) (Zhang et al., 2012) addresses this problem using multi-compartment diffusion modelling, in which restricted diffusion is modelled as a set of sticks, hindered diffusion as the dispersion of the sticks, and unrestricted diffusion as an

isotropic sphere. These metrics are not only completely agnostic to tissue type (all voxels are modeled by the same set of equations), but also provide a more comprehensive analysis of the microstructural subtleties and underlying mechanisms associated with disease or development induced changes. NODDI has been extensively used to study both pathological and normal brain development (Adluru et al., 2014; Eaton-Rosen et al., 2015; Grussu et al., 2017; Jelescu et al., 2015; Kunz et al., 2014; Wen et al., 2015), and many recent studies have explored how healthy aging can influence these metrics, shedding some light on their potential biological implications. For example, the orientation dispersion index (ODI) has been shown to decrease globally in human gray matter with age, suggesting a reduction in dendrite complexity or arborization (Nazeri et al., 2015). There have also been reports of increased neurite density index (NDI) and ODI in localized white matter regions, primarily in the frontal lobe (Billiet et al., 2015; Chang et al., 2015).

Given these advantages in NODDI, the aim of this study is to focus on aging-induced changes in neurite density, dispersion, and fiber population metrics in the medial temporal lobe and their relationship with cognitive performance. Venkatesh et al. (Venkatesh et al., 2020), have recently shown that neurite density, dispersion and free water volume concentration all increase with age in the human hippocampus, and have shown that NODDI metrics are better at predicting age than traditional diffusion tensor measures. However, there have been no reports exploring age related changes in NODDI metrics in hippocampal subfields, or how they relate to changes in memory performance. Here, we sought to determine the effect of age on both fiber metrics, as well as NODDI

properties, in the medial temporal lobe. We further assessed the relationship between changes in these metrics and cognitive performance in young and older adults. Finally, we used structural equation modelling to assess the extent to which these structural changes drive age-related cognitive decline.

2.2 METHODS

2.2.1 Participants

Forty-eight adults were recruited from the Orange County area in California. Three subjects were excluded for data segmentation issues, three subjects were excluded for registration issues, and four were excluded for neuropsychological scores more than 2 standard deviations below the mean for their age group. The final study adults consisted of 15 young (20 - 38 years, 28.4 ± 4.6 years, 8 females) and 23 older (59 - 84 years, 69.9±5.3 years, 14 females) adults. All participants provided informed consent prior to participation in this study, approved by the University of California, Irvine Institutional Review Board, and were compensated for their time.

2.2.2 Neuropsychological Battery

All participants completed a battery of neuropsychological tests to evaluate their cognitive abilities. Tests included the Mini-mental State Examination (MMSE) to screen for cognitive impairment (Folstein et al., 1975), Rey Auditory Verbal Learning Test (RAVLT) to evaluate memory recall and recognition (Rey, 1941), Geriatric Depression Scale (GDS) and Beck Depression Index (BDI) to characterize their depression profiles (Beck, 1972; Yesavage et al., 1982) (no participant was found to have a profile in the moderate-to-

severe range) (See Table 2.2). The Mini Mental State Exam (MMSE) total score is the sum of all test questions (maximum score of 30). The Rey Auditory Verbal Learning Test has three components: 5 presentations of the same 15-word lists with immediate recall, a second immediate recall test following an interference list of 15 novel words, and a final recall after a 15-minute delay. Here, the RAVLT Delay reflects the final recall score (maximum score of 15).

2.2.3 MR Image Acquisition

The participants were scanned using a Philips Achieva 3.0 Tesla MRI system, using a 32-channel SENSE receive-only head coil. Fitted padding was used to minimize head movements. A T1-weighted magnetization-prepared rapid gradient echo (MP-RAGE) scan was acquired (TR = 11ms, TE = 4.6ms, flip angle = - 18°, 200 sagittal slices and 0.75 mm isotropic resolution) for structural analysis and registration. High-resolution structural MRI images of the MTL were acquired using a T2-weighted sequence to aid in MTL segmentation (TE = 80 ms, flip angle = 90°, slices = 54, slice thickness = 3 mm, matrix size = 384 x 384, voxel size = 0.469 x 0.469 x 2mm, and an in-plane field of view = 108 x 180 mm). Both structural images were aligned as oblique coronals perpendicular to the long axis of the hippocampus and positioned to ensure MTL coverage. Three diffusion weighted scans (TR = 2174-2734ms, TE = 94 ms, 80 axial slices and 1.69 mm isotropic resolution) were acquired for four gradient values: b = 500, 1000, 2000, and 2500 s/mm². Gradients were applied in 10 directions for each scan (120 directions in total) along with 12 images with no diffusion weighting (b = 0).

Demographics	Young	Older	T-stat	p-value
N	15	23		
Mean Age	28.40 ± 4.73	69.87 ± 5.43		
Education	17.00 ± 2.17	17.30 ± 1.77		
MMSE	29.40 ± 0.74	29.48 ± 0.67	-0.33	0.37
RAVLT Total	61.13 ± 5.05	55.00 ± 8.06	2.88	0.003
RAVLT Immediate	13.80 ± 1.42	12.21 ± 2.50	2.48	0.009
RAVLT Delay	13.86 ± 1.18	12.00 ± 2.71	2.9	0.003

Table 2.2: Demographics and neuropsychological scores

2.2.4 Diffusion Data Preprocessing

All preprocessing steps employed MRtrix3 (www.mrtrix.org) commands or used MRtrix3 scripts that linked external software packages. Physiological noise arising from thermal motion of water molecules in the brain was first removed (Veraart et al., 2016), followed by removal of Gibbs ringing artifacts (Kellner et al., 2016), eddy current correction (Andersson & Sotiropoulos, 2016) and bias field correction (Tustison et al., 2014). The image intensity was then normalized across subjects in the log-domain (D. Raffelt et al., 2012).

2.2.5 Structural Data Preprocessing

The T1w images were corrected for intensity inhomogeneities using Advanced Normalization Tools (ANTs) N4 bias correction. Each individual's structural image was then nonlinearly registered to their respective preprocessed b0 image, so that the structural and diffusion images were in the same space for the rest of the analyses.

Registration was manually checked to ensure accuracy. To segment the MTL, we used a multi-atlas model created by our lab using ASHS (Yushkevich et al., 2010) and 19 independent hand-segmented brains (both the MP-RAGE and high-resolution T2 images). These segmentations included both segmentations of the parahippocampal gyrus into perirhinal (PRC), parahippocampal (PHC), and entorhinal (ERC) cortices described previously (Insausti et al., 1998; C. E. L. Stark & Okado, 2003). Similarly, we segmented the hippocampus into 3 subregions: a combined dentate gyrus and CA3 (combined due to resolution constraints; DG/CA3), CA1, and subiculum, based on our previous work (S. M. Stark & Stark, 2017b). For each of these, we created multi-atlas models in ASHS and then used these to segment each individual's high-resolution T2 scan.

2.2.6 Fiber Orientation Distribution Analysis with MRtrix3

Following preprocessing, we generated response functions for white matter, gray matter, and CSF for each participant. The response function for each tissue type was then averaged across subjects. The fiber orientation distributions (FODs) were then calculated for each tissue type from the group averaged response functions using Multi-Shell Multi-Tissue Constrained Spherical Deconvolution (MSMT-CSD) (Dhollander et al., 2016). We created a study-specific template using an iterative registration and averaging approach (D. Raffelt et al., 2011) using the white matter FODs from 20 arbitrary subjects (10 old and 10 young). All the subjects' FODs were registered to this template using a FOD-guided non-linear registration (D. Raffelt et al., 2011). The remaining analysis in MRtrix3 was performed in this study-specific template space, unless mentioned otherwise.

34

To segment the white matter tracts in a common space, we generated a tractogram from the template using whole-brain probabilistic tractography (20 million streamlines, termination cutoff = 0.6). To account for reconstruction biases, we filtered the tractogram to 2 million streamlines using the Spherical-deconvolution Informed Filtering of Tractograms algorithm (Smith et al., 2013).

The FOD images were then segmented into "fixels" (individual voxels sectioned into individual fibers) for further analysis. We calculated the fiber density (FD), fiber bundle cross-section (FC), and a combined measure of fiber density and cross section (FDC) for each subject across all white matter fixels (D. A. Raffelt et al., 2017). The FD of a given fixel is proportional to the intra-axonal volume of axons aligned in a given direction and is calculated as the integral of the FOD along that direction, using the Apparent Fiber Density framework (D. Raffelt et al., 2012). The FC metric is meant to capture macrostructural changes and is sensitive to axonal loss and pathway atrophy (Grazioplene et al., 2018; Pannek et al., 2018). It is calculated as the amount of distortion perpendicular to a given fixel's orientation that is required to warp the individual's FOD to the template FOD (D. A. Raffelt et al., 2017). We used the natural logarithm of this metric for statistical analysis to ensure that the data were normally distributed and centered around zero. Finally, since the functionality of a given fiber bundle is influenced by both the local fiber density as well as the fiber cross-section, group differences may manifest as changes to both these metrics. Hence the FDC, a combined metric, was also calculated as the product of the FD and FC for each fixel. For comparison purposes, we also computed traditional fractional anisotropy (FA) and mean diffusivity (MD) metrics.

The fixel metrics were compared across age groups at each white matter fixel using a General Linear Model, considering age as a nuisance covariate. We performed connectivity-based smoothing and statistical inference using connectivity-based fixel enhancement (CFE). Family-wise error corrected p-values were then assigned to each fixel using non-parametric permutation testing of the CFE enhanced t-statistics (Nichols & Holmes, 2002).

2.2.7 NODDI Analysis with the Microstructure Diffusion Toolbox (MDT)

Microstructure metrics were calculated using the Neurite Orientation Dispersion and Density Imaging (NODDI) model (Zhang et al., 2012) with the Microstructure Diffusion Toolbox (MDT) (Harms et al., 2017). NODDI characterizes diffusion within each brain voxel as a combination of intracellular, extracellular and CSF based components. The intracellular compartment seeks to capture neurite membranes and myelin sheaths and is modelled as a set of sticks with restricted diffusion perpendicular to the orientation of the axonal bundles and unhindered diffusion along them. The extracellular compartment is thought to capture primarily the space around the neurites, composed of glial cells and somas. The diffusion in this space is modelled as hindered Gaussian anisotropic diffusion. Finally, the CSF compartment is modelled as isotropic diffusion. The neurite density index (NDI) gives the fraction of tissue volume restricted within neurites. It scales from 0 to 1, with 0 being most extracellular-like diffusion and 1 being most intracellular-like (Billiet et al., 2015). The orientation dispersion index (ODI) is a measure of tortuosity and is calculated as the dispersion coefficient of the neurites. An ODI closer to 0 is indicative

of well-aligned neurites, while that closer to 1 indicates higher levels of dispersion. The fractional isotropy (FISO) is the percentage of the volume in each voxel that is best modelled by free-water diffusion. The 4D DWI data was passed in as input and parametric maps of NDI, ODI, and FISO were generated for each subject and then transformed into MNI space using ANTs.

2.2.8 Voxel-Based Spatial Statistics

All white matter metric calculations were performed in the study-specific template space. First, a global white matter mask was created from the Harvard-Oxford structural atlas [1–4]. This mask was nonlinearly transformed to each subject's structural image in template space, to make a subject-specific global white matter mask. All subject-specific masks were then averaged and thresholded at 90% (such that a voxel is accepted into the mask only if the voxel is part of the subject specific masks for 90% of the subjects). The diffusion metrics were then averaged within this mask to generate global white matter metrics for each subject. The same process was repeated after generating a fornix mask from the JHU White Matter Atlas (Hua et al., 2008; Mori, 2007; Wakana et al., 2007). Note that all statistical analyses in white matter were first performed in the CFE framework. The voxel-based analysis was employed for comparison purposes only.

A global gray matter mask was generated using the Harvard-Oxford structural atlas and metrics were averaged across this mask to calculate global gray matter metrics. The medial temporal lobe was segmented into the CA1, DG/CA3, subiculum, entorhinal cortex, perirhinal cortex, and parahippocampal cortex using an in-house protocol (Huffman & Stark, 2014; Kirwan & Stark, 2004). Diffusion metrics were then averaged

across each of these regions of interest in both hemispheres for each subject to make subject-specific bilateral masks. The global gray matter mask was created in the same way as the global white matter mask.

All statistical analyses were performed in Python 3 (using StatsModels (Seabold & Perktold, 2010) or SciPy (Jones et al., 2001)) or GraphPad Prism 8.3.0. (*Home - GraphPad*, n.d.) Statistical p-values were corrected for multiple comparisons (6 regions of interest for each metric) in all gray matter associated analysis by calculating the false discovery rate (Benjamini et al., 2006). Group differences were computed using student's two-tailed t tests in GraphPad Prism 8.3.0. Structural equation analysis was performed using PyProcessMacro [Model 4] (*PROCESS Macro for SPSS and SAS*, n.d.).

2.3 RESULTS

2.3.1 Fornix integrity and microstructure is modulated by age.

First, we assessed the effect of age on fornix integrity using the traditional single-tensor diffusion measures of FA and MD. Consistent with prior reports (Bennett et al., 2010; Kantarci et al., 2013) , MD in the fornix was reliably higher in the older adults (t = 3.118; p = 0.0036), while FA showed a significant reduction (t = 5.100; p < 0.0001). Moreover, both MD and FA were linearly correlated with age in the older adults alone (R^2 = 0.5370, p < 0.0001; R^2 = 0.3597, p = 0.0025 respectively; Figure 2.1a, b). We then asked whether similar age-related deterioration in the fornix could be detected with the more sophisticated measures of tract architecture. With connectivity-based fixel enhancement statistics, we found that the FD of the fornix was significantly lower in the older adults (t

= 5.959; $p < 0.0001$) and that FD decreased linearly with age in the older adults alone (R^2 = 0.3638, $p = 0.0023$; Figure 2.1c). There was no evidence for a relationship between the fiber cross section of the fornix ($p = 0.9450$) or the raw NDI ($p = 0.3520$) and age. Results also revealed that the amount of free water in the fornix voxels was significantly higher in the older subjects ($t = 2.773$; $p = 0.0087$; Figure 2.1d). Together, these findings are consistent with the hypothesis that hippocampal connectivity is altered in typical aging and further, that the differences are best attributed to small-scale changes in tract integrity.

To determine whether the differences observed were selective to the fornix and not merely a consequence of age-related global white matter decline, the fornix diffusion metrics were linearly modelled against their respective global white matter diffusion metrics. The residuals of this model were quantified as the "globally regressed" metric. Post global-regression, the FD decline with age remained robust (t-test: $t = 3.4720$; $p = 0.0014$; aged-only linear regression: $R^2 = 0.6120$, $p < 0.0001$; Figure 2.1e). Interestingly, the globally regressed NDI showed a decrease in the older adults ($t = 2.277$; $p = 0.0288$; Figure 2.1f), while this had not been observed with the raw NDI, suggesting an age-associated change in the fornix that was not a result of a global decrease. Notably, after removing global effects of age on FISO, there was no remaining effect of age, suggesting that the change observed in the raw fornix FISO was merely a consequence of a global increase in white matter free water concentration. No reliable sex differences were found in any of the fornix metrics after correcting for multiple comparisons. All significant effects were

observed in both hemispheres (results reported above were acquired from bilateral masks of a given region of interest).
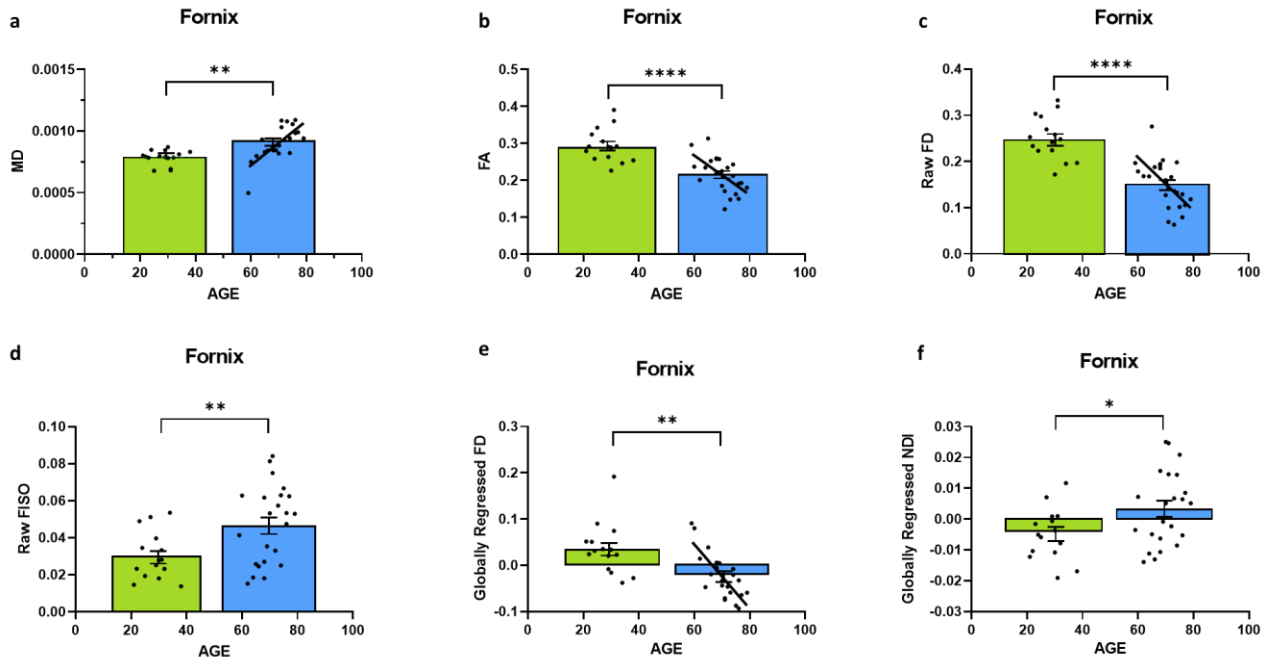
Figure 2.1: The diffusion metrics of the fornix are influenced by age. Dots indicate individuals with their age both grouped in bars and plotted along the x-axis. a-b) Traditional diffusion tensor metrics of the fornix are linearly correlated with age in the older adults and show group differences. c) The raw fornix FD decreased with age. d) The raw fornix FISO increased in the aged adults. e) The fornix FD maintains its relationship with age even after regressing out global white matter changes. f) The globally regressed fornix NDI increased with age. Error bars show the standard error of the mean. Asterisks indicate $p \leq 0.05$, $p \leq 0.01$, $p \leq 0.001$, and $p \leq 0.0001$ respectively.

2.3.2 Fornix integrity and microstructure correlate with RAVLT performance.

We then evaluated whether these individual differences in fornix architecture were correlated with hippocampal-based memory performance. RAVLT, a word-list learning

paradigm, is a standard neuropsychological measure that has proven to be sensitive to age-related changes in memory performance and neural measures (Bennett et al., 2015; Yassa et al., 2010). The raw fornix FISO was negatively linearly correlated with delayed recall RAVLT performance (R^2 = 0.319, p = 0.0002; Figure 2.2a), while the raw FD showed a positive linear relationship with RAVLT performance (R^2 = 0.2261, p = 0.0026; Figure 2.2b). There was no reliable relationship between the raw NDI and the RAVLT score after correcting for multiple comparisons.

After global regression, the FD remained positively correlated with RAVLT delay (R^2 = 0.1576, p = 0.0136; Figure 2.2c). Interestingly, and in conjunction with observations from the previous section, the globally regressed NDI showed a negative linear relationship with RAVLT performance (R^2 = 0.2830, p = 0.0006; Figure 2.2d), suggesting that the age-related decrease in FD and increase in NDI might be contributing to age-associated cognitive decline. The relationship between FISO and RAVLT delay disappeared after global regression, in line with the hypothesis that the observed FISO changes were not unique to the fornix. (R^2 = 0.07, p = 0.131)
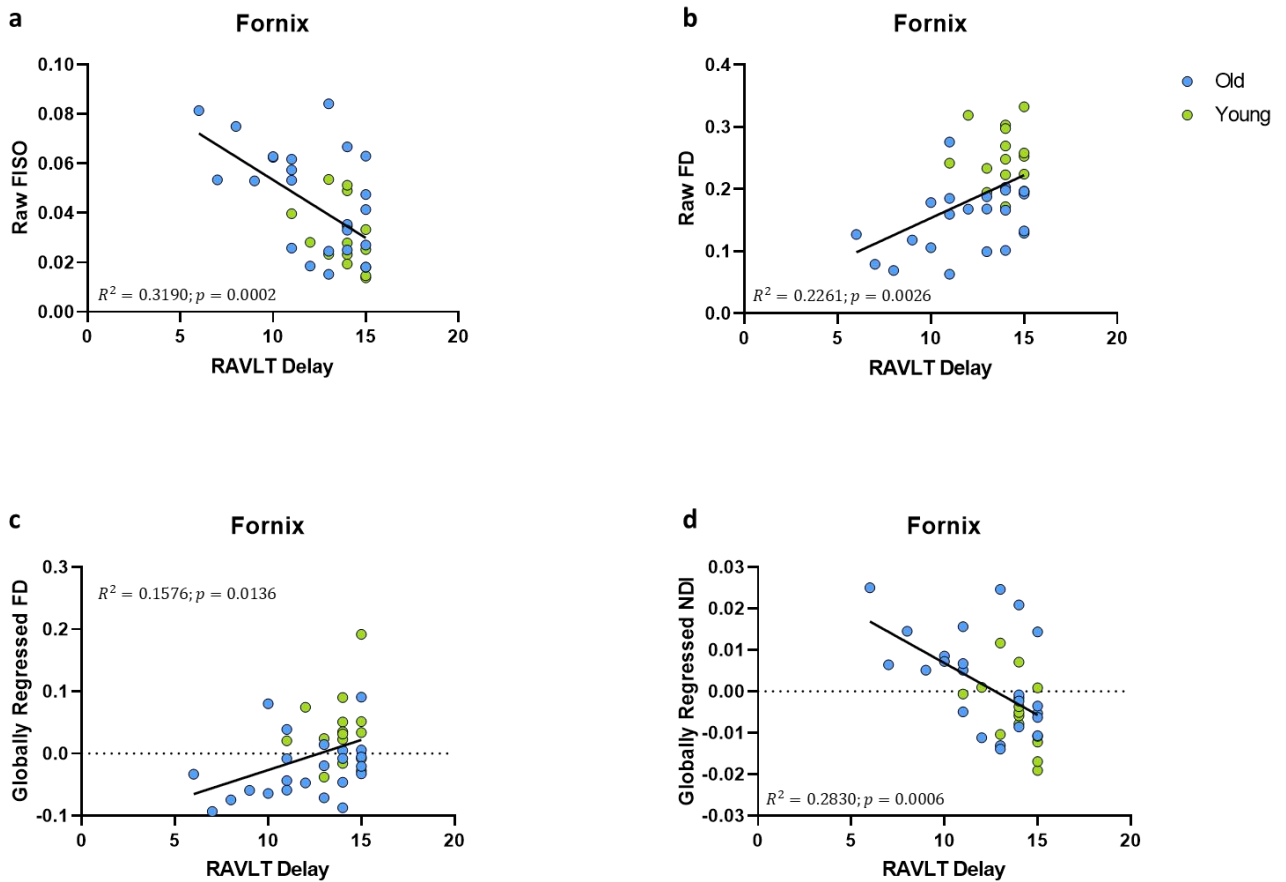
Figure 2.2: Fornix diffusion metrics were correlated with performance in the RAVLT. a-b) The raw fornix FISO and FD are positively associated with RAVLT performance. c-d) After global regression, the fornix FD and NDI were negatively correlated with RAVLT performance.

2.3.3 Gray matter microstructure of the medial temporal lobe deteriorates with age.

An advantage of the NODDI analytic framework is that each voxel is treated as a combination of several different components that lead to the observed diffusion and no distinction is drawn a priori as to whether a voxel is gray matter, white matter, or CSF (all voxels are treated as potential mixtures thereof). This approach allows us to perform

meaningful analyses of the microstructure of gray matter. In examining whether age induces any structural changes within segments of the medial temporal lobe, we observed that the raw NDI of the DG/CA3 was higher in the aged adults ($t = 2.863$, $p = 0.0069$; Figure 2.3a). We also observed higher FISO in the perirhinal cortex ($t = 3.452$, $p = 0.0014$), parahippocampal cortex ($t = 2.913$, $p = 0.0061$), DG/CA3 ($t = 4.667$, $p < 0.0001$), CA1 ($t = 2.897$, $p = 0.0064$) and the subiculum ($t = 5.817$, $p < 0.0001$) in older adults. However, we did not observe reliable age-related changes in the diffusion metrics of the entorhinal cortex.

Post global-regression, there was no age-associated increase in the FISO of the MTL segments, suggesting that the increases observed in the raw metric were simply a consequence of global atrophy due to aging. The globally regressed NDI of the parahippocampal cortex and all hippocampal subfields displayed an age-related increase (PHC: $t = 5.931$, $p < 0.0001$; DG/CA3: $t = 3.6770$, $p = 0.0008$; CA1: $t = 2.4890$, $p = 0.0176$; Subiculum: $t = 3.8080$, $p = 0.0005$; Figure 2.3b-e). Thus, the NDI change in each of these regions was greater than the global gray matter average NDI in older adults, while it was reduced in the younger adults, suggesting that the NDI increases in the MTL are beyond those associated with age in the whole brain.

No reliable sex differences were found for any of the MTL metrics, after correcting for multiple comparisons. In addition, all significant effects were observed in both hemispheres.
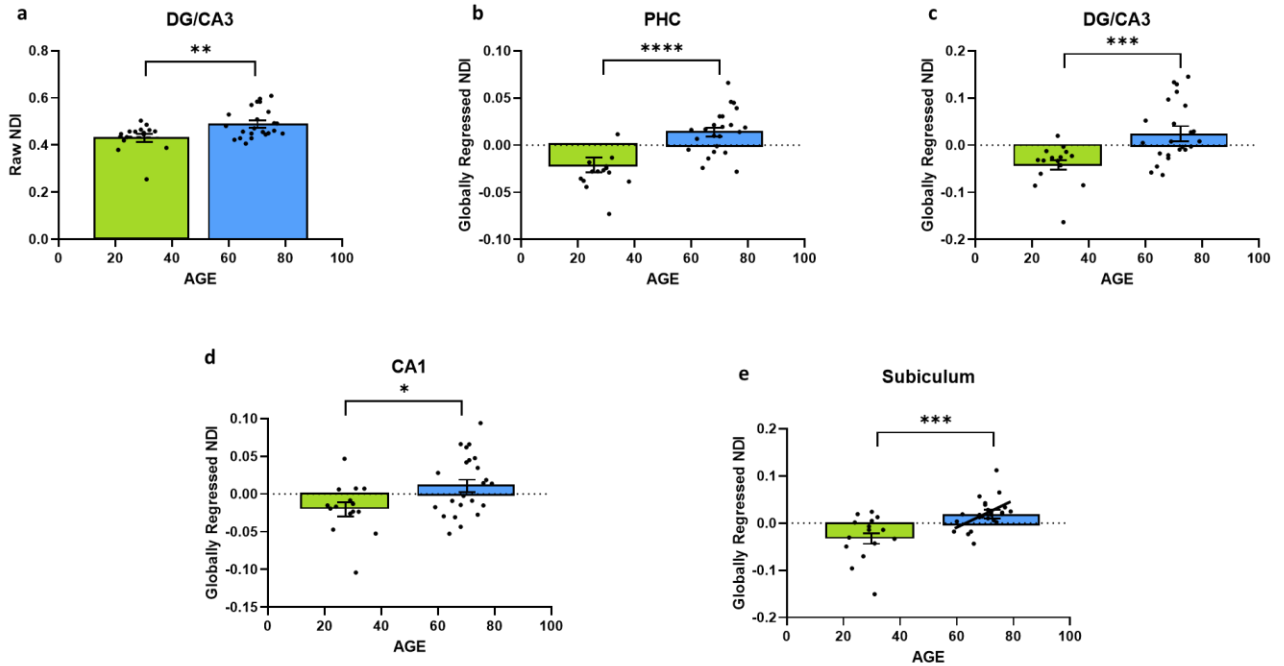
Figure 2.3: The NDI of the medial temporal lobe is greater in the aged adults. a) The raw NDI of the DG/CA3 is increased in the aged adults. b-e) After regressing out global gray matter changes, the NDI of the PHC and hippocampal subfields are increased in the aged adults. Error bars show the standard error of the mean. Asterisks indicate p ≤ 0.05, p ≤ 0.01, p ≤ 0.001, and p ≤ 0.0001 respectively.

2.3.4 NDI of the DG/CA3 and the CA1 are correlated with RAVLT performance.

We next assessed whether the diffusion metrics within the gray matter of the medial temporal lobe were associated with memory ability, particularly performance in the RAVLT. The raw FISO for each medial temporal lobe region, except for the entorhinal cortex, was negatively linearly correlated with RAVLT delay. However, this association disappeared after we regressed out global gray matter metrics, suggesting that the relationship between FISO and RAVLT performance is informed by general global gray

matter atrophy driving cognitive decline. Consistent with these results, greater FISO values are thought to be indicative of more necrotic cells and CSF presence in gray matter voxels. (Metzler-Baddeley et al., 2012; Ofori et al., 2015)

The raw NDI of both the DG/CA3 (R^2 = 0.2192, p = 0.003; Figure 2.4a) and the CA1 (R^2 = 0.1246, p < 0.0297; Figure 2.4b) showed a negative correlation with RAVLT performance (however, the effect with CA1 NDI was not reliable after correcting for multiple comparisons.) After global regression, the NDI of the DG/CA3 and the CA1 remained negatively correlated with RAVLT performance, even after correcting for multiple comparisons (Figure 2.4 c, d).
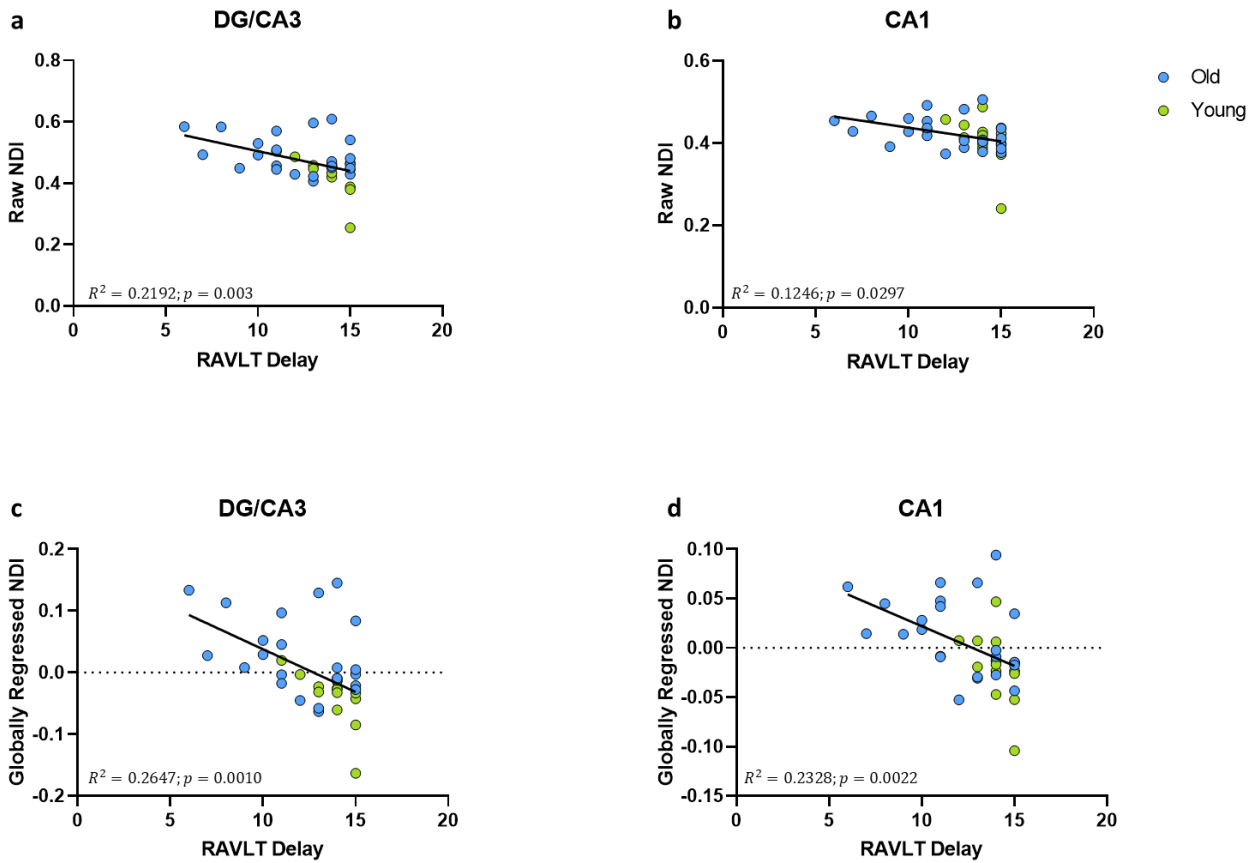
Figure 2.4: The NDI of the hippocampus has a negative relationship with RAVLT performance. a-b) The raw NDI of the DG/CA3 and CA1 decreased with increase in RAVLT delay. c-d) This relationship remained after regressing out global gray matter NDI.

2.3.5 NDI of the DG/CA3, CA1 and the fornix remain correlated with RAVLT delay, even after regressing age out

To assess whether these structural correlations with cognitive performance might reflect more than simple age-related decline, we regressed age out of the RAVLT scores in addition to regressing it out of our diffusion metrics. The age-regressed RAVLT scores can be thought of a "de-aged" RAVLT score (capturing something akin to age-invariant individual differences), as the effects of standard aging are computationally removed from the score. This regressed RAVLT score remained negatively correlated with the globally regressed NDI of the fornix ($R^2 = 0.1624$, $p = 0.0121$), DG/CA3 ($R^2 = 0.1172$, $p = 0.0354$), and the CA1 ($R^2 = 0.1481$, $p = 0.017$). We then regressed age out of the NDI as well and observed that the negative linear correlation survived (Figure 2.5). The persistence of this relationship between NDI and the RAVLT delay, even after removing the effects of age, suggests that this metric is sensitive to microstructural properties in these regions that directly influence performance in the RAVLT.
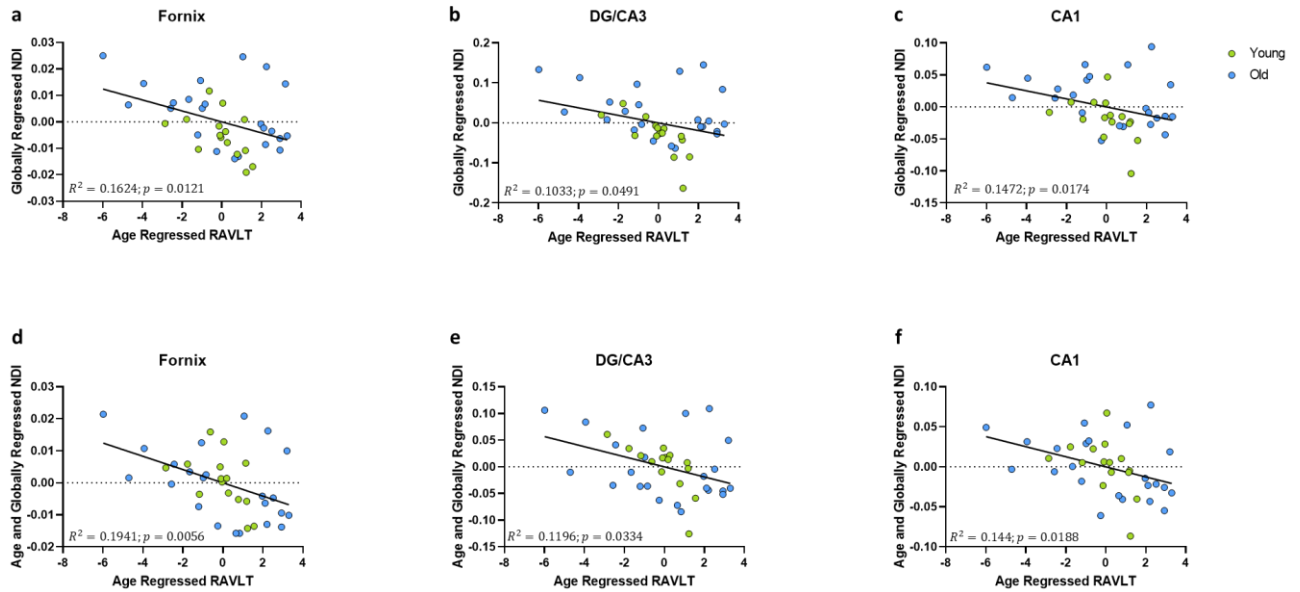
Figure 2.5: The relationship between RAVLT and NDI is retained even after regressing out the effect of age on both sides, in the fornix, DG/CA3 and CA1. a-c) The globally regressed NDI had a negative relationship with the RAVLT score, after regressing out the effect of age on the RAVLT performance. d-f) This relationship is sustained even after regressing out the effect of age on the globally regressed NDI.

The above correlations suggest a clear relationship amongst age, integrity of the hippocampus (and its connectivity via the fornix), and memory performance. To model the most parsimonious account of these interrelationships, we performed a mediation analysis. An increase in the hippocampus NDI, more specifically, the DG/CA3 NDI, mediated the negative relationship between age and RAVLT delay. Removing the effect of the DG/CA3 NDI change resulted in age having no residual effect on the RAVLT delay. Similarly, a decrease in the FD of the fornix significantly mediated the relationship between age and RAVLT delay. In both cases, we observed that the effect of age on cognitive decline disappeared upon removing the effect of the mediators. No other diffusion metric studied showed this effect (Figure 2.6). It must be noted that this result

must be interpreted cautiously as this is not a longitudinal study and we lack middle-aged participants that would allow for a continuous distribution of ages. However, despite these limitations, this observation bolsters the theory that NDI and FD in DG/CA3, and the fornix respectively may be heavily influencing verbal recall.
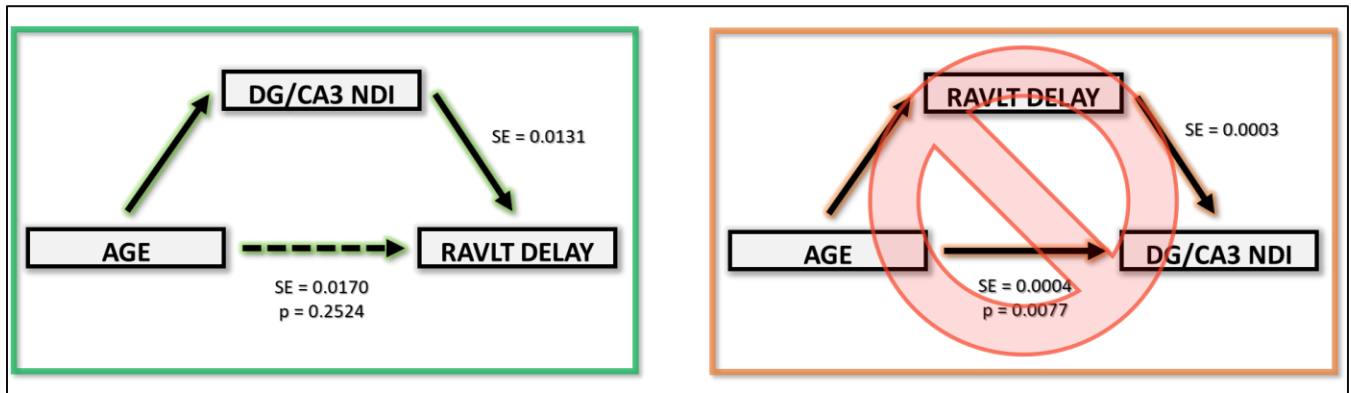
Figure 2.6: Age-related RAVLT decline can be mediated by NDI increase in the DG/CA3.

2.3.6 Fiber cross sectional differences in the fornix are found with voxel-based statistics but disappear with fixel-wise analyses.

It is important to note the differences observed between fixel-based analysis and voxel-based analysis techniques when looking at white matter fiber tracts. A single voxel might have multiple fiber tracts passing through it, causing interference and noise in the measure. Moreover, crossing, fanning and kissing fibers further alleviate this issue as the "density" of a tract may be corrupted by another tract in the voxel that seems to overlap it. This makes most voxel-based analysis techniques undesirably non-specific. A fixel-wise analysis solves this problem by performing statistics on specific fiber populations within the voxel, ensuring that the effect observed is in the pathway that is being studied.

This issue is further demonstrated in our observation that connectivity-based fixel-enhancement statistics showed no significant age effects on the fiber cross-section of the fornix, while a voxel-based statistical analysis of the same metric showed a significant difference between age groups (p = 0.001). Care must be taken when reporting voxel-based white matter results for this reason. Interestingly, the observed robustness of fornix fiber cross section with age suggests that large scale structural changes may not be the focus of age-related architectural changes in the fornix.

2.4 DISCUSSION

In this study, we examined the age-related effects of diffusion metrics of the medial temporal lobe and their relationship with memory performance. We first replicated previous studies showing that the fractional anisotropy of the fornix declines with age, while mean diffusivity increases. We then demonstrated age-related changes in fornix architecture with more comprehensive diffusion metrics, observing a decrease in FD, and an increase in the NDI. Notably, these changes were correlated with poorer RAVLT performance, suggesting that age-related microstructural deterioration of the fornix may play a role in age-related cognitive decline. We also observed similar trends in the gray matter of the medial temporal lobe: showing that the NDI of hippocampal subfields and the parahippocampal cortex increased with age and had a negative correlation with RAVLT performance for DG/CA3 and CA1. Interestingly, we observed that the NDI of the fornix, DG/CA3 and CA1 maintained its relationship with RAVLT performance, even after regressing age out from both the structural metric and the cognitive score, suggesting that this metric is inherently sensitive to a neurobiological property within the hippocampus

that corresponds to cognitive performance independent of age. We also demonstrated that traditional methods of analyzing diffusion metrics are not only insufficient for identifying such microarchitectural differences but may also provide unreliable results. Finally, through structural equation modelling, we showed that the DG/CA3 NDI increase and fornix FD decrease mediated age-related decline in RAVLT performance.

Though previous studies have shown that the integrity of the fornix declines with age, none to our knowledge, have explored this change with more nuanced diffusion metrics to arrive at a more neurobiologically detailed explanation. A decrease in FA could mean a myriad of structural alterations: from demyelination and decrease in axon diameter to a decrease in axon packing density(Sampaio-Baptista & Johansen-Berg, 2017). The fornix has been shown to undergo age related axonal degeneration in both rats (Naranjo & Greene, 1977) and monkeys (Peters et al., 2010); and our findings on fiber density reductions bolster the idea that an analogous change may be occurring in humans. This, along with our observation that FC remains unchanged, suggests that age-related fornix deterioration may more likely to be caused by microstructural alterations, like changes in axon packing density or loss of myelinated fibers(Peters et al., 2010), more so than macrostructural alterations like an overall reduction in the diameter of the fiber bundle. While this explanation is in no way conclusive, it helps shed more light on the underlying mechanisms behind age-related structural decline. Moreover, the linear relationship we observe between fornix fiber density and age in the older adults alone suggests the existence of a "tipping point" in age- after which fornix deterioration begins to occur consistently and linearly. Unfortunately, the lack of middle-aged adults or longitudinal

data prevents us from accurately establishing the age of this tipping point based on these data.

Moreover, NODDI analysis of the diffusion signal enables us to directly compare changes in different tissue types, which is valuable when studying more systemic changes in the medial temporal lobe. As NODDI does not directly discriminate between gray and white matter, we are able to agnostically measure structural changes and their relationship with cognition. A major caveat of this technique, however, is that there exists very little information on what these metrics may cytoarchitecturally mean. NODDI is a recent technique and its metrics have not been adequately histologically validated, especially in human tissue. The nomenclature of these metrics can also be quite misleading. An increase in the neurite density index does not necessarily correspond to an actual increase in the number of neurites in a voxel. It must be kept in mind that diffusion weighted imaging currently does not have the resolution to measure differences at such a microscopic level. That said, NODDI has proven to be extremely valuable in parsing out information from highly complex voxels, and studies that have correlated its metrics with neurobiological properties have been promising. (Sato et al., 2017; Schilling et al., 2018; Sepehrband et al., 2015)

With NODDI, we found an increase in FISO with age in the fornix, parahippocampal cortex, perirhinal cortex, and all hippocampal subfields, suggesting that these regions are either getting corrupted by an influx of cerebrospinal fluid or other factors that result in an increase in free water concentration (such as an increase in the number of necrotic cells). Increases in FISO could also be caused by neuropathological factors like

edema(Pasternak et al., 2009), inflammation(Wang et al., 2011), and atrophy(Metzler-Baddeley et al., 2011, p.). These factors may also clarify the negative relationship we observed between FISO and RAVLT performance. Interestingly, the effect of age on FISO and the influence of FISO on RAVLT performance disappeared when we regressed out the global change in FISO, suggesting that the increase we had previously observed was merely a consequence of overall brain atrophy with age. More importantly, this global regression introduced an effect of age on the NDI in the fornix, parahippocampal cortex and all hippocampal subfields, indicating that the NDI in these regions may have a more focused increase than the generalized global metric during aging. This selective increase in NDI may indicate a decrease in dendritic complexity, perhaps caused by atrophy of the surrounding cortical layers. (Colgan et al., 2016) This speculation is further invigorated by the retention of the relationship between NDI and RAVLT performance in the fornix, DG/CA3 and CA1, even after regressing out the effect of age in both the structural metric and the cognitive score. A similar dynamic is observed between the fiber density of the fornix and RAVLT performance as well- suggesting that both NODDI and MRtrix may be capable of capturing specialized distortions like reductions in myelination or dendritic complexity. This possibility is especially exciting as its clinical applications are endless: the diagnosis of many neurodegenerative disorders could be aided by the context of the NODDI metrics(Sampaio-Baptista & Johansen-Berg, 2017), with the added advantage that NODDI is relatively easy to implement and process. Another speculation that could rise from the relationship between NDI and RAVLT in the DG/CA3, CA1 and fornix, despite the regression of age, is that this metric is capturing a neurobiological property (like dendritic arborization) that is inherently correlated with verbal recall- suggesting

that exploring these metrics might enable us to get at the neurobiological basis of specific cognitive functions.

These findings also raise the speculation that changes in the neurite density index due to age might be partially driving age-related cognitive decline, at least in the context of delayed verbal recall. This theory is further bolstered with results from our mediation analysis, where we showed that the effect of age on RAVLT performance is no longer reliable once we regress out NDI and FD changes of the DG/CA3 and fornix. Though further evidence is required, these results may indicate that neurite density related structural changes in the fornix and the hippocampus may be responsible for instigating age-related memory decline.

Our results also challenge the validity of current voxel-based analysis methods used in diffusion weighted imaging, especially in white matter regions. We show that fiber cross section of the fornix does not significantly change with age when we performed connectivity-based fixel enhancement statistics, but the same measure was sensitive when we computed simple voxel averages about the region of interest. This discrepancy might be explained by the fact that MRI voxels are relatively large and contain multiple fiber pathways running through them, a nuance that simple voxel-based analysis methods do not fully appreciate. For example, the fornix also has other white matter pathways running across it (ex: the cingulum), which may also be changing with age. Fixel-based analysis works around this issue by separating the multiple fiber populations in a single voxel using constrained spherical deconvolution, enabling us to examine individual pathways with more accuracy. More interesting patterns may be found if we map the

distributions of metrics across all voxels in the region instead of simply averaging metrics across a region of interest. More specific, non-linear analyses of the voxel-wise distribution of a metric within a given ROI can provide a more comprehensive assessment of how these metrics change. Thus, our results have shown that diffusion weighted imaging may have more power if we move beyond simple voxel-based averaging analysis methods.

MRtrix and NODDI put together may be able to give us the most detailed view of the microstructure of the live human brain possible with the current technological state of diffusion weighted imaging. No other study to our knowledge has examined healthy aging related microstructural changes in the medial temporal lobe and its relationship with cognitive performance at this level of detail before. It is worth noting that our sample size is relatively small and longitudinal data is required to fully determine the progression of these changes. Lack of reverse phase encoded acquisitions also makes our signal more susceptible to EPI distortions. Moreover, NODDI assumes that intrinsic diffusivity is uniform throughout the brain, but this measure might be susceptible to age-related changes. While these NODDI metrics may be more sensitive to gray and white matter integrity, more research is necessary to understand the underlying neurobiological of each of them. Therefore, future studies tying together diffusion weighted imaging with the underlying histology will hence be immensely valuable.

References

Abe, O., Aoki, S., Hayashi, N., Yamada, H., Kunimatsu, A., Mori, H., Yoshikawa, T., Okubo, T., & Ohtomo, K. (2002). Normal aging in the central nervous system: Quantitative MR diffusion-tensor analysis. *Neurobiology of Aging*, *23*(3), 433–441. https://doi.org/10.1016/S0197-4580(01)00318-9

Adluru, G., Gur, Y., Anderson, J. S., Richards, L. G., Adluru, N., & DiBella, E. V. R. (2014). Assessment of white matter microstructure in stroke patients using NODDI. *Conference Proceedings: … Annual International Conference of the IEEE Engineering in Medicine and Biology Society. IEEE Engineering in Medicine and Biology Society. Annual Conference*, *2014*, 742–745. https://doi.org/10.1109/EMBC.2014.6943697

Ahmad, A., & Spear, P. D. (1993). Effects of aging on the size, density, and number of rhesus monkey lateral geniculate neurons. *Journal of Comparative Neurology*, *334*(4), 631–643. https://doi.org/10.1002/cne.903340410

Andersson, J. L. R., & Sotiropoulos, S. N. (2016). An integrated approach to correction for off-resonance effects and subject movement in diffusion MR imaging. *NeuroImage*, *125*, 1063–1078. https://doi.org/10.1016/j.neuroimage.2015.10.019

Beck, A. (1972). *Depression: Causes and Treatment*. University of Pennsylvania Press.

Benjamini, Y., Krieger, A. M., & Yekutieli, D. (2006). Adaptive linear step-up procedures that control the false discovery rate. *Biometrika*, *93*(3), 491–507. https://doi.org/10.1093/biomet/93.3.491

Bennett, I. J., Huffman, D. J., & Stark, C. E. L. (2015). Limbic Tract Integrity Contributes to Pattern Separation Performance Across the Lifespan. *Cerebral Cortex (New York, N.Y.: 1991)*, *25*(9), 2988–2999. https://doi.org/10.1093/cercor/bhu093

Bennett, I. J., & Madden, D. J. (2014). Disconnected aging: Cerebral white matter integrity and age-related differences in cognition. *Neuroscience*, *276*, 187–205. https://doi.org/10.1016/j.neuroscience.2013.11.026

Bennett, I. J., Madden, D. J., Vaidya, C. J., Howard, D. V., & Howard, J. J. (2010). Age-related differences in multiple measures of white matter integrity: A diffusion tensor imaging study of healthy aging. *Hum Brain Mapp*, *31*, 378–390. https://doi.org/10.1002/hbm.20872

Bennett, I. J., & Stark, C. E. L. (2015). Mnemonic Discrimination Relates to Perforant Path Integrity: An Ultra-High Resolution Diffusion Tensor Imaging Study. *Neurobiology of Learning and Memory*, *129*, 107–112. https://doi.org/10.1016/j.nlm.2015.06.014

Billiet, T., Vandenbulcke, M., Mädler, B., Peeters, R., Dhollander, T., Zhang, H., Deprez, S., Van den Bergh, B. R. H., Sunaert, S., & Emsell, L. (2015). Age-related microstructural differences quantified using myelin water imaging and advanced diffusion MRI. *Neurobiology of Aging*, *36*(6), 2107–2121. https://doi.org/10.1016/j.neurobiolaging.2015.02.029

Budde, M. D., Kim, J. H., Liang, H.-F., Schmidt, R. E., Russell, J. H., Cross, A. H., & Song, S.-K. (2007). Toward accurate diagnosis of white matter pathology using diffusion tensor imaging. *Magnetic Resonance in Medicine*, *57*(4), 688–695. https://doi.org/10.1002/mrm.21200

Chang, Y. S., Owen, J. P., Pojman, N. J., Thieu, T., Bukshpun, P., Wakahiro, M. L. J., Berman, J. I., Roberts, T. P. L., Nagarajan, S. S., Sherr, E. H., & Mukherjee, P. (2015). White Matter Changes of Neurite Density and Fiber Orientation Dispersion during Human Brain Maturation. *PLOS ONE*, *10*(6), e0123656. https://doi.org/10.1371/journal.pone.0123656

Charlton, R. A., McIntyre, D. J., Howe, F. A., Morris, R. G., & Markus, H. S. (2007). The relationship between white matter brain metabolites and cognition in normal aging: The GENIE study. *Brain Res*, *1164*, 108–116. https://doi.org/10.1016/j.brainres.2007.06.027

Colgan, N., Siow, B., O'Callaghan, J. M., Harrison, I. F., Wells, J. A., Holmes, H. E., Ismail, O., Richardson, S., Alexander, D. C., Collins, E. C., Fisher, E. M., Johnson, R., Schwarz, A. J., Ahmed, Z., O'Neill, M. J., Murray, T. K., Zhang, H., & Lythgoe, M. F. (2016). Application of neurite orientation dispersion and density imaging (NODDI) to a tau pathology model of Alzheimer's disease. *NeuroImage*, *125*, 739–744. https://doi.org/10.1016/j.neuroimage.2015.10.043

Dhollander, T., Raffelt, D., & Connelly, A. (2016). *Unsupervised 3-tissue response function estimation from single-shell or multi-shell diffusion MR data without a co-registered T1 image*.

Eaton-Rosen, Z., Melbourne, A., Orasanu, E., Cardoso, M. J., Modat, M., Bainbridge, A., Kendall, G. S., Robertson, N. J., Marlow, N., & Ourselin, S. (2015). Longitudinal measurement of the developing grey matter in preterm subjects using multi-modal MRI. *NeuroImage*, *111*, 580–589. https://doi.org/10.1016/j.neuroimage.2015.02.010

Eckert, M. A. (2011). Slowing Down: Age-Related Neurobiological Predictors of Processing Speed. *Frontiers in Neuroscience*, *5*. https://doi.org/10.3389/fnins.2011.00025

Fjell, A. M., Sneve, M. H., Storsve, A. B., Grydeland, H., Yendiki, A., & Walhovd, K. B. (2016). Brain Events Underlying Episodic Memory Changes in Aging: A Longitudinal Investigation of Structural and Functional Connectivity. *Cerebral Cortex*, *26*(3), 1272–1286. https://doi.org/10.1093/cercor/bhv102

Folstein, M. F., Folstein, S. E., & McHugh, P. R. (1975). "Mini-mental state". A practical method for grading the cognitive state of patients for the clinician. *Journal of Psychiatric Research*, *12*(3), 189–198.

Glisky, E. L. (2007). Changes in Cognitive Function in Human Aging. In D. R. Riddle (Ed.), *Brain Aging: Models, Methods, and Mechanisms*. CRC Press/Taylor & Francis. http://www.ncbi.nlm.nih.gov/books/NBK3885/

Grazioplene, R. G., Bearden, C. E., Subotnik, K. L., Ventura, J., Haut, K., Nuechterlein, K. H., & Cannon, T. D. (2018). Connectivity-enhanced diffusion analysis reveals white matter density disruptions in first episode and chronic schizophrenia. *NeuroImage: Clinical*, *18*, 608–616. https://doi.org/10.1016/j.nicl.2018.02.015

Grieve, S. M., Williams, L. M., Paul, R. H., Clark, C. R., & Gordon, E. (2007). Cognitive aging, executive function, and fractional anisotropy: A diffusion tensor MR imaging study. *AJNR. American Journal of Neuroradiology*, *28*(2), 226–235.

Grussu, F., Schneider, T., Tur, C., Yates, R. L., Tachrount, M., Ianuş, A., Yiannakas, M. C., Newcombe, J., Zhang, H., Alexander, D. C., DeLuca, G. C., & Gandini Wheeler-Kingshott, C. A. M. (2017). Neurite dispersion: A new marker of multiple sclerosis spinal cord pathology? *Annals of Clinical and Translational Neurology*, *4*(9), 663–679. https://doi.org/10.1002/acn3.445

Gunning-Dixon, F. M., Brickman, A. M., Cheng, J. C., & Alexopoulos, G. S. (2009). Aging of Cerebral White Matter: A Review of MRI Findings. *International Journal of Geriatric Psychiatry*, *24*(2), 109–117. https://doi.org/10.1002/gps.2087

Harms, R. L., Fritz, F. J., Tobisch, A., Goebel, R., & Roebroeck, A. (2017). Robust and fast nonlinear optimization of diffusion MRI microstructure models. *NeuroImage*, *155*, 82–96. https://doi.org/10.1016/j.neuroimage.2017.04.064

Home—GraphPad. (n.d.). Retrieved November 19, 2019, from https://www.graphpad.com/

Hsu, J.-L., Leemans, A., Bai, C.-H., Lee, C.-H., Tsai, Y.-F., Chiu, H.-C., & Chen, W.-H. (2008). Gender differences and age-related white matter changes of the human brain: A diffusion tensor imaging study. *NeuroImage*, *39*(2), 566–577. https://doi.org/10.1016/j.neuroimage.2007.09.017

Hua, K., Zhang, J., Wakana, S., Jiang, H., Li, X., Reich, D. S., Calabresi, P. A., Pekar, J. J., van Zijl, P. C. M., & Mori, S. (2008). Tract probability maps in stereotaxic spaces: Analyses of white matter anatomy and tract-specific quantification. *NeuroImage*, *39*(1), 336–347. https://doi.org/10.1016/j.neuroimage.2007.07.053

Huffman, D. J., & Stark, C. E. L. (2014). Multivariate pattern analysis of the human medial temporal lobe revealed representationally categorical cortex and representationally agnostic hippocampus. *Hippocampus*, *24*(11), 1394–1403. https://doi.org/10.1002/hipo.22321

Insausti, R., Juottonen, K., Soininen, H., Insausti, A. M., Partanen, K., Vainio, P., Laakso, M. P., & Pitkanen, A. (1998). MR volumetric analysis of the human entorhinal, perirhinal, and temporopolar cortices. *AJNR.American Journal of Neuroradiology*, *19*(4), 659–671.

Jack, C. R., Petersen, R. C., Xu, Y., O'Brien, P. C., Smith, G. E., Ivnik, R. J., Tangalos, E. G., & Kokmen, R. (1998). The rate of medial temporal lobe atrophy in typical aging and Alzheimer's disease. *Neurology*, *51*, 993–999.

Jelescu, I. O., Veraart, J., Adisetiyo, V., Milla, S. S., Novikov, D. S., & Fieremans, E. (2015). One diffusion acquisition and different white matter models: How does microstructure change in human early development based on WMTI and NODDI? *NeuroImage*, *107*, 242–256. https://doi.org/10.1016/j.neuroimage.2014.12.009

Jeurissen, B., Leemans, A., Tournier, J.-D., Jones, D. K., & Sijbers, J. (2013). Investigating the prevalence of complex fiber configurations in white matter tissue with diffusion magnetic resonance imaging. *Human Brain Mapping*, *34*(11), 2747–2766. https://doi.org/10.1002/hbm.22099

Johnson, M. K. (1997). *Source monitoring and memory distortion*. Philosophical Transactions of the Royal Society of London Series B-Biological Sciences.

Jones, E., Oliphant, T., & Peterson, P. (2001). *SciPy: Open Source Scientific Tools for Python*. SciPy.Org. https://www.scipy.org

Kantarci, K. (2014). Fractional Anisotropy of the Fornix and Hippocampal Atrophy in Alzheimer's Disease. *Frontiers in Aging Neuroscience*, *6*. https://doi.org/10.3389/fnagi.2014.00316

Kantarci, K., Weigand, S. D., Przybelski, S. A., Preboske, G. M., Pankratz, V. S., Vemuri, P., Senjem, M. L., Murphy, M. C., Gunter, J. L., Machulda, M. M., Ivnik, R. J., Roberts, R. O., Boeve, B. F., Rocca, W. A., Knopman, D. S., Petersen, R. C., & Jack, C. J. (2013). MRI and MRS predictors of mild cognitive impairment in a population-based sample. *Neurology*, *81*, 126–133. https://doi.org/10.1212/WNL.0b013e31829a3329

Kellner, E., Dhital, B., Kiselev, V. G., & Reisert, M. (2016). Gibbs-ringing artifact removal based on local subvoxel-shifts: Gibbs-Ringing Artifact Removal. *Magnetic Resonance in Medicine*, *76*(5), 1574–1581. https://doi.org/10.1002/mrm.26054

King, M. D., Houseman, J., Roussel, S. A., van Bruggen, N., Williams, S. R., & Gadian, D. G. (1994). Q-Space imaging of the brain. *Magnetic Resonance in Medicine*, *32*(6), 707–713.

Kirwan, C. B., & Stark, C. E. L. (2004). Medial temporal lobe activation during encoding and retrieval of novel face-name pairs. *Hippocampus*, *14*, 910–930.

Kochunov, P., Williamson, D. E., Lancaster, J., Fox, P., Cornell, J., Blangero, J., & Glahn, D. (2012). Fractional anisotropy of water diffusion in cerebral white matter across the lifespan. *Neurobiology of Aging*, *33*(1), 9–20. https://doi.org/10.1016/j.neurobiolaging.2010.01.014

Kövari Enikö, Gold Gabriel, Herrmann François R., Canuto Alessandra, Hof Patrick R., Michel Jean-Pierre, Bouras Constantin, & Giannakopoulos Panteleimon. (2004). Cortical Microinfarcts and Demyelination Significantly Affect Cognition in Brain Aging. *Stroke*, *35*(2), 410–414. https://doi.org/10.1161/01.STR.0000110791.51378.4E

Kunz, N., Zhang, H., Vasung, L., O'Brien, K. R., Assaf, Y., Lazeyras, F., Alexander, D. C., & Hüppi, P. S. (2014). Assessing white matter microstructure of the newborn with multi-shell diffusion MRI and biophysical compartment models. *NeuroImage*, *96*, 288–299. https://doi.org/10.1016/j.neuroimage.2014.03.057

Madden, D. J., Bennett, I. J., Burzynska, A., Potter, G. G., Chen, N. K., & Song, A. W. (2012). Diffusion tensor imaging of cerebral white matter integrity in cognitive aging. *Biochim Biophys Acta*, *1822*, 386–400. https://doi.org/10.1016/j.bbadis.2011.08.003

Metzler-Baddeley, C., Jones, D. K., Belaroussi, B., Aggleton, J. P., & O'Sullivan, M. J. (2011). Frontotemporal connections in episodic memory and aging: A diffusion MRI tractography study. *The Journal of Neuroscience: The Official Journal of the Society for Neuroscience*, *31*(37), 13236–13245. https://doi.org/10.1523/JNEUROSCI.2317-11.2011

Metzler-Baddeley, C., O'Sullivan, M. J., Bells, S., Pasternak, O., & Jones, D. K. (2012). How and how not to correct for CSF-contamination in diffusion MRI. *NeuroImage*, *59*(2), 1394–1403. https://doi.org/10.1016/j.neuroimage.2011.08.043

Mito, R., Raffelt, D., Dhollander, T., Vaughan, D. N., Tournier, J.-D., Salvado, O., Brodtmann, A., Rowe, C. C., Villemagne, V. L., & Connelly, A. (2018). Fibre-specific white matter reductions in Alzheimer's disease and mild cognitive impairment. *Brain*, *141*(3), 888–902. https://doi.org/10.1093/brain/awx355

Mori, S. (2007). *Introduction to Diffusion Tensor Imaging*. Elsevier Science.

Morrison, J. H., & Baxter, M. G. (2012). The ageing cortical synapse: Hallmarks and implications for cognitive decline. *Nature Reviews Neuroscience*, *13*, 240–250.

Naranjo, N., & Greene, E. (1977). Use of reduced silver staining to show loss of connections in aged rat brain. *Brain Research Bulletin*, *2*, 71–74.

Nazeri, A., Chakravarty, M. M., Rotenberg, D. J., Rajji, T. K., Rathi, Y., Michailovich, O. V., & Voineskos, A. N. (2015). Functional consequences of neurite orientation dispersion and density in humans across the adult lifespan. *The Journal of Neuroscience: The Official Journal of the Society for Neuroscience*, *35*(4), 1753–1762. https://doi.org/10.1523/JNEUROSCI.3979-14.2015

Nichols, T. E., & Holmes, A. P. (2002). Nonparametric permutation tests for functional neuroimaging: A primer with examples. *Human Brain Mapping*, *15*(1), 1–25.

Ofori, E., Pasternak, O., Planetta, P. J., Burciu, R., Snyder, A., Febo, M., Golde, T. E., Okun, M. S., & Vaillancourt, D. E. (2015). Increased free-water in the substantia nigra of Parkinson's disease: A single-site and multi-site study. *Neurobiology of Aging*, *36*(2), 1097–1104. https://doi.org/10.1016/j.neurobiolaging.2014.10.029

Pannek, K., Fripp, J., George, J. M., Fiori, S., Colditz, P. B., Boyd, R. N., & Rose, S. E. (2018). Fixel-based analysis reveals alterations is brain microstructure and macrostructure of preterm-born infants at term equivalent age. *NeuroImage: Clinical*, *18*, 51–59. https://doi.org/10.1016/j.nicl.2018.01.003

Pasternak, O., Sochen, N., Gur, Y., Intrator, N., & Assaf, Y. (2009). Free water elimination and mapping from diffusion MRI. *Magnetic Resonance in Medicine*, *62*(3), 717–730. https://doi.org/10.1002/mrm.22055

Peters, A. (2002). The effects of normal aging on myelin and nerve fibers: A review. *Journal of Neurocytology*, *31*(8), 581–593. https://doi.org/10.1023/A:1025731309829

Peters, A., Sethares, C., & Moss, M. B. (2010). How the primate fornix is affected by age. *The Journal of Comparative Neurology*, *518*(19), 3962–3980. https://doi.org/10.1002/cne.22434

Petralia, R. S., Mattson, M. P., & Yao, P. J. (2014). Communication Breakdown: The Impact of Ageing on Synapse Structure. *Ageing Research Reviews*, *14*, 31–42. https://doi.org/10.1016/j.arr.2014.01.003

PROCESS macro for SPSS and SAS. (n.d.). The PROCESS Macro for SPSS and SAS. Retrieved November 6, 2019, from http://processmacro.org/

Raffelt, D. A., Smith, R. E., Ridgway, G. R., Tournier, J.-D., Vaughan, D. N., Rose, S., Henderson, R., & Connelly, A. (2015). Connectivity-based fixel enhancement: Whole-brain statistical analysis of diffusion MRI measures in the presence of crossing fibres. *NeuroImage*, *117*, 40–55. https://doi.org/10.1016/j.neuroimage.2015.05.039

Raffelt, D. A., Tournier, J.-D., Smith, R. E., Vaughan, D. N., Jackson, G., Ridgway, G. R., & Connelly, A. (2017). Investigating white matter fibre density and morphology using fixel-based analysis. *NeuroImage*, *144*, 58–73. https://doi.org/10.1016/j.neuroimage.2016.09.029

Raffelt, D., Tournier, J.-D., Fripp, J., Crozier, S., Connelly, A., & Salvado, O. (2011). Symmetric diffeomorphic registration of fibre orientation distributions. *NeuroImage*, *56*(3), 1171–1180. https://doi.org/10.1016/j.neuroimage.2011.02.014

Raffelt, D., Tournier, J.-D., Rose, S., Ridgway, G. R., Henderson, R., Crozier, S., Salvado, O., & Connelly, A. (2012). Apparent Fibre Density: A novel measure for the analysis of diffusion-weighted magnetic resonance images. *NeuroImage*, *59*(4), 3976–3994. https://doi.org/10.1016/j.neuroimage.2011.10.045

Raz, N., Lindenberger, U., Rodrigue, K. M., Kennedy, K. M., Head, D., Williamson, A., Dahle, C., Gerstorf, D., & Acker, J. D. (2005). Regional brain changes in aging healthy adults: General trends, individual differences and modifiers. *Cerebral Cortex (New York, N.Y.: 1991)*, *15*(11), 1676–1689.

Rey, A. (1941). L'examen psychologique dans les cas d'encephalopathie traumatique. *Arch Psychol*, *28*, 286–340.

Salvadores, N., Sanhueza, M., Manque, P., & Court, F. A. (2017). Axonal Degeneration during Aging and Its Functional Role in Neurodegenerative Disorders. *Frontiers in Neuroscience*, *11*. https://doi.org/10.3389/fnins.2017.00451

Sampaio-Baptista, C., & Johansen-Berg, H. (2017). White Matter Plasticity in the Adult Brain. *Neuron*, *96*(6), 1239–1251. https://doi.org/10.1016/j.neuron.2017.11.026

Sato, K., Kerever, A., Kamagata, K., Tsuruta, K., Irie, R., Tagawa, K., Okazawa, H., Arikawa-Hirasawa, E., Nitta, N., Aoki, I., & Aoki, S. (2017). Understanding microstructure of the brain by comparison of neurite orientation dispersion and density imaging (NODDI) with transparent mouse brain. *Acta Radiologica Open*, *6*(4). https://doi.org/10.1177/2058460117703816

Schacter, D. L., Buckner, R. L., Koutstaal, W., Dale, A. M., & Rosen, B. R. (1997). Late onset of anterior prefrontal activity during true and false recognition: An event-related fMRI study. *NeuroImage*, *6*, 259–269.

Scheibel, M. E., Lindsay, R. D., Tomiyasu, U., & Scheibel, A. B. (1975). Progressive dendritic changes in aging human cortex. *Experimental Neurology*, *47*(3), 392–403. https://doi.org/10.1016/0014-4886(75)90072-2

Schilling, K. G., Janve, V., Gao, Y., Stepniewska, I., Landman, B. A., & Anderson, A. W. (2018). Histological validation of diffusion MRI fiber orientation distributions and dispersion. *NeuroImage*, *165*, 200–221. https://doi.org/10.1016/j.neuroimage.2017.10.046

Seabold, S., & Perktold, J. (2010). *Statsmodels: Econometric and Statistical Modeling with Python*. 5.

Sepehrband, F., Clark, K. A., Ullmann, J. F. P., Kurniawan, N. D., Leanage, G., Reutens, D. C., & Yang, Z. (2015). Brain tissue compartment density estimated using diffusion-weighted MRI yields tissue parameters consistent with histology. *Human Brain Mapping*, *36*(9), 3687–3702. https://doi.org/10.1002/hbm.22872

Sharaf, A., Krieglstein, K., & Spittau, B. (2013). Distribution of microglia in the postnatal murine nigrostriatal system. *Cell and Tissue Research*, *351*(3), 373–382. https://doi.org/10.1007/s00441-012-1537-y

Smith, R. E., Tournier, J.-D., Calamante, F., & Connelly, A. (2013). SIFT: Spherical-deconvolution informed filtering of tractograms. *NeuroImage*, *67*, 298–312. https://doi.org/10.1016/j.neuroimage.2012.11.049

Song, S.-K., Sun, S.-W., Ju, W.-K., Lin, S.-J., Cross, A. H., & Neufeld, A. H. (2003). Diffusion tensor imaging detects and differentiates axon and myelin degeneration in mouse optic nerve after retinal ischemia. *NeuroImage*, *20*(3), 1714–1722.

Stark, C. E. L., & Okado, Y. (2003). Making memories without trying: Medial temporal lobe activity associated with incidental memory formation during recognition. *The Journal of Neuroscience*, *23*, 6748–6753.

Stark, S. M., & Stark, C. E. L. (2017a). The Aging Hippocampus: Linking Animal and Human Research. In *Cognitive Neuroscience of Aging* (2nd ed., pp. 273–300). Oxford University Press.

Stark, S. M., & Stark, C. E. L. (2017b). Age-related deficits in the mnemonic similarity task for objects and scenes. *Behavioural Brain Research*, *333*, 109–117. https://doi.org/10.1016/j.bbr.2017.06.049

Takahashi, M., Ono, J., Harada, K., Maeda, M., & Hackney, D. B. (2000). Diffusional Anisotropy in Cranial Nerves with Maturation: Quantitative Evaluation with Diffusion MR Imaging in Rats. *Radiology*, *216*(3), 881–885. https://doi.org/10.1148/radiology.216.3.r00se41881

Tournier, J.-D., Calamante, F., Gadian, D. G., & Connelly, A. (2004). Direct estimation of the fiber orientation density function from diffusion-weighted MRI data using spherical deconvolution. *NeuroImage*, *23*(3), 1176–1185. https://doi.org/10.1016/j.neuroimage.2004.07.037

Tuch, D. S. (2004). Q-ball imaging. *Magnetic Resonance in Medicine*, *52*(6), 1358–1372. https://doi.org/10.1002/mrm.20279

Tustison, N. J., Cook, P. A., Klein, A., Song, G., Das, S. R., Duda, J. T., Kandel, B. M., van Strien, N., Stone, J. R., Gee, J. C., & Avants, B. B. (2014). Large-scale evaluation of ANTs and FreeSurfer cortical thickness measurements. *Neuroimage*, *99*, 166–179. https://doi.org/10.1016/j.neuroimage.2014.05.044

Venkatesh, A., Stark, S. M., Stark, C. E. L., & Bennett, I. J. (2020). Age- and memory- related differences in hippocampal gray matter integrity are better captured by NODDI compared to single-tensor diffusion imaging. *Neurobiology of Aging*, *96*, 12–21. https://doi.org/10.1016/j.neurobiolaging.2020.08.004

Veraart, J., Fieremans, E., & Novikov, D. S. (2016). Diffusion MRI noise mapping using random matrix theory: Diffusion MRI Noise Mapping. *Magnetic Resonance in Medicine*, *76*(5), 1582–1593. https://doi.org/10.1002/mrm.26059

Wakana, S., Caprihan, A., Panzenboeck, M. M., Fallon, J. H., Perry, M., Gollub, R. L., Hua, K., Zhang, J., Jiang, H., Dubey, P., Blitz, A., van Zijl, P., & Mori, S. (2007). Reproducibility of quantitative tractography methods applied to cerebral white matter. *NeuroImage*, *36*(3), 630–644. https://doi.org/10.1016/j.neuroimage.2007.02.049

Wang, Y., Wang, Q., Haldar, J. P., Yeh, F.-C., Xie, M., Sun, P., Tu, T.-W., Trinkaus, K., Klein, R. S., Cross, A. H., & Song, S.-K. (2011). Quantification of increased cellularity during inflammatory demyelination. *Brain: A Journal of Neurology*, *134*(Pt 12), 3590–3601. https://doi.org/10.1093/brain/awr307

Wen, Q., Kelley, D. A. C., Banerjee, S., Lupo, J. M., Chang, S. M., Xu, D., Hess, C. P., & Nelson, S. J. (2015). Clinically feasible NODDI characterization of glioma using multiband EPI at 7 T. *NeuroImage : Clinical*, *9*, 291–299. https://doi.org/10.1016/j.nicl.2015.08.017

Yassa, M. A., Muftuler, L. T., & Stark, C. E. L. (2010). Ultrahigh-resolution microstructural diffusion tensor imaging (msDTI) reveals perforant path degradation in aged humans in vivo. *Proc Natl Acad Sci U S A*, *107*, 12687–12691.

Yesavage, J. A., Brink, T. L., Rose, T. L., Lum, O., Huang, V., Adey, M., & Leirer, V. O. (1982). Development and validation of a geriatric depression screening scale: A preliminary report. *Journal of Psychiatric Research*, *17*(1), 37–49.

Yushkevich, P. A., Wang, H., Pluta, J., Das, S. R., Craige, C., Avants, B. B., Weiner, M. W., & Mueller, S. (2010). Nearly Automatic Segmentation of Hippocampal Subfields in In Vivo Focal T2-Weighted MRI. *NeuroImage*, *53*(4), 1208–1224. https://doi.org/10.1016/j.neuroimage.2010.06.040

Zhang, H., Schneider, T., Wheeler-Kingshott, C. A., & Alexander, D. C. (2012). NODDI: Practical in vivo neurite orientation dispersion and density imaging of the human brain. *NeuroImage*, *61*(4), 1000–1016. https://doi.org/10.1016/j.neuroimage.2012.03.072

Higher-order diffusion measures complement tensor metrics and volume in gray matter when predicting age and cognition.

In Chapter 2, we established that NODDI metrics were indeed sensitive to aging-related changes in hippocampal microstructure and could inform cognitive consequences. However, the multi-shell sequences required to derive these diffusion metrics can double or triple the scan time depending on the number of shells added, and the value of these metrics over traditional tensor metrics in gray matter has not yet been adequately examined. Moreover, the study described in the previous chapter involved a modest sample size, and we were not sure whether these results would translate to larger populations. In this chapter, we first replicated the previous study with a larger sample size (about 3x) and demonstrate that NODDI metrics are robust and reliable across studies. We then investigated how these subfield-specific NODDI metrics compared to more traditional metrics like tensor metrics and volume, in predicting age and memory ability- and discovered that combining the NODDI and tensor measures significantly improved the predictive power of our logistic models! We use these results to encourage neuroimaging data collection efforts to include a multi-shell diffusion MRI sequence in their protocols, as these metrics may be able to capture microstructural variance that might be missed by

traditional approaches, even in gray matter studies. These results provide a comprehensive insight into the advantage of NODDI metrics in studying gray matter microstructure and may even be extended to fields beyond cognitive aging.

NB: A version of this chapter is currently under review at Neuroimage.

3.1 INTRODUCTION

Magnetic Resonance Imaging (MRI) studies have been very valuable in non-invasively detecting structural changes associated with behavior, cognition, function, and pathology. While there are a range of MRI techniques that can capture different types of information, acquisition time is always at a premium in any study. It is challenging to determine which acquisition protocols to include in a study while finding the best balance between scan time and information received. Structural Magnetic Resonance Imaging (sMRI) techniques like T1-weighted, T2-weighted, and Fluid Attenuated Inversion Recovery (FLAIR) imaging have been crucial in understanding the anatomical alterations that the brain experiences, both in research and clinical contexts (Brans et al., 2010; Dekaban & Sadowsky, 1978; Hedman et al., 2011; Ho et al., 1980; Jernigan et al., 2001; Morrison & Hof, 1997; Peter R., 1979; Raz et al., 2004; Taki et al., 2011; van Haren et al., 2008). For example, being able to trace the outline and subsequently calculate the volume of the hippocampus using T1-weighted images has been extremely valuable when studying diseases like Alzheimer's (Fox & Freeborough, 1997). However, while these techniques can detect useful macrostructural properties like regional volume and cortical thickness,

dramatic changes like gross atrophy or cortical thinning likely follow a myriad of more subtle microstructural changes that cannot be detected by standard T1- and T2-weighted imaging and their analogs (Jack et al., 2018). Cytoarchitectural properties like dendritic complexity, glial density, and cellular characteristics may be more reflective of individual differences in cognitive and pathological identities. Observing these microstructural characteristics in the brain non-invasively had been a major challenge to the field until recent advances in MRI technology.

Diffusion-weighted imaging (DWI) (Stejskal & Tanner, 1965) is increasingly becoming a key solution to this problem, given its ability to provide a range of quantitative measures describing neural microstructure within only minutes of acquisition (Johansen-Berg & Behrens, 2014). Until recently, DWI was almost exclusively associated with the characterization of white matter. Diffusion tensor metrics and tractography revealed how important features like axonal integrity, myelination, and specific structural connections change through healthy and pathological conditions and how they influence cognitive performance and other behavior (Assaf & Pasternak, 2008; Sasson et al., 2010; Thomason & Thompson, 2011). Given this, diffusion imaging has been considered a general microstructural probe as the geometry, organization, and morphology of any tissue type influences the diffusion signal. More recently, studies have been conducted using diffusion metrics to investigate gray matter microstructure (Aggarwal et al., 2015; Assaf, 2019; Budde & Annese, 2013; Colgan et al., 2016; Radhakrishnan et al., 2020; Venkatesh et al., 2020). However, the ratio of current publications that use diffusion MRI to study white mater vs gray matter is a striking 5:1, perhaps because early modeling algorithms

67

could not accommodate the cytoarchitectural complexity of gray matter, and DWI used to provide poor image resolution in gray matter sub-structures (Assaf, 2019; Nazeri et al., 2020). Recent advances in both diffusion image acquisition and analysis techniques may be able to resolve some of these issues (Frank, 2001; D. K. Jones, 2004; Papadakis et al., 1999).

A promising acquisition technique has been multi-shell DWI, which acquires scans at multiple gradient strengths (b-values). These images can then be analyzed using biophysically plausible models like Neurite Orientation Dispersion and Density Imaging (NODDI) (Zhang et al., 2012), which yield microstructural metrics that correspond to "intracellular", "extracellular" and free water sources of the diffusion signal across tissue types. While NODDI may be well-suited to characterize the cytoarchitectural properties of gray matter, it has been seldom utilized to do so, especially in large-scale studies which usually only collect single-shelled diffusion data, and any multi-shelled data is collected in a much smaller sample size (Beekly et al., 2004; Petersen et al., 2010). This is mainly because increasing the number of shells can double or triple scan time (depending on the number of shells added), which can be a valuable commodity, especially when studying sensitive populations. The counterargument for including additional DWI shells may be strengthened if their advantage in deciphering gray matter microstructure can be documented, as proposed here.

In this study, we asked whether metrics derived from multi-shell diffusion protocols provide enough additional information over traditional tensor and volume metrics to justify the added acquisition time. To simplify this question and directly determine the

value of NODDI metrics over other metrics in a test case, we observed the effect of aging in the hippocampal subfields, and the relationship of this phenomenon with two popular hippocampal-dependent memory tasks. We first reproduced prior results from our lab and others (Radhakrishnan et al., 2020; Venkatesh et al., 2020) in a larger study population showing that NODDI metrics are sensitive to aging-related microstructural differences in hippocampal subfields and that differences in these NODDI metrics may be associated with cognitive decline. Our central question beyond this replication was how the hippocampal NODDI metrics compare to traditional tensor metrics and volume when predicting age or cognitive performance. We found that NODDI metrics do indeed complement both tensor metrics and volume, even while exclusively examining gray matter, and including the NODDI metrics greatly improves the predictive power of our models in estimating both age as well as cognition. We use these results to urge neuroimaging data collection consortiums to include multi-shell diffusion sequences in their protocol as these metrics may be able to capture microstructural variance not captured by conventional methods.

3.2 METHODS

3.2.1 Participants

Participants were recruited from the University of California, Riverside and surrounding communities. Before enrollment, participants were screened for neurological conditions (e.g., depression, stroke, etc.) and scanner-related contraindications (e.g., claustrophobia, pregnancy, etc.). After scanning, sixteen of the 170 participants were excluded based on data segmentation issues and/or registration artefacts. The final

sample consisted of 79 younger adults (20.41 ± 1.89 years, 46 females) and 75 older adults (73.56 ± 6.26 years, 45 females) (Table 3.1). All participants provided informed consent before participation in this study and were compensated for their time. All experimental procedures were approved by the University of California, Riverside Review Board.

3.2.2 Cognitive testing

All participants completed a battery of neuropsychological tests to evaluate their cognitive abilities. We assessed participants' memory using the Rey Auditory Verbal Learning Test (RAVLT) (Rey, 1941) and the two-choice Mnemonic Similarity Test (MST) (Kirwan & Stark, 2007; Stark et al., 2013, 2019). The RAVLT has three components: 5 presentations of the same 15-word list with immediate recall, a second immediate recall test following an interference list of 15 new words, and a final delayed recall of the initial list after 15 minutes. The RAVLT Delay score reflects the final recall score, on a scale of 0 to 15.

The MST is a modified recognition memory task that was designed to tax "pattern separation" processes in an explicit attempt to rely on hippocampal processing and its link to the hippocampus has been validated in a wide range of domains (see Stark et al., 2019 for review). In the MST, participants viewed 128 images of everyday objects during an incidental encoding phase. During the test phase, participants were shown repeated images, novel foils, and items that were similar to, but not the same as studied images. On each trial, participants had to judge them as either "old" (repeated targets) or "new" (novel foils and similar lures) using a two-choice button press. A lure discrimination index (LDI) was calculated using signal detection theory as the discrimination d' between repeated targets and similar lures (Kirwan & Stark, 2007; Stark et al., 2015). A traditional

recognition measure was calculated as the *d'* between repeated targets and novel foils. Participants who had >20% omitted trials or an extremely poor recognition score (greater than 2.5 standard deviations from the mean [REC < 0.5]) were excluded. The final sample size for the MST analyses was 78 younger adults (20.41 ± 1.89 years, 46 females) and 69 older adults (74.04 ± 6.35 years, 35 females).

	Young	Old
N	79	75
Age*	20.41 ± 1.89	73.56 ± 6.26
Female (%)	58.2%	60%
Education	13.98 ± 2.26	14.56 ± 2.30
RAVLT Immediate*	11.29 ± 2.50	8.30 ± 3.02
RAVLT Delay*	10.68 ± 3.00	7.67 ± 3.40
MST LDI*	0.83 ± 0.50	1.12 ± 0.57
MST REC	2.67 ± 0.94	2.97 ± 0.72

Table 3.1: Demographics and cognitive test scores. *Rows in blue indicate p<0.05 in a t-test between young and old groups.

3.2.3 MR Image Acquisition

The participants were scanned using a Siemens Prisma 3T MRI scanner (Siemens Healthineers, Malvern, PA), fitted with a 32-channel receive-only head coil. Fitted padding was used to minimize head movements.

T1W: A T1-weighted magnetization-prepared rapid gradient echo (MP-RAGE) scan was acquired with the following parameters: echo time (TE)/repetition time (TR) = 2.72/2400 ms, 208 axial slices, GRAPPA acceleration factor = 2, and in 0.8mm isotropic resolution.

DWI: Axial diffusion-weighted echo-planar images were acquired in both anterior-posterior and posterior-anterior phase encodings with b = 1500 s/mm^2 and b = 3000 s/mm^2 applied in 64 orthogonal directions each with the following parameters: TE/TR = 102/3500 ms, FOV = 212 x 182 mm, 64 axial slices, multi-band acceleration factor = 4 and in 1.7 mm isotropic resolution. Twelve images with no diffusion weighting (b = 0; half in each encoding direction) were also collected.

3.2.4 Diffusion data preprocessing

All preprocessing steps employed MRtrix3 (Tournier et al., 2012) (www.mrtrix.org) commands or used Mrtrix3 scripts that linked external software packages. Physiological noise arising from thermal motion of water molecules in the brain was first removed (Veraart et al., 2016), followed by removal of Gibbs ringing artifacts (Kellner et al., 2016), eddy current correction (Andersson & Sotiropoulos, 2016), motion correction (Andersson et al., 2003), susceptibility-induced distortion correction (Skare & Bammer, 2009) and bias field correction (Tustison et al., 2014). The image intensity was then normalized across subjects in the log-domain (Raffelt et al., 2012). Images with no diffusion weighting (b=0) were extracted and averaged to aid with structural registration.

3.2.5 Structural data processing

Each participant's structural image was nonlinearly co-registered to the average of their respective preprocessed b0 images using the ANTS Registration SyN algorithm with a b-spline transform (Avants et al., 2008; Tustison and Avants, 2013). Registration was manually checked to ensure accuracy, and DWI-registered T1w images were used for the rest of the analyses. The T1-weighted images were then processed using FMRIPREP

version 20.2.1 (Esteban et al., 2018; Gorgolewski et al., 2011). Each volume was corrected for intensity non-uniformity using N4 Bias Field Correction from Advanced Normalization Tools (ANTS v2.3.4) (Tustison et al., 2010). The images were then skull stripped using the OASIS template. Brain surfaces were reconstructed using recon-all from FreeSurfer v7 (Dale et al., 1999) and the brain mask estimated previously was refined with a custom variation of the method to reconcile ANTs-derived and FreeSurfer-derived segmentations of the cortical gray-matter of Mindboggle (Klein et al., 2017). The hippocampus was previously hand-segmented on a template image into 3 subregions: a combined dentate gyrus and CA3 (combined due to resolution constraints; DG/CA3), CA1, and subiculum, based on our previous work (Stark and Stark, 2017). As the hippocampal atlas was in template space, spatial normalization to the ICBM 152 Nonlinear Asymmetrical template version 2009c (Fonov et al., 2009) was performed through nonlinear registration with ANTs, using brain-extracted versions of both T1w volume and template and using ANTs MultiLabel resampling technique. Regional volume was calculated by transforming the masks back to subject space and calculating the number of voxels encompassing each subfield multiplied with the image resolution. Brain tissue segmentation of cerebrospinal fluid (CSF), white-matter (WM), and gray-matter (GM) was performed on the brain-extracted T1w using FAST from FSL v6.0.

3.2.6 Deriving diffusion metrics

We calculated traditional tensor metrics using MRtrix3 with data from all shells. Although there are concerns about estimating tensor metrics from multi-shell data due to diffusion being non-Gaussian at high b values, the increased number of averages and diffusion

directions used here attenuates these fit issues. A weighted least squares (WLS) approach was first used to fit the diffusion tensor to the log signal, using weights based on empirical signal intensities (Basser et al., 1994). We repeated the weighted least squares with weights determined by the signal predictions from the previous step (Veraart et al., 2013). We then generated maps of the following tensor-derived parameters: the mean apparent diffusion coefficient (ADC, sometimes also referred to as Mean Diffusivity or MD), fractional anisotropy (FA), axial diffusivity (AD, same as principal eigen value) and radial diffusivity (RD, equal to mean of the two non-principal eigen values) (Westin, 1997).

While these traditional tensor metrics are widely used, they were not originally designed to capture the complex cytoarchitectural properties of gray matter. Hence, we derived higher-order multi-compartment metrics using the Neurite Orientation Dispersion and Density Imaging (NODDI) (Zhang et al., 2012) model in the Microstructure Diffusion Toolbox (Harms et al., 2017). NODDI's metrics are tissue type agnostic and can readily be used in gray matter as it characterizes diffusion within each voxel as a combination of intracellular, extracellular, and CSF-based components. Here, we focus on three NODDI-derived parameters: the neurite density index (NDI), the orientation dispersion index (ODI), and the fractional isotropy (FISO). The NDI measures intracellular volume fraction and is calculated as the proportion of the voxel expressing unhindered diffusion along a given set of sticks, and restricted diffusion perpendicular to the same set of sticks. The ODI is a measure of tortuosity coupling an intracellular and extracellular space and models the extracellular space as hindered, gaussian anisotropic diffusion (very similar to, and hence highly correlated with, the tensor-derived FA). The amount of isotropic free

volume within a voxel is measured by FISO and is usually proportional to the amount of CSF in a voxel. The intrinsic diffusivity was set to 1.7 μm² ms⁻¹. Note that if this intrinsic diffusivity values is suboptimal for gray matter as suggested by some prior work (Guerrero et al., 2019), it would be expected to overestimate absolute NDI values but have minimal effect of the age group differences of interest. Because there was no significant age group difference in the number of voxels that may have insufficient signal to accurately estimate the NODDI metrics (i.e., voxels with NDI > 0.99; (Emmenegger et al., 2021), no thresholding was applied. The diffusion metrics in each of the hippocampal subfields were calculated by averaging the parameter maps using AFNI (Cox, 1996).

3.2.7 Statistical Analyses

All statistical analyses were performed in Python's Scipy (E. Jones et al., 2001) or GraphPad Prism 9.1.0. Group differences were computed using Student's two-tailed t-tests (Student, 1908). All regression analyses were simple linear regressions. Statistical p-values were corrected for multiple comparisons by calculating the false discovery rate (Benjamini et al., 2006), unless running tests with *a priori* hypotheses. Receiver operating characteristic (ROC) curves and their corresponding areas under the curve (AUC) were calculated using statsmodels (Seabold & Perktold, 2010).

3.3 RESULTS

We had previously shown in Chapter 2 that NDI of the DG/CA3 was increased in older adults, and was negatively associated with RAVLT Delay (n = 38) (Radhakrishnan et al., 2020). We first reproduced these results in a larger population before diving into more complex analyses.

3.3.1 NDI of all hippocampal subfields is increased in older adults

With this larger sample size, we found that the NDI of all the hippocampal subfields is greater in the older group as compared to the younger group (Two sample t-test. DG/CA3 : t = 5.30, p < 0.0001 ; CA1 : t = 4.32, p < 0.0001 ; Subiculum : t = 4.10, p<0.0001). Moreover, the NDI of the DG/CA3 and CA1 subfields increased with age within the older subpopulation alone (Linear regression. DG/CA3: R^2 = 0.09, p = 0.04; CA1: R^2 = 0.179, p = 0.002; Subiculum: R^2 = 0.025, p = 0.277). Because of the lack of variance in age in the younger population and the absence of middle-aged data, we could not perform correlations with age in just the young group or across the lifespan, in any meaningful way.

To determine whether these relationships had any sort of selectivity towards the hippocampal subfields and were not just a consequence of age-related global gray matter decline, we modelled the subfield-specific NDI linearly against the average whole brain gray matter NDI as described in our previous study. The residuals of this highly correlated model were quantified as the "globally regressed" NDI for each subfield. Post global-regression, we found that the older adults not only still had higher hippocampal NDI, the globally regressed NDI for older adults was largely positive, while that for the younger adults was largely negative: indicating that young adults tend to have a hippocampal NDI that is below the whole brain average, but as one grows older the hippocampal NDI relatively increases so much that it becomes well above the whole brain average, suggesting a focused NDI increase in the hippocampal subfields (Figure 3.1; Two sample t-test. DG/CA3 : t = 3.89, p = 0.0002 ; CA1 : t = 4.63, p < 0.0001 ; Subiculum : t = 4.28,

p<0.0001). The globally regressed NDI was also positively correlated with age within the older subpopulation in the DG/CA3 and CA1, but not in the subiculum. (Figure 3.1; Linear regression. DG/CA3: R^2 = 0.081, p = 0.019; CA1: R^2 = 0.132, p = 0.002; Subiculum: R^2 = 0.005, p = 0.847). To ensure that nothing about our sample was driving the observed effect and that any deviation from normality might be altering our results, we performed 1000 random samplings of 70% of our data. The resulting slopes were entirely consistent with our regression-based confidence intervals.

We found no differences between hemispheric metrics for all subfields. The NDI was greater in biologically male participants compared to biologically female participants for all subfields (Two sample t-test. DG/CA3: t = 2.04, p = 0.043; CA1: t = 2.036, p = 0.044; Subiculum: t = 3.74, p = 0.0003), but the previously described age effects remained significant after controlling for sex.
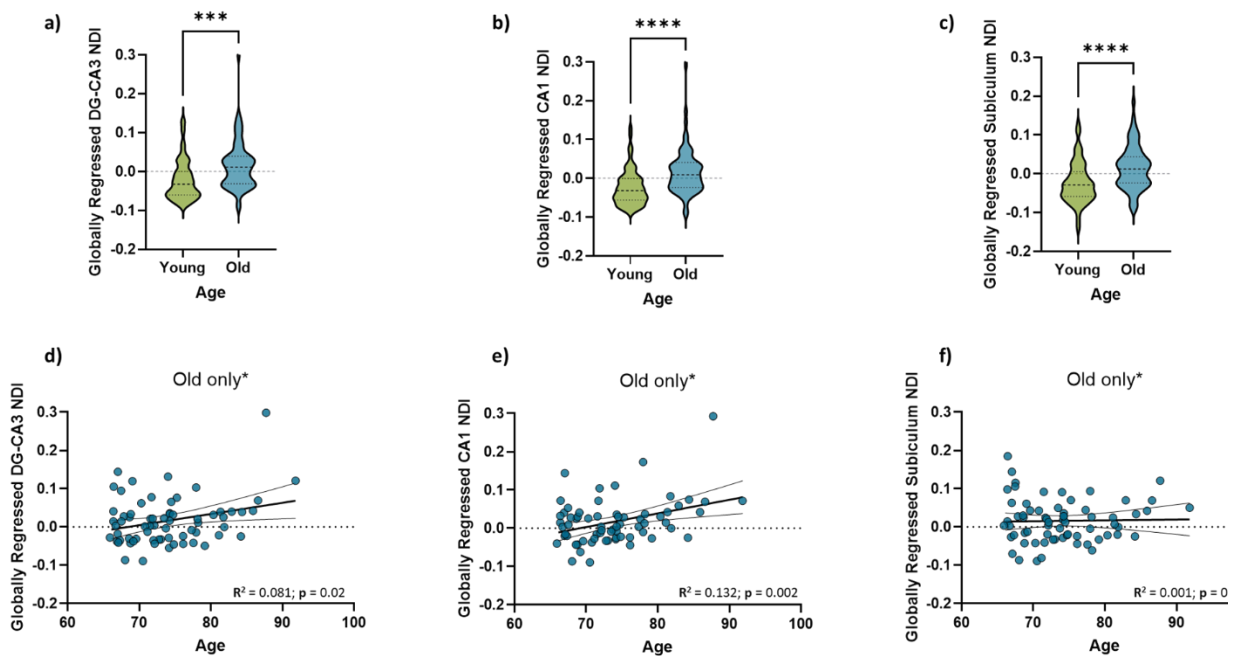
Figure 3.1: (a-c) Hippocampal NDI is significantly greater in older adults as compared to young adults- for all three hippocampal subfields. Moreover, the NDI of the DG/CA3 (d) and CA1 (e) linearly increases with age within the older subpopulation, while that of the subiculum (f) does not.

3.3.2 Hippocampal NDI is negatively associated with RAVLT Delay, and more weakly with the LDI

We were also able to replicate our previous finding that the hippocampal subfield NDI was negatively correlated with RAVLT performance, even after factoring in age as a regressor. While previously (Radhakrishnan et al., 2020), we observed reliable correlations in only the DG/CA3, here the NDI of all hippocampal subfields was negatively correlated with RAVLT delay, both before and after global regression, suggesting that this relationship in the hippocampus may not be a general brain-wide phenomenon (Figure 3.2). Within the older subpopulation, age was not significantly correlated with RAVLT Delay. However, the NDI of all hippocampal subfields still trended towards a negative relationship with the RAVLT delay in both the younger age group (Linear regression. DG/CA3: $R^2 = 0.059$, $p = 0.007$; CA1: $R^2 = 0.075$, $p = 0.001$; Subiculum: $R^2 = 0.143$, $p < 0.0001$) as well as the older age group (Linear regression. DG/CA3: $R^2 = 0.054$, $p = 0.05$; CA1: $R^2 = 0.080$, $p = 0.021$; Subiculum: $R^2 = 0.195$, $p = 0.0002$), with the subiculum NDI having the strongest relationship in both groups, suggesting that this relationship was beyond just an effect of age, and that hippocampal subfield NDI might be capable of capturing individual differences associated with cognition.

A more selective and weaker relationship was found between performance in the MST, as measured by the LDI, and the NDI of the hippocampal subfields. While the raw NDI of

78

both the DG/CA3 and subiculum were negatively associated with LDI (Linear regression. DG/CA3: R^2 = 0.030, p = 0.043; CA1: R^2 = 0.021, p = 0.087; Subiculum: R^2 = 0.1, p = 0.0002), this relationship was only weakly significant in the subiculum after global regression (Linear regression. DG/CA3: R^2 = 0.002, p = 0.557; CA1: R^2 = 0.007, p = 0.346; Subiculum: R^2 = 0.03, p = 0.0434). As in the previous analysis, we performed 1000 samplings of 70% of our data for both RAVLT delay and LDI, and all resulting slopes were consistent with our confidence intervals.
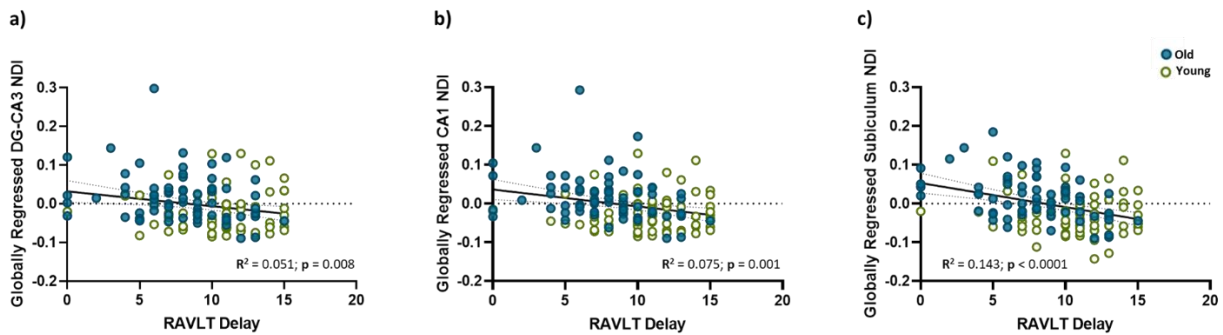
Figure 3.2: Globally regressed NDI is negatively associated with RAVLT Delay in all three hippocampal subfields, in both the younger and older groups, with the subiculum NDI having the strongest relationship with RAVLT performance. Green dots indicate the younger adults (18 – 29 years), while blue dots represent the older adults (65 – 92 years).

3.3.3 Tensor, NODDI and volumetric measures of hippocampal subfields can all successfully predict age group.

The results in sections 3.1 and 3.2 reproduce previously reported findings in a larger dataset and establish that the relationships between age, NDI and cognition are reliable and consistent. We next wanted to assess how NDI and other NODDI metrics compare to

tensor metrics and coarse volume in their relationships with age and cognition. Note that some hippocampal diffusion metrics like AD and ADC were not correlated with their global averages, so we used only *raw* diffusion metrics (not globally regressed) for the rest of the study to be consistent across metrics.

As an initial test, we sought to determine how well the various diffusion and volumetric measures from the hippocampus could classify participants into their age group. To do this, we used ROC curves to evaluate the performance of each metric in accurately distinguishing between young and old groups. We calculated the AUC for each measure, by passing in the metric for each subfield split by hemisphere (for a total of 6 input features) and fitting a logistic regression model to derive the ROC and consequently predict the age group. We used hemisphere-specific metrics instead of bilateral ones simply because they generated the greatest AUC for most metrics (Supplementary Table S3.5). Since the input features were highly collinear (Supplementary Figure S3.1), we used the newton conjugate gradient method (Buckley, 1978; Knoll & Keyes, 2004) for optimization to prevent a non-Hessian matrix error. To calculate the null distribution and estimate the p-value, we conducted a permutation analysis by randomly shuffling the old/young labels and estimating the AUC over 5000 iterations using the volumetric input features (since the null distributions would essentially remain equivalent across all metrics). We found that all metrics studied could successfully distinguish between young and old age groups well above chance with just the six inputs from that metric in each hippocampal subfield alone (Figure 3.4), with the ODI, volume and FA yielding the highest AUCs. Given the difference in age between the groups and considering that aging

causes very dramatic changes in the brain, it is unsurprising that all metrics, even volume, are sensitive to these changes.
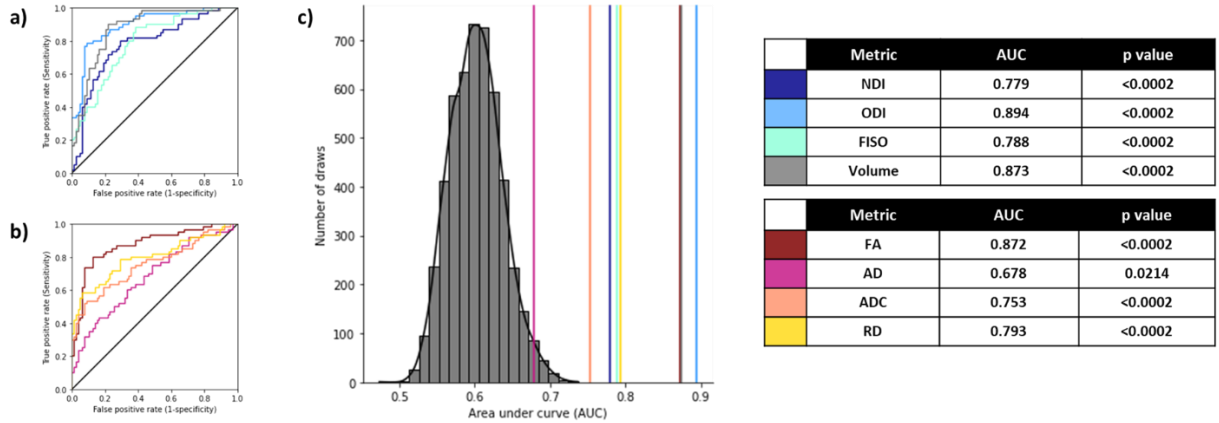
Figure 3.3: Using diffusion and structural metrics of the hippocampal subfields to predict age group. All metrics can successfully predict age group, with ODI, volume and FA being the best predictors and AD being the worst predictor (a-b). The histogram represents the null distribution (random permutation of old/young labels), and the colored lines represent the AUC of each of the metrics from all 6 subfields (c).

We then asked whether we could achieve higher prediction accuracy inputting a specific combination of these metrics, instead of a single metric from all subfields, and whether having the NODDI metrics posed any advantage over just the tensor metrics and volume in predicting age group. To answer this, we calculated the AUC for each combination of 6 input features from either a) a composite of tensor metrics and volume [$^{30}_6C$ = 593,775 combinations] b) NODDI metrics [$^{18}_6C$ = 18,564 combinations] or c) a composite of all metrics studied i.e., volume, tensor and NODDI metrics [$^{48}_6C$ = 12,271,512 combinations] (Figure 3.5 a-c). We found that the 99th percentile of the AUC distribution from permuting over just the NODDI metrics (0.90) was higher than that sampled from the tensor metrics and volume (0.77) or even from a combination of all metrics (0.86), suggesting that the NODDI metrics were providing highly valuable information for capturing aging-related microstructural differences by themselves. More specifically, the 99th percentile of the

tensor + volume distribution was equal to the 57.94^{th} percentile of the all metrics distribution, while the 99th percentile of the just NODDI distribution was equal to 99.88^{th} percentile of the all metrics distribution. To isolate this and understand it more completely, we then asked which individual features were most often contributing to the highest AUC values (top 1000) over all the combinations (Figure 3.5d). Within these best-performing combinations, we found that all NODDI (blues) and volume (grey) metrics occurred far more frequently in the input features than any of the tensor metrics (reds/yellow).

Note that the distributions were non-Gaussian when volume was included in the selection features, due to the lack of collinearity of volume with the other metrics while using the newton conjugate gradient optimization algorithm (see supplementary Figure S3.1).
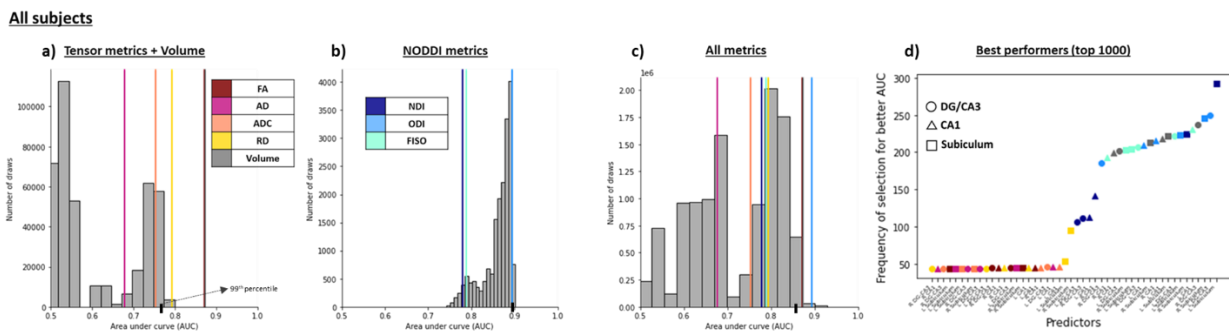
Figure 3.4: A combination of NODDI metrics results in the highest AUC peaks, compared to just the tensor metrics and volume or all the metrics combined. Histograms represent the AUCs generated following and exhaustive n-choose-6 analysis to determine how well various combinations of 6 Region x Metric regressors could model age group. (a) Analysis of only the traditional tensor and volume metrics; (b) Analysis of only the NODDI metrics; and (c) Analysis of all metrics combined. The colored lines represent the AUCs of each metric from all 6 subfields. (d) Plot of the frequency of selection of a given Region x Metric combination in the top 1000 AUCs in the All metrics analysis. Here, NODDI metrics and volume also showed up the most frequently across subfields as input features contributing to the highest AUCs.

3.3.4 A combination of NODDI, tensor metrics and volume predict RAVLT performance better than any of them alone.

We then repeated the same analysis as the previous section, this time for predicting RAVLT delay. We binarized the RAVLT score at a threshold of 9, such that all those who scored higher than 9 were considered "high performing", and those who scored 9 or below were considered "low performing", consistent with previous findings for these age groups (Stark et al., 2010, 2013). Binarizing the RAVLT in this way also helped reduce noise that might arise from screener differences or individual participants having "off" days (it is more likely that a binarized RAVLT score would remain consistent over multiple testing days, compared to the continuous score, speaking to its robustness). Note, even though classified as "low performing", none of these individuals were clinically diagnosed as cognitively impaired. While calculating the AUC for predicting high/low RAVLT delay this way in *the entire subpopulation*, using each metric from all 6 subfield features, we found that all metrics except FISO and AD performed well above chance, with ODI having the largest AUC, followed by RD, FA, and NDI [Figure 3.6].

Metric	AUC	p value
NDI	0.707	0.002
ODI	0.744	<0.0002
FISO	0.645	0.110
Volume	0.659	0.048

Metric	AUC	p value
FA	0.713	0.001
AD	0.614	0.341
ADC	0.701	0.002
RD	0.720	0.0006
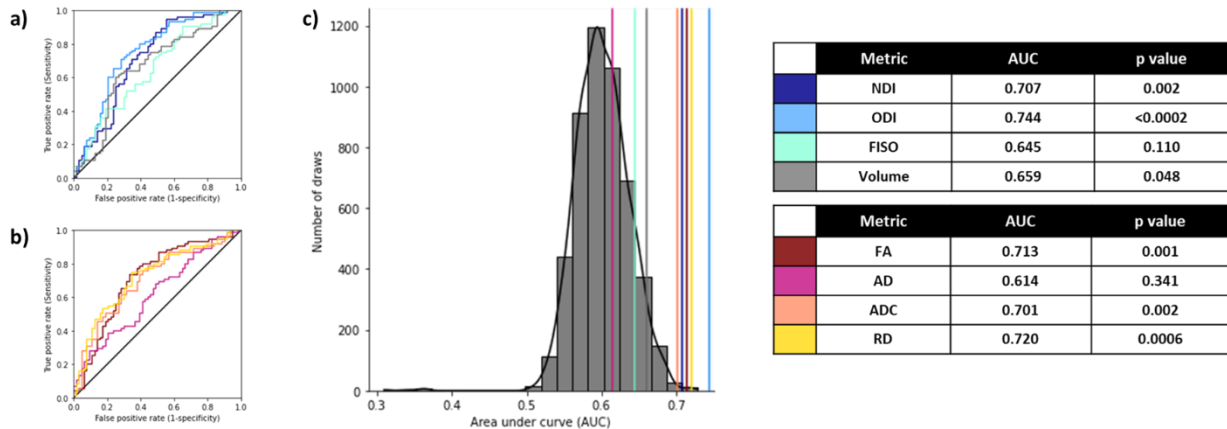
Figure 3.5: Using diffusion and structural metrics of the hippocampal subfields to *predict RAVLT performance (<9)*. Except FISO and AD, all metrics can successfully predict RAVLT status as well- with ODI being the best

predictor. The histogram (c) represents the null distribution (randomly permuting the high/low RAVLT labels), and the colored lines represent the AUC of each of the metrics from all 6 subfields.

We next performed the same $^{48}_{6}C$ analysis of all possible combinations of metrics. Notably, when examining AUCs resulting from combinations of only NODDI metrics and AUCs resulting from only tensor+volume metrics, we observed similar distributions with AUCs at the 99th percentile of 0.78 and 0.77 respectively. However, when combinations of NODDI and tensor+volume metrics were included, we observed a bimodal distribution with the AUC at the 99th percentile = 0.93 (Figure 3.7), and the AUCs of the separate distributions were both equal to about the ~55th percentile of the all metrics distribution. This indicates that NODDI and tensor+volume metrics, while correlated, contain independent aspects of variance that is useful in modeling RAVLT performance. As expected from these results, the input features that most frequently contributed to the top 1000 AUCs spanned all metrics and all subfields.

Given the correlation between age and RAVLT performance, it is certainly possible that our prediction of RAVLT status is driven by our ability to predict age group (note, 75% of the high-performing RAVLT participants belong to the younger age group). To assess whether these metrics were capturing cognitive difference beyond just a function of age, we repeated this analysis separately in the younger and older subpopulations. In the older group, we found that these results were just as reliable (99th percentile of AUC distribution with Tensor metrics + Volume: 0.89; NODDI metrics: 0.84; All metrics: 0.98). The peak AUCs of all conditions were greater when predicting the RAVLT delay in just the older group and compared to the entire study sample. Notably, the features that

contributed to the highest AUCs here were not in the same order as with the entire sample size, but still appeared to span across all metrics and subfields evenly. In the younger group, we found that combining the metrics did not result in a significantly higher AUC distribution over just the traditional metrics or NODDI metrics (99th percentile of AUC distribution with Tensor metrics + Volume: 0.75; NODDI metrics: 0.71; All metrics: 0.75), possibly due to the low number of poor performers, or because these metrics weren't sensitive to microstructural properties that contributed to low RAVLT delay at a young age.

Figure 3.6: Combining NODDI and tensor metrics results in a significantly higher AUC after selecting for best performing features in predicting high/low RAVLT performance, as compared to just traditional measures or just NODDI measures both when examining the full study population (a-d) and when examining only the older subpopulation (e-h). (a, e) Analysis of only the traditional tensor and volume metrics; (b, f) Analysis of only the NODDI metrics; and (c, g) Analysis of all metrics combined. Histograms represent the distribution of AUCs generated following and exhaustive n-choose-6 analysis to determine how well various combinations of 6 Region x Metric regressors could model high/low RAVLT group. The colored lines represent the AUCs of each metric from all 6 subfields. (d, h) Plot of the frequency of selection of a given Region x Metric combination in the top 1000 AUCs in the All metrics analysis.

3.3.5 A combination of NODDI and tensor metrics predicts MST performance better than either of them alone.

We also found similar results when predicting MST performance, as relayed by the LDI. Here, we binarized the LDI at a threshold of 1.25, to match the proportion used in our RAVLT analysis. We found that the AUCs for predicting high/low LDI were lower overall than the corresponding high/low RAVLT or age group (Figure 3.8) when restricting ourselves to individual metrics from all 6 subfields. Here, the only individual predictors were ODI, FA, volume, and FISO.

Metric	AUC	p value
NDI	0.599	0.408
ODI	0.677	0.012
FISO	0.614	0.246
Volume	0.660	0.03

Metric	AUC	p value
FA	0.676	0.012
AD	0.587	0.559
ADC	0.588	0.538
RD	0.610	0.292
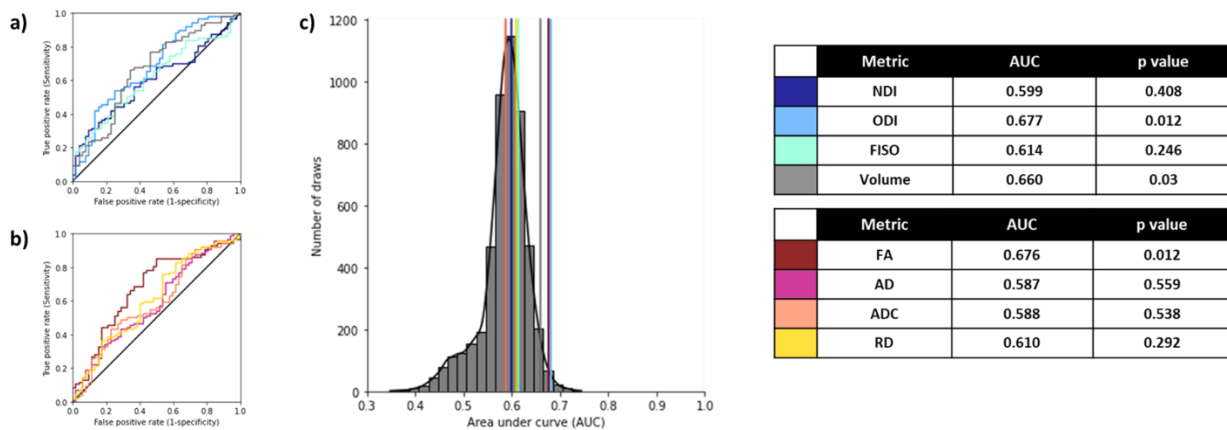
Figure 3.7: Using diffusion and structural metrics of the hippocampal subfields to *predict LDI (<1.25)*. Only ODI, FA and volume could predict MST performance slightly better than chance. The histogram represents the null distribution (randomly permuting the high/low labels), and the colored lines represent the AUC of each of the metrics from all 6 subfields.

Turning to the n-choose-6 permutations, we observed a familiar pattern. The 99th percentile of the AUC distribution obtained from using just the NODDI metrics or just the tensor metrics + volume were 0.67 and 0.75 respectively but using a combination of all metrics resulted in a bimodal distribution with a 99th percentile AUC of 0.87 (Figure 3.9), again with the separate distributions having their 99th percentile equal to below the 60th

86

percentile in the complete distribution. As with the RAVLT delay, the most informative input features spanned all metrics across all subfields. We were also able to reproduce these results in just the older subgroup (99th percentile of AUC distribution with Tensor metrics + Volume: 0.85; NODDI metrics: 0.75; All metrics: 0.96). As with the RAVLT performance, combining the metrics did not help the AUC in the younger subgroup (99th percentile of AUC distribution with Tensor metrics + Volume: 0.74; NODDI metrics: 0.77; All metrics: 0.76). These results again indicate that while NODDI and traditional diffusion metrics can be correlated with each other, they provide unique information and contributions to the variance that can be used to model cognition.
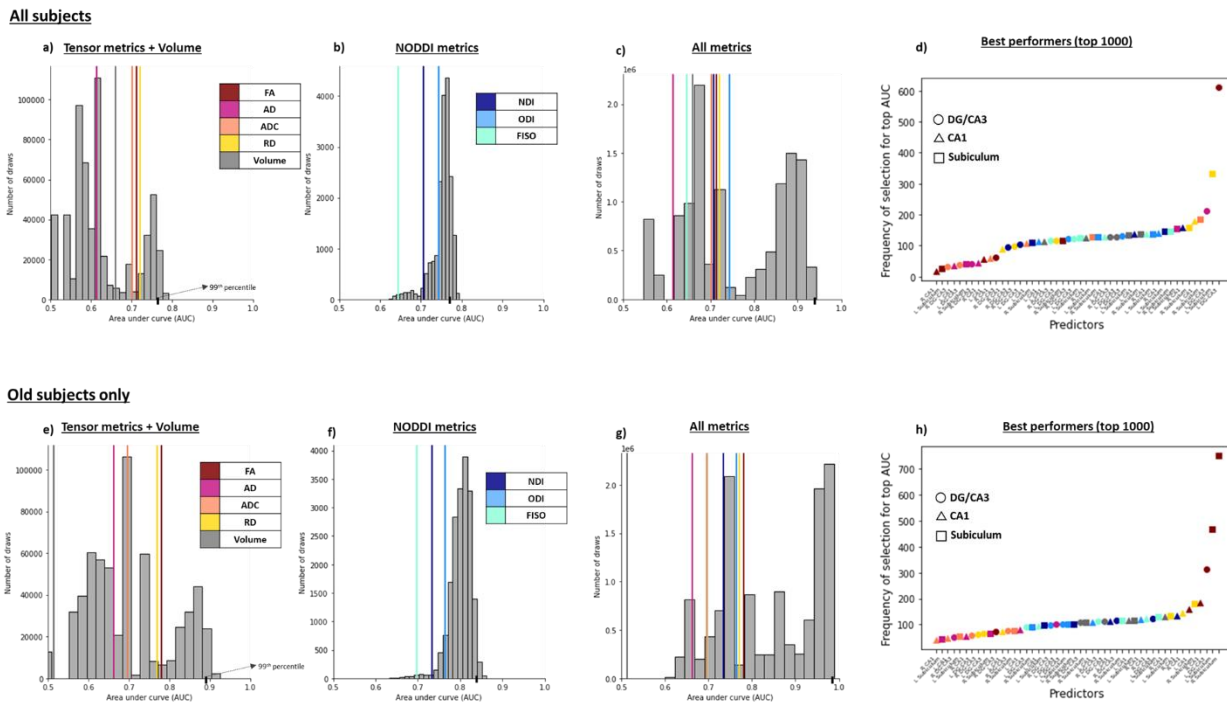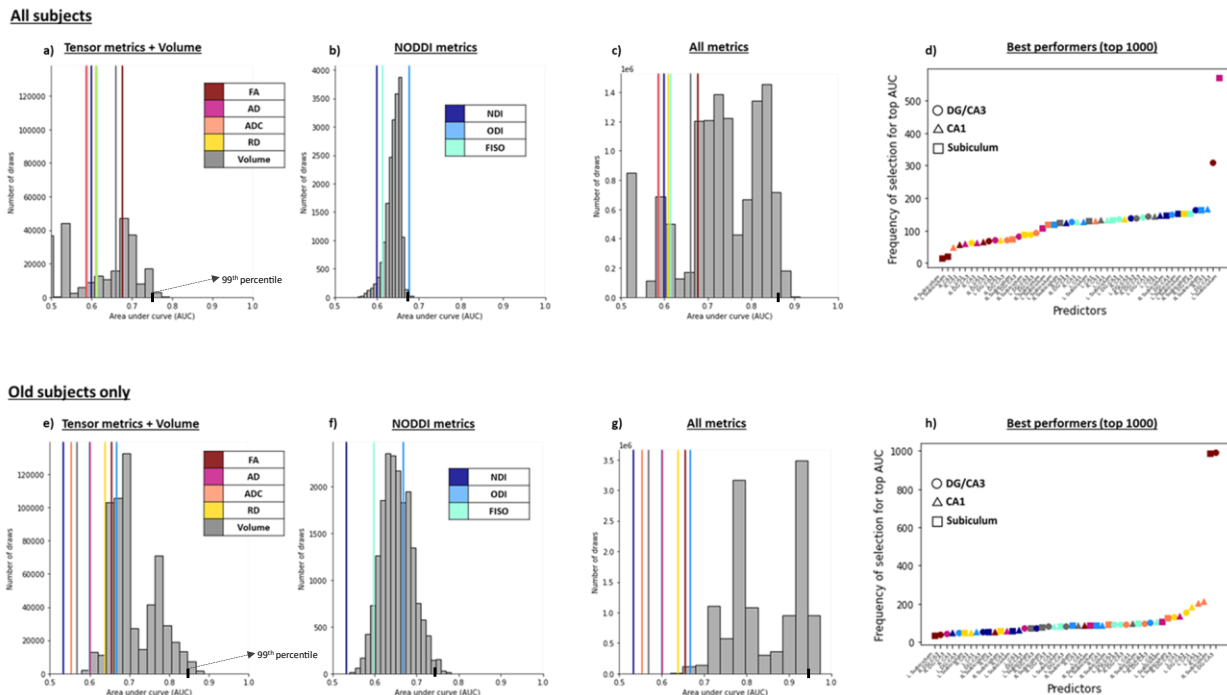

Figure 3.8: Combining NODDI and tensor metrics results in a significantly higher AUC after selecting for best performing features in predicting high/low MST performance, as compared to just traditional measures or just NODDI measures, in both the full study population (a-d), as well as in the older subpopulation (e-h). a, e) Analysis of only the traditional tensor and volume metrics; (b, f) Analysis of only the NODDI metrics; and (c, g) Analysis of all metrics combined. Histograms represent the distribution of AUCs generated following and exhaustive n-choose-6 analysis to determine how well various combinations of 6 Region x Metric regressors could model high/low RAVLT group. The colored lines represent the AUCs of each metric from all 6 subfields. (d, h) Plot of the frequency of selection of a given Region x Metric combination in the top 1000 AUCs in the All metrics analysis.

87

3.4 DISCUSSION

In this study, we show that multi-shelled diffusion-weighted imaging can provide significant advantages in determining aging-associated microstructural differences in the hippocampal subfields and their cognitive consequences. We first reproduced our previous studies in a larger sample size (about three-fold of that reported in our prior publications) showing that the NODDI metric NDI is increased in older adults, and this increase may be partially driving aging associated memory decline. The ability to reproduce these effects across independent populations and study centers speaks to the robustness and reliability of these relationships.

We also found that NDI increases with age within the older population alone (ages 65 – 92) in the DG-CA3 and CA1, but not in the subiculum. However, the negative relationship between NDI and RAVLT performance was strongest in the subiculum in both the entire study population as well as the older subgroup alone, suggesting a subfield-specific pattern of NDI differentially associating with cognition at the outset of aging. The other hippocampal diffusion metrics derived from both the NODDI and the tensor models had selective relationships with age and RAVLT delay and LDI across the subfields (see supplementary material) that are consistent with prior reports in the literature (Fukutomi et al., 2019; Mortimer et al., 2004; Müller et al., 2005; Nazeri et al., 2015; Nobis et al., 2019; Yassa et al., 2011). Also consistent with several previous studies (Aggarwal et al., 2015; Assaf, 2019; Leuze et al., 2014; Truong et al., 2014), we found that even the most basic diffusion metrics like FA and RD were sensitive to age and cognitive measures. They

88

could detect specific microstructural properties of gray matter and were mainly better than volume in detecting individual cognitive differences. Interestingly, relationships between these diffusion metrics and aging/cognition were largely independent of hippocampal volume. Moreover, despite being highly correlated with each other, none of the diffusion metrics were associated with volume in any of the subfields. These observations suggest that hippocampal microstructure as relayed by the diffusion metrics, and macrostructure measured by subfield volume, could represent independent processes in normal aging.

Not only could diffusion metrics be reliably used in gray matter to make inferences about aging and cognition, but we also found that including multi-shell diffusion sequences greatly improved the ability of our statistical models to predict age and cognition. While all metrics studied (**Tensors**: AD, ADC, FA, RD; **NODDI**: NDI, ODI, FISO; **T1w**: Volume) could predict age group well above chance, a combination of the NODDI metrics alone consistently resulted in higher AUCs, compared to any of the other combinations. Moreover, when examining the distribution of the highest AUCs possible from all combinations of input features, we noticed that all the NODDI metrics and volume in all the subfields appeared far more frequently than any of the tensor metrics in any of the subfields. These observations suggest that the NODDI metrics may be able to capture almost all the microstructural variance that can distinguish between the young and old populations and speak to the collective power that acquiring multi-shell data can have in at least aging studies.

Interestingly, when using the same model to predict memory performance, we observed that while combinations of just tensor metrics and volume, or just NODDI metrics yielded laudable AUCs, combining the tensor metrics, volume and NODDI metrics could result in a near-perfect prediction model. Additionally, when predicting both RAVLT and MST performance, this effect only got stronger when looking at just the older subpopulation (resulting in AUCs of over 0.98). This enhancement could be because the neurobiological properties that help define cognitive performance are more likely to be consistent under the common effect of aging, as compared to a much wider age range. The increase in the predictive power of the model in the older group also demonstrates that these metrics could be capturing neurobiological properties that go beyond just the dramatic effect of age and might be sensitive to individual differences as well.

The results in this paper collectively present a strong case in support of including multi-shelled diffusion sequences in study protocols, despite the increase in acquisition time. The full diffusion sequence here required ~16 minutes to acquire both phase encoding directions. However, excellent results are still possible with diffusion data from one phase encoding and only b0 images from the reverse (or a separate phase map), reducing the acquisition time to ~9 minutes. Adding just a single shell and a modest number of directions over typical DTI protocols allowed for NODDI analyses that generated metrics that immensely improved the predictive power of our model, showing that these multi-shelled acquisition and analysis techniques could uncover large effects not discernible by more conventional methods. We posit that these results observed in hippocampal aging likely extend to other domains of interest, like in development or neuropsychiatric

conditions, directing large data collection studies to prioritize acquiring at least one extra shell.

 Of course, this study is not without limitations. Increasing scan times, even by small amounts, result in many issues in studies involving children or participants with neurological conditions. To accommodate for research where long scan times are not feasible, more work that examines the benefits of additional shells over additional directions are required. Moreover, since the data presented here are cross-sectional, we cannot conclude that NODDI metrics would display the same advantage when studying the temporal dynamics of phenomena like aging. Longitudinal studies and studies monitoring interventions (Eaton-Rosen et al., 2015; Kamiya et al., 2020; Radhakrishnan et al., 2021) could greatly enhance our understanding on the benefits of these metrics. Another limitation is that our models binarize age and continuous cognitive measures, so we cannot evaluate whether NODDI metrics would complement tensors and volume so clearly when predicting absolute age and cognition. However, these binarized cognitive scores are far more robust than the continuous scores, and much less prone to noise or sample bias. Though this study is fairly well-balanced by sex, it is also important to note the role of other demographic differences (like race and socioeconomic status) often rising from volunteer and selection biases in most human neuroimaging studies.

In conclusion, we have shown that two shells are better than one. The extra diffusion-weighted shell provides predictive and neurobiologically relevant information that would have not been available without it. NODDI metrics offer obvious value beyond and/or in conjunction with traditional tensor and volumetric measures when studying gray matter

microstructure and might even be able to explain individual differences in cognition or behavior.

Diffusion and tensor metrics have differential relationships with age and cognition and are highly correlated with each other.

We evaluated the linear relationships between these metrics and age/cognition in each subfield. We found that all diffusion metrics were significantly different between the young and old populations in at least two of the subfields, while volume only differed between the groups in the DG-CA3 (Table S3.1). We also found that the diffusion metrics and volumes of the hippocampal subfields were correlated with age and cognition (RAVLT delay and LDI) differentially (Tables S3.2-4). Some of these other metrics had subfield-specific selectivity as well in these relationships, similar to what was observed with the NDI. These results suggest that different metrics could be differentially capturing different age and behavior-associated structural properties separately in these subfields.

We then assessed the relationships of these metrics with each other, in all three subfields. We found that many diffusion metrics were highly correlated with each other, while none of them were correlated with volume. We also found that, despite the subfields having slight variations in microstructure, the relationships between the diffusion metrics remained mostly the same across subfields (Figure S3.1).

DG-CA3

Metric	t value	p value
NDI	-3.27	0.001
ODI	-5.05	<0.0001
FISO	-5.28	<0.0001
AD	-1.72	0.08
ADC	-4.34	<0.0001
FA	4.22	<0.0001
RD	-5.59	<0.0001
Volume	4.15	<0.0001

CA1

Metric	t value	p value
NDI	-4.50	<0.0001
ODI	-6.52	<0.0001
FISO	-5.75	<0.0001
AD	-1.97	0.05
ADC	-4.37	<0.0001
FA	5.20	<0.0001
RD	-5.41	<0.0001
Volume	0.64	0.52

Subiculum

Metric	t value	p value
NDI	-4.80	<0.0001
ODI	-4.18	<0.0001
FISO	-5.33	<0.0001
AD	-0.97	0.33
ADC	-2.29	0.02
FA	2.77	0.006
RD	-2.74	0.006
Volume	0.74	0.46

Table S3.1: T-test results between young and old age groups. Items in bold indicate p < 0.05 (to account for multiple comparisons: Bonferroni corrected p value for each subfield = 0.003). Red rows indicate an increase with age (Old > Young) and blue rows indicate a decrease with age (Young > Old).

DG-CA3

Metric	R squared	P value
NDI	0.09334	0.0101
ODI	0.000723	0.8252
FISO	0.07939	0.0181
AD	0.1775	0.0003
ADC	0.2024	<0.0001
FA	0.03193	0.1389
RD	0.2004	0.0001
Volume	5.07E-05	0.9533

CA1

Metric	R squared	P value
NDI	0.1769	0.0003
ODI	0.000308	0.8853
FISO	0.1302	0.0021
AD	0.2321	<0.0001
ADC	0.2205	<0.0001
FA	0.0623	0.0372
RD	0.2094	<0.0001
Volume	0.005164	0.5544

Subiculum

Metric	R squared	P value
NDI	0.000267	0.8931
ODI	0.03626	0.1144
FISO	0.01296	0.3481
AD	0.1637	0.0005
ADC	0.1387	0.0015
FA	0.09474	0.0095
RD	0.1192	0.0034
Volume	0.000376	0.8734

Table S3.2: Relationship between age and hippocampal subfield metrics, in just the older subpopulation. NDI, AD, ADC and RD are positively associated with age, while FA is negatively associated with age. Items in bold indicate p < 0.05. Red rows denote a positive relationship while blue rows denote a negative relationship.

DG-CA3

Metric	R squared	P value
NDI	0.04969	0.0067
ODI	0.1534	<0.0001
FISO	2.04E-07	0.9957
AD	0.005094	0.3903
ADC	0.008659	0.2623
FA	0.05091	0.006
RD	0.02979	0.0366
Volume	0.000404	0.8091

CA1

Metric	R squared	P value
NDI	0.06542	0.0018
ODI	0.1726	<0.0001
FISO	4.76E-06	0.9791
AD	0.000188	0.869
ADC	0.01883	0.0975
FA	0.05318	0.005
RD	0.03409	0.0252
Volume	0.008151	0.2768

Subiculum

Metric	R squared	P value
NDI	0.1887	<0.0001
ODI	0.008681	0.2617
FISO	0.007608	0.2935
AD	0.02111	0.0791
ADC	0.01162	0.1938
FA	0.004527	0.4181
RD	0.00858	0.2645
Volume	0.003125	0.5013

Table S3.3: Relationship between RAVLT Delay and hippocampal subfield metrics, in the whole study population. NDI and FISO of the DG/CA3 and CA1, and the tensor metrics of all subfields were significantly associated with RAVLT performance. Items in bold indicate $p < 0.05$. Red rows denote a positive relationship while blue rows denote a negative relationship.

DG-CA3

Metric	R squared	P value
NDI	0.001	0.6739
ODI	**0.071**	**0.0015**
FISO	0.001	0.6512
AD	0.01	0.196
ADC	0	0.9777
FA	0.03	0.0223
RD	0.001	0.5966
Volume	**0.03**	**0.0282**

CA1

Metric	R squared	P value
NDI	0.01204	0.1968
ODI	**0.1026**	**0.0001**
FISO	0.000283	0.8436
AD	0.002597	0.5498
ADC	0.002244	0.5784
FA	**0.04976**	**0.0081**
RD	0.007279	0.3162
Volume	0.00569	0.3757

Subiculum

Metric	R squared	P value
NDI	**0.0369**	**0.0228**
ODI	0.002	0.5943
FISO	0.002	0.5892
AD	0.0111	0.2153
ADC	0.0043	0.4441
FA	0.0005	0.8006
RD	0.0030	0.5178
Volume	0.0057	0.3744

Table S3.4: Relationship between LDI and hippocampal subfield metrics, in the whole study population. NDI, AD, and RD are negatively associated with age, while FA is negatively associated with age. Items in bold indicate $p < 0.05$. Red rows denote a positive relationship while blue rows denote a negative relationship.
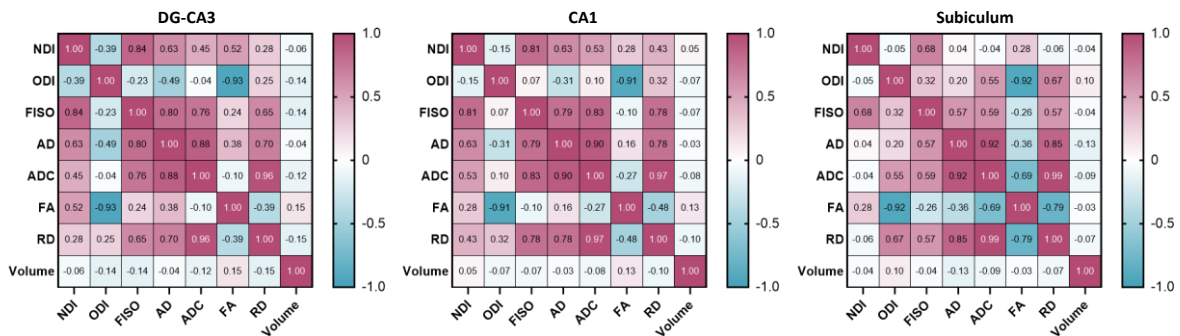
Figure S3.1: The NODDI and tensor metrics are highly correlated to each other. None of the diffusion metrics are significantly correlated with volume for all subfields. Despite the slight difference in subfield microstructure, the relationship between metrics remains consistent across all three hippocampal subfields. The correlation matrix represents Pearson coefficients (r).

95

	Metric	AUC from Hippocampus as a whole (1 input feature)	AUC from hippocampus split by hemisphere (2 input features)	AUC from hippocampus split by subfields, bilaterally (3 input features)	AUC from hippocampus split by subfields and hemisphere (6 input features)
Predicting age group	NDI	0.755	0.754	0.761	**0.779**
	ODI	0.854	0.860	0.885	**0.894**
	FISO	0.789	**0.791**	0.777	0.789
	AD	0.538	0.563	0.548	**0.678**
	ADC	0.652	0.652	0.689	**0.753**
	FA	0.822	0.824	**0.872**	**0.872**
	RD	0.705	0.708	0.773	**0.793**
	Volume	0.607	0.531	0.870	**0.874**
Predicting RAVLT delay	NDI	0.669	0.671	0.701	**0.707**
	ODI	0.704	0.704	0.741	**0.744**
	FISO	0.637	0.635	0.630	**0.645**
	AD	0.570	0.575	0.583	**0.614**
	ADC	0.463	0.477	0.650	**0.702**
	FA	0.650	0.650	0.685	**0.713**
	RD	0.494	0.528	0.676	**0.721**
	Volume	0.516	0.535	0.651	**0.660**
Predicting LDI (MST)	NDI	0.547	0.553	0.591	**0.600**
	ODI	0.654	0.664	0.670	**0.677**
	FISO	0.600	0.609	0.599	**0.614**
	AD	0.542	0.584	0.552	**0.587**
	ADC	0.517	0.553	0.539	**0.588**
	FA	0.656	0.657	**0.676**	**0.676**
	RD	0.554	0.563	0.589	**0.610**
	Volume	0.501	0.563	0.587	**0.660**

Table S3.5: Input features split by hemisphere as well as subfields consistently generated the highest AUCs as compared to other splitting methods, when predicting all targets. Cells in bold indicate the highest AUC for that row.

References

Aggarwal, M., Nauen, D. W., Troncoso, J. C., & Mori, S. (2015). Probing region-specific microstructure of human cortical areas using high angular and spatial resolution diffusion MRI. *NeuroImage*, *105*, 198–207. https://doi.org/10.1016/j.neuroimage.2014.10.053

Andersson, J. L. R., Skare, S., & Ashburner, J. (2003). How to correct susceptibility distortions in spin-echo echo-planar images: Application to diffusion tensor imaging. *NeuroImage*, *20*(2), 870–888. https://doi.org/10.1016/S1053-8119(03)00336-7

Andersson, J. L. R., & Sotiropoulos, S. N. (2016). An integrated approach to correction for off-resonance effects and subject movement in diffusion MR imaging. *NeuroImage*, *125*, 1063–1078. https://doi.org/10.1016/j.neuroimage.2015.10.019

Assaf, Y. (2019). Imaging laminar structures in the gray matter with diffusion MRI. *NeuroImage*, *197*, 677–688. https://doi.org/10.1016/j.neuroimage.2017.12.096

Assaf, Y., & Pasternak, O. (2008). Diffusion Tensor Imaging (DTI)-based White Matter Mapping in Brain Research: A Review. *Journal of Molecular Neuroscience*, *34*(1), 51–61. https://doi.org/10.1007/s12031-007-0029-0

Basser, P. J., Mattiello, J., & Lebihan, D. (1994). Estimation of the Effective Self-Diffusion Tensor from the NMR Spin Echo. *Journal of Magnetic Resonance, Series B*, *103*(3), 247–254. https://doi.org/10.1006/jmrb.1994.1037

Beekly, D. L., Ramos, E. M., van Belle, G., Deitrich, W., Clark, A. D., Jacka, M. E., Kukull, W. A., & NIA-Alzheimer's Disease Centers. (2004). The National Alzheimer's Coordinating Center (NACC) Database: An Alzheimer disease database. *Alzheimer Disease and Associated Disorders*, *18*(4), 270–277.

Benjamini, Y., Krieger, A. M., & Yekutieli, D. (2006). Adaptive linear step-up procedures that control the false discovery rate. *Biometrika*, *93*(3), 491–507. https://doi.org/10.1093/biomet/93.3.491

Brans, R. G. H., Kahn, R. S., Schnack, H. G., Baal, G. C. M. van, Posthuma, D., Haren, N. E. M. van, Lepage, C., Lerch, J. P., Collins, D. L., Evans, A. C., Boomsma, D. I., & Pol, H. E. H. (2010). Brain Plasticity and Intellectual Ability Are Influenced by Shared Genes. *Journal of Neuroscience*, *30*(16), 5519–5524. https://doi.org/10.1523/JNEUROSCI.5841-09.2010

Buckley, A. G. (1978). A combined conjugate-gradient quasi-Newton minimization algorithm. *Mathematical Programming*, *15*(1), 200–210. https://doi.org/10.1007/BF01609018

Budde, M., & Annese, J. (2013). Quantification of anisotropy and fiber orientation in human brain histological sections. *Frontiers in Integrative Neuroscience*, *7*, 3. https://doi.org/10.3389/fnint.2013.00003

Colgan, N., Siow, B., O'Callaghan, J. M., Harrison, I. F., Wells, J. A., Holmes, H. E., Ismail, O., Richardson, S., Alexander, D. C., Collins, E. C., Fisher, E. M., Johnson, R., Schwarz, A. J., Ahmed, Z., O'Neill, M. J., Murray, T. K., Zhang, H., & Lythgoe, M. F. (2016). Application of neurite orientation dispersion and density imaging (NODDI) to a tau pathology model of Alzheimer's disease. *NeuroImage*, *125*, 739–744. https://doi.org/10.1016/j.neuroimage.2015.10.043

Cox, R. W. (1996). AFNI: software for analysis and visualization of functional magnetic resonance neuroimages. *Computers and Biomedical Research*, *29*(3), 162–173.

Dale, A. M., Fischl, B., & Sereno, M. I. (1999). Cortical surface-based analysis. I. Segmentation and surface reconstruction. *NeuroImage*, *9*(2), 179–194. https://doi.org/10.1006/nimg.1998.0395

Dekaban, A. S., & Sadowsky, D. (1978). Changes in brain weights during the span of human life: Relation of brain weights to body heights and body weights. *Annals of Neurology*, *4*(4), 345–356. https://doi.org/10.1002/ana.410040410

Eaton-Rosen, Z., Melbourne, A., Orasanu, E., Cardoso, M. J., Modat, M., Bainbridge, A., Kendall, G. S., Robertson, N. J., Marlow, N., & Ourselin, S. (2015). Longitudinal measurement of the developing grey matter in preterm subjects using multi-modal MRI. *NeuroImage*, *111*, 580–589. https://doi.org/10.1016/j.neuroimage.2015.02.010

Emmenegger, T. M., David, G., Ashtarayeh, M., Fritz, F. J., Ellerbrock, I., Helms, G., Balteau, E., Freund, P., & Mohammadi, S. (2021). The Influence of Radio-Frequency Transmit Field Inhomogeneities on the Accuracy of G-ratio Weighted Imaging. *Frontiers in Neuroscience*, *15*, 770. https://doi.org/10.3389/fnins.2021.674719

Esteban, O., Markiewicz, C., Blair, R. W., Moodie, C., Isik, A. I., Erramuzpe Aliaga, A., Kent, J., Goncalves, M., DuPre, E., Snyder, M., Oya, H., Ghosh, S., Wright, J., Durnez, J., Poldrack, R., & Gorgolewski, K. J. (2018). *FMRIPrep: A robust preprocessing pipeline for functional MRI*. https://doi.org/10.1101/306951

Fonov, V. S., Evans, A. C., McKinstry, R. C., Almli, C. R., & Collins, D. L. (2009). Unbiased nonlinear average age-appropriate brain templates from birth to adulthood. *NeuroImage*, *47*, S102. https://doi.org/10.1016/S1053-8119(09)70884-5

Fox, N. C., & Freeborough, P. A. (1997). Brain atrophy progression measured from registered serial MRI: Validation and application to Alzheimer's disease. *Journal of Magnetic Resonance Imaging: JMRI*, *7*(6), 1069–1075. https://doi.org/10.1002/jmri.1880070620

Frank, L. R. (2001). Anisotropy in high angular resolution diffusion-weighted MRI. *Magnetic Resonance in Medicine*, *45*(6), 935–939. https://doi.org/10.1002/mrm.1125

Fukutomi, H., Glasser, M. F., Murata, K., Akasaka, T., Fujimoto, K., Yamamoto, T., Autio, J. A., Okada, T., Togashi, K., Zhang, H., Van Essen, D. C., & Hayashi, T. (2019). Diffusion Tensor Model links to Neurite Orientation Dispersion and Density Imaging at high b-value in Cerebral Cortical Gray Matter. *Scientific Reports*, *9*(1), 12246. https://doi.org/10.1038/s41598-019-48671-7

Gorgolewski, K., Burns, C. D., Madison, C., Clark, D., Halchenko, Y. O., Waskom, M. L., & Ghosh, S. S. (2011). Nipype: A Flexible, Lightweight and Extensible Neuroimaging Data Processing Framework in Python. *Frontiers in Neuroinformatics*, *5*. https://doi.org/10.3389/fninf.2011.00013

Guerrero, J. M., Adluru, N., Bendlin, B. B., Goldsmith, H. H., Schaefer, S. M., Davidson, R. J., Kecskemeti, S. R., Zhang, H., & Alexander, A. L. (2019). Optimizing the intrinsic parallel diffusivity in NODDI: An extensive empirical evaluation. *PLOS ONE*, *14*(9), e0217118. https://doi.org/10.1371/journal.pone.0217118

Harms, R. L., Fritz, F. J., Tobisch, A., Goebel, R., & Roebroeck, A. (2017). Robust and fast nonlinear optimization of diffusion MRI microstructure models. *NeuroImage*, *155*, 82–96. https://doi.org/10.1016/j.neuroimage.2017.04.064

Hedman, A. M., van Haren, N. E. M., Schnack, H. G., Kahn, R. S., & Hulshoff Pol, H. E. (2011). Human brain changes across the life span: A review of 56 longitudinal magnetic resonance imaging studies. *Human Brain Mapping*, *33*(8), 1987–2002. https://doi.org/10.1002/hbm.21334

Ho, K. C., Roessmann, U., Straumfjord, J. V., & Monroe, G. (1980). Analysis of brain weight. I. Adult brain weight in relation to sex, race, and age. *Archives of Pathology & Laboratory Medicine*, *104*(12), 635–639.

Jack, C. R., Bennett, D. A., Blennow, K., Carrillo, M. C., Dunn, B., Haeberlein, S. B., Holtzman, D. M., Jagust, W., Jessen, F., Karlawish, J., Liu, E., Molinuevo, J. L., Montine, T., Phelps, C., Rankin, K. P., Rowe, C. C., Scheltens, P., Siemers, E., Snyder, H. M., & Sperling, R. (2018). NIA-AA Research Framework: Toward a biological definition of Alzheimer's disease. *Alzheimer's & Dementia : The Journal of the Alzheimer's Association*, *14*(4), 535–562. https://doi.org/10.1016/j.jalz.2018.02.018

Jernigan, T. L., Archibald, S. L., Fennema-Notestine, C., Gamst, A. C., Stout, J. C., Bonner, J., & Hesselink, J. R. (2001). Effects of age on tissues and regions of the cerebrum and cerebellum. *Neurobiology of Aging*, *22*(4), 581–594.

Johansen-Berg, H., & Behrens, T. E. J. (Eds.). (2014). *Diffusion MRI: From quantitative measurement to in-vivo neuroanatomy* (2nd ed). Elsevier/Academic Press.

Jones, D. K. (2004). The effect of gradient sampling schemes on measures derived from diffusion tensor MRI: A Monte Carlo study†. *Magnetic Resonance in Medicine*, *51*(4), 807–815. https://doi.org/10.1002/mrm.20033

Jones, E., Oliphant, T., & Peterson, P. (2001). *SciPy: Open Source Scientific Tools for Python*. SciPy.Org. https://www.scipy.org

Kamiya, K., Hori, M., & Aoki, S. (2020). NODDI in clinical research. *Journal of Neuroscience Methods*, *346*, 108908. https://doi.org/10.1016/j.jneumeth.2020.108908

Kellner, E., Dhital, B., Kiselev, V. G., & Reisert, M. (2016). Gibbs-ringing artifact removal based on local subvoxel-shifts: Gibbs-Ringing Artifact Removal. *Magnetic Resonance in Medicine*, *76*(5), 1574–1581. https://doi.org/10.1002/mrm.26054

Kirwan, C. B., & Stark, C. E. L. (2007). Overcoming interference: An fMRI investigation of pattern separation in the medial temporal lobe. *Learning and Memory*, *14*, 625–633.

Klein, A., Ghosh, S. S., Bao, F. S., Giard, J., Häme, Y., Stavsky, E., Lee, N., Rossa, B., Reuter, M., Chaibub Neto, E., & Keshavan, A. (2017). Mindboggling morphometry of human brains. *PLOS Computational Biology*, *13*(2), e1005350. https://doi.org/10.1371/journal.pcbi.1005350

Knoll, D. A., & Keyes, D. E. (2004). Jacobian-free Newton–Krylov methods: A survey of approaches and applications. *Journal of Computational Physics*, *193*(2), 357–397. https://doi.org/10.1016/j.jcp.2003.08.010

Leuze, C. W. U., Anwander, A., Bazin, P.-L., Dhital, B., Stüber, C., Reimann, K., Geyer, S., & Turner, R. (2014). Layer-Specific Intracortical Connectivity Revealed with Diffusion MRI. *Cerebral Cortex*, *24*(2), 328–339. https://doi.org/10.1093/cercor/bhs311

Morrison, J. H., & Hof, P. R. (1997). Life and Death of Neurons in the Aging Brain. *Science*, *278*(5337), 412–419. https://doi.org/10.1126/science.278.5337.412

Mortimer, J. A., Gosche, K. M., Riley, K. P., Markesbery, W. R., & Snowdon, D. A. (2004). Delayed recall, hippocampal volume and Alzheimer neuropathology: Findings from the Nun Study. *Neurology*, *62*(3), 428–432. https://doi.org/10.1212/01.WNL.0000106463.66966.65

Müller, M. J., Greverus, D., Dellani, P. R., Weibrich, C., Wille, P. R., Scheurich, A., Stoeter, P., & Fellgiebel, A. (2005). Functional implications of hippocampal volume and diffusivity in mild cognitive impairment. *NeuroImage*, *28*(4), 1033–1042. https://doi.org/10.1016/j.neuroimage.2005.06.029

Nazeri, A., Chakravarty, M. M., Rotenberg, D. J., Rajji, T. K., Rathi, Y., Michailovich, O. V., & Voineskos, A. N. (2015). Functional Consequences of Neurite Orientation Dispersion and Density in Humans across the Adult Lifespan. *Journal of Neuroscience*, *35*(4), 1753–1762. https://doi.org/10.1523/JNEUROSCI.3979-14.2015

Nazeri, A., Schifani, C., Anderson, J. A. E., Ameis, S. H., & Voineskos, A. N. (2020). In Vivo Imaging of Gray Matter Microstructure in Major Psychiatric Disorders: Opportunities for Clinical Translation. *Biological Psychiatry: Cognitive Neuroscience and Neuroimaging*, *5*(9), 855–864. https://doi.org/10.1016/j.bpsc.2020.03.003

Nobis, L., Manohar, S. G., Smith, S. M., Alfaro-Almagro, F., Jenkinson, M., Mackay, C. E., & Husain, M. (2019). Hippocampal volume across age: Nomograms derived from over 19,700 people in UK Biobank. *NeuroImage: Clinical*, *23*, 101904. https://doi.org/10.1016/j.nicl.2019.101904

Papadakis, N. G., Xing, D., Huang, C. L.-H., Hall, L. D., & Carpenter, T. A. (1999). A Comparative Study of Acquisition Schemes for Diffusion Tensor Imaging Using MRI. *Journal of Magnetic Resonance*, *137*(1), 67–82. https://doi.org/10.1006/jmre.1998.1673

Peter R., H. (1979). Synaptic density in human frontal cortex—Developmental changes and effects of aging. *Brain Research*, *163*(2), 195–205. https://doi.org/10.1016/0006-8993(79)90349-4

Petersen, R. C., Aisen, P. S., Beckett, L. A., Donohue, M. C., Gamst, A. C., Harvey, D. J., Jack, C. R., Jagust, W. J., Shaw, L. M., Toga, A. W., Trojanowski, J. Q., & Weiner, M. W. (2010).

Alzheimer's Disease Neuroimaging Initiative (ADNI). *Neurology*, *74*(3), 201–209. https://doi.org/10.1212/WNL.0b013e3181cb3e25

Radhakrishnan, H., Stark, S. M., & Stark, C. E. L. (2020). Microstructural Alterations in Hippocampal Subfields Mediate Age-Related Memory Decline in Humans. *Frontiers in Aging Neuroscience*, *12*, 94. https://doi.org/10.3389/fnagi.2020.00094

Radhakrishnan, H., Ubele, M. F., Krumholz, S. M., Boaz, K., Mefford, J. L., Jones, E. D., Meacham, B., Smiley, J., Puskás, L. G., Powell, D. K., Norris, C. M., Stark, C. E. L., & Head, E. (2021). Tacrolimus Protects against Age-Associated Microstructural Changes in the Beagle Brain. *Journal of Neuroscience*, *41*(23), 5124–5133. https://doi.org/10.1523/JNEUROSCI.0361-21.2021

Raffelt, D., Tournier, J.-D., Rose, S., Ridgway, G. R., Henderson, R., Crozier, S., Salvado, O., & Connelly, A. (2012). Apparent Fibre Density: A novel measure for the analysis of diffusion-weighted magnetic resonance images. *NeuroImage*, *59*(4), 3976–3994. https://doi.org/10.1016/j.neuroimage.2011.10.045

Raz, N., Gunning-Dixon, F., Head, D., Rodrigue, K. M., Williamson, A., & Acker, J. D. (2004). Aging, sexual dimorphism, and hemispheric asymmetry of the cerebral cortex: Replicability of regional differences in volume. *Neurobiology of Aging*, *25*(3), 377–396. https://doi.org/10.1016/S0197-4580(03)00118-0

Rey, A. (1941). L'examen psychologique dans les cas d'encephalopathie traumatique. *Arch Psychol*, *28*, 286–340.

Sasson, E., Doniger, G. M., Pasternak, O., & Assaf, Y. (2010). Structural correlates of memory performance with diffusion tensor imaging. *Neuroimage*, *50*, 1231–1242. https://doi.org/10.1016/j.neuroimage.2009.12.079

Seabold, S., & Perktold, J. (2010). *Statsmodels: Econometric and Statistical Modeling with Python*. 5.

Skare, S., & Bammer, R. (2009). *Jacobian weighting of distortion corrected EPI data*. https://www.semanticscholar.org/paper/Jacobian-weighting-of-distortion-corrected-EPI-data-Skare-Bammer/7ed01244fd7c4ab273656d40b8b76fcbdc4bee7d

Stark, S. M., Kirwan, C. B., & Stark, C. E. L. (2019). Mnemonic Similarity Task: A Tool for Assessing Hippocampal Integrity. *Trends in Cognitive Sciences*, *23*(11), 938–951. https://doi.org/10.1016/j.tics.2019.08.003

Stark, S. M., & Stark, C. E. L. (2017). Age-related deficits in the mnemonic similarity task for objects and scenes. *Behavioural Brain Research*, *333*, 109–117. https://doi.org/10.1016/j.bbr.2017.06.049

Stark, S. M., Stevenson, R., Wu, C., Rutledge, S., & Stark, C. E. L. (2015). Stability of age-related deficits in the mnemonic similarity task across task variations. *Behavioral Neuroscience*, *129*(3), 257–268. https://doi.org/10.1037/bne0000055

Stark, S. M., Yassa, M. A., Lacy, J. W., & Stark, C. E. (2013). A task to assess behavioral pattern separation (BPS) in humans: Data from healthy aging and mild cognitive impairment. *Neuropsychologia*, *51*, 2442–2449. https://doi.org/10.1016/j.neuropsychologia.2012.12.014

Stark, S. M., Yassa, M. A., & Stark, C. E. L. (2010). Individual differences in spatial pattern separation performance associated with healthy aging in humans. *Learning & Memory*, *17*(6), 284–288.

Stejskal, E. O., & Tanner, J. E. (1965). Spin Diffusion Measurements: Spin Echoes in the Presence of a Time-Dependent Field Gradient. *The Journal of Chemical Physics*, *42*(1), 288–292. https://doi.org/10.1063/1.1695690

Student. (1908). The Probable Error of a Mean. *Biometrika*, *6*(1), 1–25. https://doi.org/10.2307/2331554

Taki, Y., Kinomura, S., Sato, K., Goto, R., Kawashima, R., & Fukuda, H. (2011). A longitudinal study of gray matter volume decline with age and modifying factors. *Neurobiology of Aging*, *32*(5), 907–915. https://doi.org/10.1016/j.neurobiolaging.2009.05.003

Thomason, M. E., & Thompson, P. M. (2011). Diffusion Imaging, White Matter, and Psychopathology. *Annual Review of Clinical Psychology*, *7*(1), 63–85. https://doi.org/10.1146/annurev-clinpsy-032210-104507

Tournier, J.-D., Calamante, F., & Connelly, A. (2012). MRtrix: Diffusion tractography in crossing fiber regions. *International Journal of Imaging Systems and Technology*, *22*(1), 53–66. https://doi.org/10.1002/ima.22005

Truong, T.-K., Guidon, A., & Song, A. W. (2014). Cortical Depth Dependence of the Diffusion Anisotropy in the Human Cortical Gray Matter In Vivo. *PLOS ONE*, *9*(3), e91424. https://doi.org/10.1371/journal.pone.0091424

Tustison, N. J., Avants, B. B., Cook, P. A., Yuanjie Zheng, Egan, A., Yushkevich, P. A., & Gee, J. C. (2010). N4ITK: Improved N3 Bias Correction. *IEEE Transactions on Medical Imaging*, *29*(6), 1310–1320. https://doi.org/10.1109/TMI.2010.2046908

Tustison, N. J., Cook, P. A., Klein, A., Song, G., Das, S. R., Duda, J. T., Kandel, B. M., van Strien, N., Stone, J. R., Gee, J. C., & Avants, B. B. (2014). Large-scale evaluation of ANTs and FreeSurfer cortical thickness measurements. *Neuroimage*, *99*, 166–179. https://doi.org/10.1016/j.neuroimage.2014.05.044

van Haren, N. E. M., Pol, H. E. H., Schnack, H. G., Cahn, W., Brans, R., Carati, I., Rais, M., & Kahn, R. S. (2008). Progressive Brain Volume Loss in Schizophrenia Over the Course of the Illness: Evidence of Maturational Abnormalities in Early Adulthood. *Biological Psychiatry*, *63*(1), 106–113. https://doi.org/10.1016/j.biopsych.2007.01.004

Venkatesh, A., Stark, S. M., Stark, C. E. L., & Bennett, I. J. (2020). Age- and memory- related differences in hippocampal gray matter integrity are better captured by NODDI compared to single-tensor diffusion imaging. *Neurobiology of Aging*, *96*, 12–21. https://doi.org/10.1016/j.neurobiolaging.2020.08.004

Veraart, J., Fieremans, E., & Novikov, D. S. (2016). Diffusion MRI noise mapping using random matrix theory: Diffusion MRI Noise Mapping. *Magnetic Resonance in Medicine*, *76*(5), 1582–1593. https://doi.org/10.1002/mrm.26059

Veraart, J., Sijbers, J., Sunaert, S., Leemans, A., & Jeurissen, B. (2013). Weighted linear least squares estimation of diffusion MRI parameters: Strengths, limitations, and pitfalls. *NeuroImage*, *81*, 335–346. https://doi.org/10.1016/j.neuroimage.2013.05.028

Westin. (1997). Geometrical diffusion measures for MRI from tensor basis analysis. *Proc. ISMRM'97*. https://ci.nii.ac.jp/naid/10021111885/

Yassa, M. A., Mattfeld, A. T., Stark, S. M., & Stark, C. E. L. (2011). Age-related memory deficits linked to circuit-specific disruptions in the hippocampus. *Proceedings of the National Academy of Sciences*, *108*(21), 8873–8878. https://doi.org/10.1073/pnas.1101567108

Yushkevich, P. A., Wang, H., Pluta, J., Das, S. R., Craige, C., Avants, B. B., Weiner, M. W., & Mueller, S. (2010). Nearly Automatic Segmentation of Hippocampal Subfields in In Vivo Focal T2-Weighted MRI. *NeuroImage*, *53*(4), 1208–1224. https://doi.org/10.1016/j.neuroimage.2010.06.040

Zhang, H., Schneider, T., Wheeler-Kingshott, C. A., & Alexander, D. C. (2012). NODDI: Practical in vivo neurite orientation dispersion and density imaging of the human brain. *NeuroImage*, *61*(4), 1000–1016. https://doi.org/10.1016/j.neuroimage.2012.03.072

CHAPTER 4:

TACROLIMUS PROTECTS AGAINST AGE-ASSOCIATED MICROSTRUCTURAL CHANGES IN THE BEAGLE BRAIN.

In Chapters 2 and 3, we demonstrated that NODDI and tensor metrics have the potential to resolve gray matter cytoarchitectural properties in cross-sectional studies. However, very few studies have explored the possible advantages of diffusion metrics, especially that of NODDI metrics, in examining more subtle cellular changes- like those observed longitudinally in intervention studies. In this study, we asked whether these diffusion metrics are sensitive enough to measure the efficacy of intervention studies designed to protect against aging-related structural changes. Since such studies are challenging to conduct in humans, we investigated whether diffusion metrics could detect any microstructural changes over time in the beagle brain following a year-long treatment with the calcineurin inhibiting drug, tacrolimus. We hypothesized that controlling the expression of calcineurin before gross aging-related cognitive deficits are observable, might be able to protect against aging-related structural deterioration, and we challenged whether diffusion metrics would be able to detect microstructural consequences of the intervention over just a year. Not only were we able to replicate the effect that hippocampal NDI was increased in the older dogs at baseline, administering tacrolimus over a year decreased the NDI in both the hippocampus and parahippocampal gyrus! Other

diffusion metrics like parahippocampal ODI and prefrontal FA could also detect the drug potentially protecting against aging-related structural changes in gray matter, speaking not only to the benefits of tacrolimus, but also to the power of diffusion metrics in longitudinal studies!

NB: A version of this chapter was first published in Radhakrishnan et al., Journal of Neuroscience, 2021.

4.1 INTRODUCTION

Alzheimer's Disease (AD) is the most prevalent neurodegenerative disorder in the world, affecting more than 45 million people (Dos Santos Picanco et al., 2018). It is primarily characterized by dementia, a decline in memory, and other cognitive skills beyond what is typically observed in healthy aging (Reitz & Mayeux, 2014). The greatest risk factor for AD remains age, and most people who develop the disease are older than 65 years (Inouye et al., 2010).

The two major neuropathological features of AD are abnormally folded beta-amyloid (Aβ) peptides and the accumulation of hyperphosphorylated tau proteins in amyloid plaques and neurofibrillary tangles (Forestier et al., 2015; Hendrie et al., 2015; Holtzman et al., 2011; J. Liu et al., 2015; Perl, 2010; Stancu et al., 2014). Because of the overwhelming evidence that Aβ plaques play a role in AD and the amyloid cascade hypothesis (Hardy & Higgins, 1992), most therapeutic strategies have focused on reducing or at least controlling the formation of these plaques. However, clinical trials that use Aβ reducing approaches have shown limited clinical efficacy, prompting the exploration of treatments

that target other factors or pathways driving this disease, perhaps upstream of Aβ accumulation (Pahnke et al., 2009).

Mounting evidence suggests that the Ca^{2+}/calmodulin dependent protein phosphatase, calcineurin, and downstream signaling pathways are an attractive target for ameliorating cognitive decline in AD and related disorders (Reese & Taglialatela, 2011; Sompol & Norris, 2018). Calcineurin is found at high levels in neurons and reactive glial cells where it modulates synaptic plasticity, neuroinflammation, glutamate regulation, and memory formation (Mansuy, 2003). Elevated levels of calcineurin expression and signaling are found in the hippocampus and other cortical areas at the outset of cognitive decline in humans (Abdul et al., 2009; Mohmmad Abdul et al., 2011) and are highly correlated with pathological features in later disease stages (Abdul et al., 2009; F. Liu et al., 2005). Overexpression or hyperactivation of calcineurin in experimental models recapitulates key features of AD including glial reactivity (Norris et al., 2005), synaptic degeneration (Wu et al., 2010), and cognitive dysfunction (Malleret et al., 2001). Conversely, inhibition of calcineurin signaling via genetic or pharmacologic means reverses many of these AD-related biomarkers in animal models (Furman et al., 2012; Hudry et al., 2012; A. Kumar & Singh, 2017; Reese et al., 2008; Rojanathammanee et al., 2015; Rozkalne et al., 2011; Sompol et al., 2017; Taglialatela et al., 2009). In the clinic, calcineurin inhibitors, like tacrolimus, are used primarily as immunosuppressants to combat organ transplant rejection and other autoimmune disorders. However, an epidemiological study in 2015 showed that kidney transplant patients treated with tacrolimus had a significantly lower incidence of dementia relative to age-matched individuals in the general population

(Taglialatela et al., 2015). Collectively, this work suggests that tacrolimus and other FDA-approved calcineurin inhibitors could be repurposed for the prevention of AD and dementia.

The FDA-approved status, and well-known safety profiles and contraindications of calcineurin inhibitors, would certainly make the path to AD clinical trials easier. But, to ensure that calcineurin inhibitors have the best chance of succeeding as anti-AD therapeutics requires further optimization in a preclinical model that better approximates human metabolism, neural function, treatment course, and biomarker milestones.

Dogs have a very similar metabolism compared to humans and are excellent preclinical models for testing pharmacological agents (Dalgaard, 2015). More importantly for investigating anti-AD treatments, dogs *naturally* show age-related amyloid plaque pathology, neuroinflammation, and neurodegeneration (Sarasa and Pesini 2009; Prpar Mihevc and Majdič 2019). Human-like deficits in cognition also arise with aging and correlate well with pathological features. Because of their longer lifespan, larger brain size and complexity, and ease of training, dogs are amenable to the longitudinal assessment of neurological function using complex cognitive/behavioral batteries and brain imaging, common to most modern human clinical trials. (Hoffman et al., 2018; Patronek et al., 1997). Given these clear benefits, we explored the microstructural consequences of tacrolimus on the brain of a preclinical aging beagle model (aged 4-8 years) using diffusion-weighted imaging (DWI). Though traditional MRI procedures (like T1 and T2-weighted imaging) are non-invasive, they only provide a mesoscopic view as even their highest resolutions are well too coarse to resolve changes at the expected

microscopic level, at least directly. In contrast, DWI provides measures that are sensitive to the underlying microstructure and its changes in disorders such as AD (Chua et al., 2008). Here, we use two types of diffusion analysis techniques: 1) traditional diffusion tensor fitting (Basser et al., 1994), and 2) Neurite Orientation Dispersion and Density Imaging (NODDI) analysis (Zhang et al., 2012), to survey the potential cytoarchitectural changes (or lack thereof) that tacrolimus could induce in the beagle brain.

4.2 METHODS

4.2.1 Animals and drug delivery

Forty-five (7 males and 38 females) purpose-bred beagles ranging from 5-8 years old were assessed for general health status and cognition as described previously (Christie et al., 2005; Head et al., 1998a; Milgram et al., 1999, 2002; Studzinski et al., 2006; Tapp et al., 2003). Dogs ranged in weight from 8.6 kg to 14.5 kg. Since tacrolimus has previously been associated with nephrotoxicity in renal transplant patients (Randhawa et al., 1997), blood samples were taken every six months to monitor the dogs' overall health and assess blood urea nitrogen (BUN), creatine and phosphorous levels.

4.2.2. Cognitive testing

Cognitive testing used a modified Wisconsin General Test Apparatus described previously (Head et al., 2008). Dogs were given 10 to 12 trials/day, 5 days a week depending on the cognitive task. All tasks were reward-motivated and based upon visual cues. Dogs were given baseline tests of visual discrimination learning and reversal learning to assess learning and executive function. Subsequently, a spatial delayed non-match to sample task was used to assess spatial learning and memory. At the end of baseline testing, dogs

were ranked according to cognitive test scores and balanced into 3 groups of 15 animals/group. Groups were also balanced for age.

4.2.3 Drug administration

Oral tacrolimus at 0.075 mg/kg twice a day (n = 15; Males = 2) or an oral placebo control (n = 15; Males = 2) was administered for one year. The remaining 15 animals were assigned to another intervention study not relevant to this study- only their baseline data is included here to improve the statistical power of age associations. The concentration of the drugs was designed to provide minimal immunosuppression to reduce adverse effects (Margarit et al., 1998).

4.2.4 MRI Image Acquisition

Dogs were placed under general anesthesia using Propofol (4-8 mg/kg by slow IV injection to effect). After orotracheal intubation and maintenance on Isoflurane 1-4%, delivered in 100% O_2, dogs were scanned using a Siemens Prisma 3T MRI scanner both at baseline before treatment and after one year of treatment.

T1W: A high-resolution T1 weighted MPRAGE image was collected (repetition time (TR) = 2530 milliseconds, echo time (TE) = 2.49 milliseconds, flip angle = 7°, Matrix size = 0.4 x 0.4 x 0.7 mm, Averages = 1, Average acquisition time = 10 minutes, 30 seconds) for structural analysis and image registration.

DWI: Diffusion imaging (TR = 5700 milliseconds, TE = 62 milliseconds, 48 coronal slices in the animal reference frame, Phase encoding: Superior-Inferior, Average acquisition time = 12 minutes, 30 seconds) was performed using a double refocused echo-planar

sequence with an isotropic 1.6 mm voxel for three gradient values: b = 500, 1000, and 2000 s/mm². Gradients were applied in a total of 114 directions, along with 13 images with no diffusion weighting (b = 0).

4.2.5 Diffusion data preprocessing

All preprocessing steps used MRtrix3 (Tournier et al., 2012) (www.mrtrix.org) commands or MRtrix3 scripts that linked external software packages. Physiological noise arising from thermal motion of water molecules in the brain was first removed (Veraart et al., 2016), followed by the removal of Gibbs ringing artifacts (Kellner et al., 2016). The image intensity was then normalized across subjects in the log-domain (Andersson & Sotiropoulos, 2016; Raffelt et al., 2012).

4.2.6 Structural data processing

The T1w images were corrected for intensity inhomogeneities using Advanced Normalizations Tools' (ANTs) N4 bias field correction (Tustison et al., 2010). Each dog's structural image was then non-linearly co-registered to their respective preprocessed b0 image, so that the structural and diffusion images were in the same space for the rest of the analyses. To help standardize our results, we used the Aguirre high-resolution *ex vivo* template (Datta et al., 2012). In this space, we generated a high-resolution central tendency template from the structural scans using ANTs with an initial cohort of 10 animals and a bootstrapping approach. We then used this template to generate initial priors for both brain extraction and tissue type segmentation (gray matter, white matter, cerebrospinal fluid, deep gray matter, and cerebellum) again using ANTs and a bootstrapping approach with more refined priors. The result was a set of priors that can

be used in a modified ANTs' cortical thickness pipeline to generate final tissue segments for each subject. Though the Aguirre template provides an excellent standard template space complete with high-resolution *ex vivo* scans, it does not provide adequate labels for ROI specific analyses. To solve this problem, we co-registered two different atlases, hereby referred to as the Nitzsche (Nitzsche et al., 2019) and Czeibert (Czeibert et al., 2019) atlases to the same template space using the affine+SyN nonlinear registration in ANTs. The Nitzsche atlas was used for large area ROIs like entire lobes, while the Czeibert atlas was used for more specific sub-regions like the hippocampus. All resulting images were visually inspected for quality and rerun with new command line parameters when necessary (Figure 4.1). Region-wise volumes were determined by warping the annotated atlas back to each individual's subject space and quantifying the number of voxels that made up each region of interest.
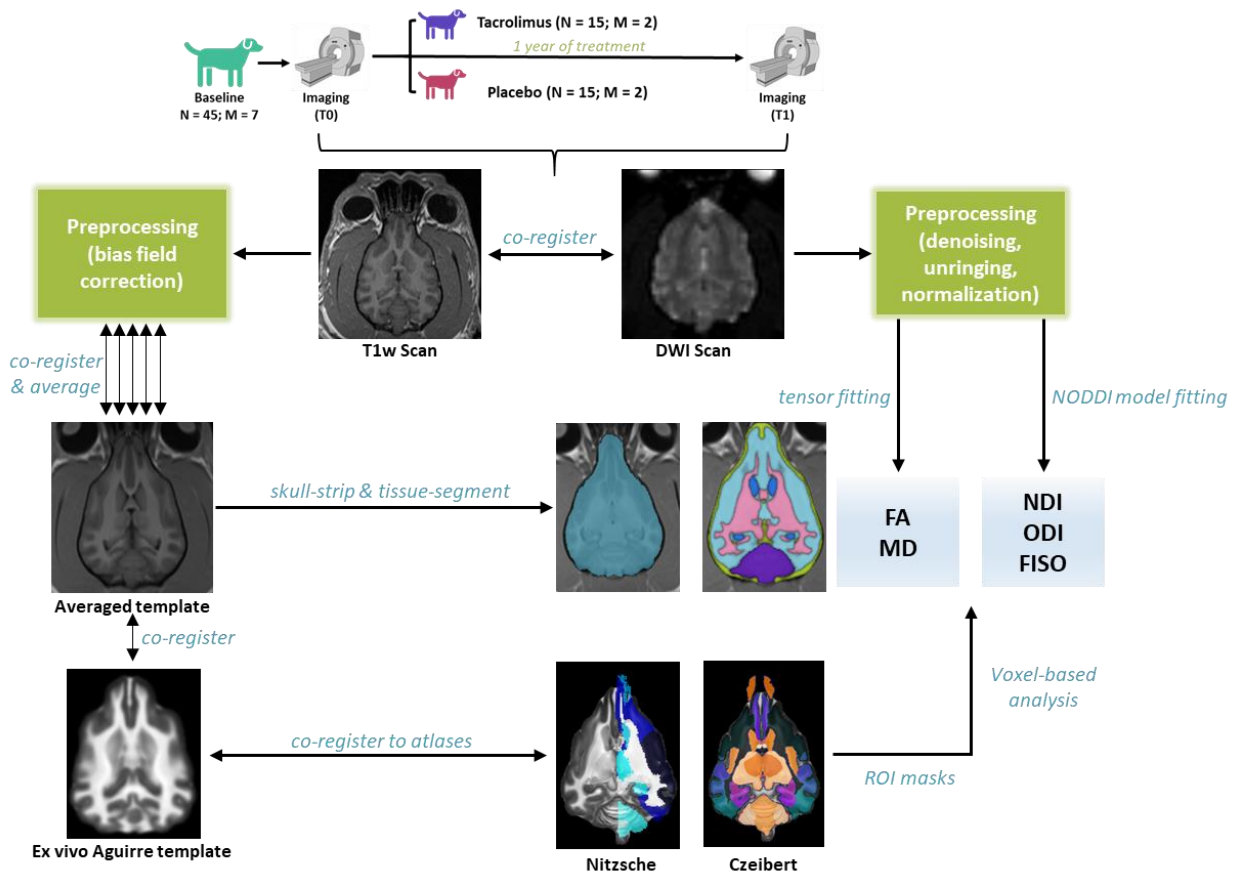
Figure 4.1: Summary of the analysis pipeline

4.2.7 Deriving diffusion metrics.

We calculated traditional tensor metrics (FA and MD) using FSL (v.6.0.1) (Jenkinson et al., 2012) and higher-order, multi-compartment metrics (NDI, ODI, and FISO) using the Neurite Orientation Dispersion and Density Imaging (NODDI) (Zhang et al., 2012) model with the Microstructure Diffusion Toolbox (Harms et al., 2017). The traditional tensor metrics are widely used, but typically only applied to white matter. NODDI's metrics are tissue type agnostic and can readily be used in gray matter as it characterizes diffusion

within each voxel as a combination of intracellular, extracellular, and CSF-based components. The intracellular compartment ostensibly captures neurite membranes and myelin sheaths and is modeled as a set of sticks with restricted diffusion perpendicular to the orientation of the axonal bundles and unhindered diffusion along them. The extracellular compartment is designed to model the space around the neurites, composed of glia and somas, as hindered gaussian anisotropic diffusion. The CSF is modeled as isotropic diffusion. A summary of all the diffusion metrics used is provided in Table 4.1.

The hippocampus, parahippocampal gyrus, and prefrontal cortex were selected as *a priori* regions because aging and AD presents early changes in these regions in dogs (Ezekiel et al., 2004; Head, 2011; Hwang et al., 2008; Shimada et al., 1992; Su et al., 2005; Tapp et al., 2004, 2006; Thal et al., 2002). Region-specific averages were obtained by aligning the Czeibert atlas (Czeibert et al., 2019) to each subject's parametric maps. Diffusion metrics were then averaged across each region of interest using AFNI (Cox, 1996). All statistical analyses were performed in Python - Scipy (Jones et al., 2001) or GraphPad Prism 8.3.0. All regression analyses were simple linear regressions. Effects of interventions were assessed with ANOVA, and multiple comparisons were corrected using Holm-Sidak statistical hypothesis testing (Holm, 1979).

Whole brain exploratory analysis was conducted to measure global longitudinal changes in each group separately using a paired t-test in a voxel-wise manner using AFNI's 3dttest++. AFNI's cluster-wise simulations (Forman et al., 1995) were used to correct for multiple comparisons. Parametric maps of each subject were passed in after they were registered to a common space, and a brain mask was passed in to improve power. To

assess the interaction between intervention and time, a difference image was created (T0-T1) for each metric and each subject, and the difference images of each group were compared through an unpaired t-test. The *-clustsim* option was used to determine the minimum cluster threshold for each individual test to maintain a final alpha of 0.05.

Code for data processing and analysis is available at https://github.uci.edu/Stark-Lab/Woofusion.

4.3 Results

4.3.1 The NDI of the beagle hippocampus and parahippocampal gyrus increases with age.

Our first question was whether diffusion within hippocampal and parahippocampal grey matter was affected by age. Previous work in our lab has shown that the NDI of the hippocampus as a whole (Venkatesh et al., 2020), and specifically the DG/CA3 subfields (Radhakrishnan et al., 2020), is higher in older humans (59-84 years) than young adults (20-38 years) and that this increase is negatively correlated with memory performance (Radhakrishnan et al., 2020). Here, we found a similar relationship between age and hippocampal NDI at baseline, before treatment, in the canine model across all groups (Simple linear regression: R^2 = 0.111, p = 0.031; Figure 4.2). Moreover, we observed a similar relationship between age and parahippocampal NDI (R^2 = 0.131, p = 0.018; Figure 4.2). This relationship between age and NDI was insignificant overall when averaging over the entire temporal lobe (R^2 = 0.008, p = 0.567), suggesting a focused change in these regions with age.

To determine whether these results were driven by gray matter or white matter voxels, we classified individual voxels in these regions into gray or white matter by FA-thresholding. Those voxels with FA > 0.4 were classified as likely-white matter voxels while those with FA < 0.4 were classified as likely-gray matter voxels (M. Kumar et al., 2016). We found that the ratio of gray matter to white matter voxels was, on average, 7.48 : 1 in the hippocampus and 9.07 : 1 in the parahippocampal gyrus, suggesting that a clear majority of the signal we were detecting in these ROIs was driven by gray matter. Moreover, removal of the white matter voxels from the regions of interest when averaging across the parametric maps did not significantly change the results.

None of the other studied metrics showed a reliable relationship with age in the hippocampus or the parahippocampal gyrus- further bolstering our claim that the NDI might be capturing unique aging-associated microstructural properties in hippocampal and parahippocampal gray matter not typically detected by simple tensor metrics. We found no significant differences in NDI between hemispheres in both regions. Our male/female distribution did not permit us to test for sex differences.
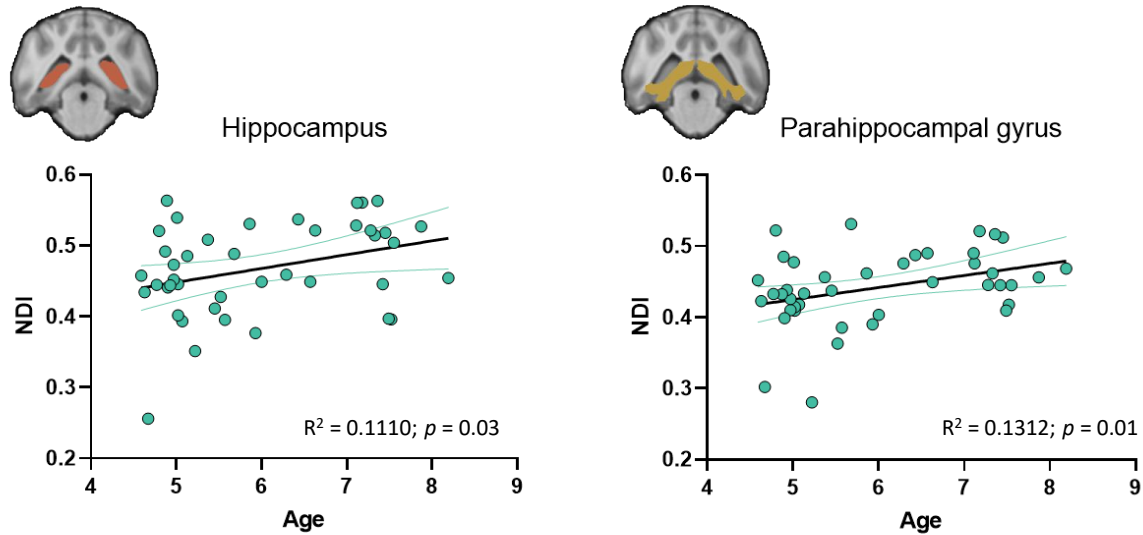
Figure 4.2: At baseline, before treatment, the NDI of the hippocampus and the parahippocampal gyrus are positively correlated with age. Individual dots represent individual subjects. The line of best fit is in black, and the teal lines represent 95% confident intervals.

4.3.2 One-year treatment with tacrolimus results in a decrease in hippocampal and parahippocampal NDI and an increase in parahippocampal ODI.

Dogs treated with tacrolimus for a year had significantly lowered hippocampal (Repeated measures ANOVA, Šídák's multiple comparisons test: t = 3.976, p = 0.001, DF = 25) and parahippocampal (t = 3.711, p = 0.002, DF = 25) NDI as compared to baseline, suggesting that the drug might be rescuing some level of age-associated change (Figure 4.3). Such a change was not observed between the time points for the control dogs in either of the regions. Though the dogs are not old enough to be exhibiting significant cognitive deficits (Milgram, 2003), previous studies in humans using structural equation modeling show that increased hippocampal NDI mediates age-related cognitive decline (Radhakrishnan

118

et al., 2020), indicating that the drug may have the potential to protect against cognitive deficits if administered for a longer period of time.

The parahippocampal ODI significantly increased after a year in the control dogs (t = 3.197, p = 0.007), but not in the dogs treated with tacrolimus (t = 0.082, p = 0.995). We also observed a critical interaction between drug and time on ODI (F = 4.660, p = 0.040, ANOVA). We did not notice any correlations between parahippocampal ODI and age at baseline (R^2 = 0.039, p = 0.805; Figure 4.4), possibly because the dogs are middle-aged, and we have a relatively restricted range. However, age-related increases in ODI have been reported in human studies with negative consequences (Mole et al., 2020; Nazeri et al., 2015; Venkatesh et al., 2020).

As with the previous analysis, removal of the white matter voxels from the regions of interest when averaging across the parametric maps did not significantly change the results. No other studied metric showed an effect of time or intervention in these regions. We found no significant difference in the diffusion metrics between hemispheres for all regions studied.
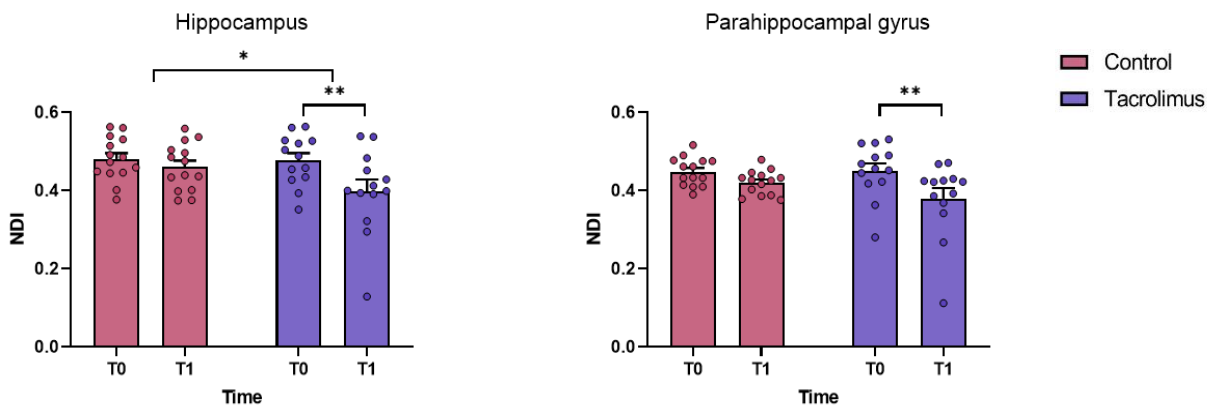
Figure 4.3: One-year treatment of tacrolimus significantly reduces the NDI in both the hippocampus (t = 3.976, p = 0.001) and the parahippocampal gyrus (t = 3.711, p = 0.002). There was a significant interaction between intervention and time in the hippocampus (F = 4.482, p = 0.044, ANOVA), but not in the parahippocampal gyrus (F = 2.579, p = 0.120). Error bars show standard error of the mean.
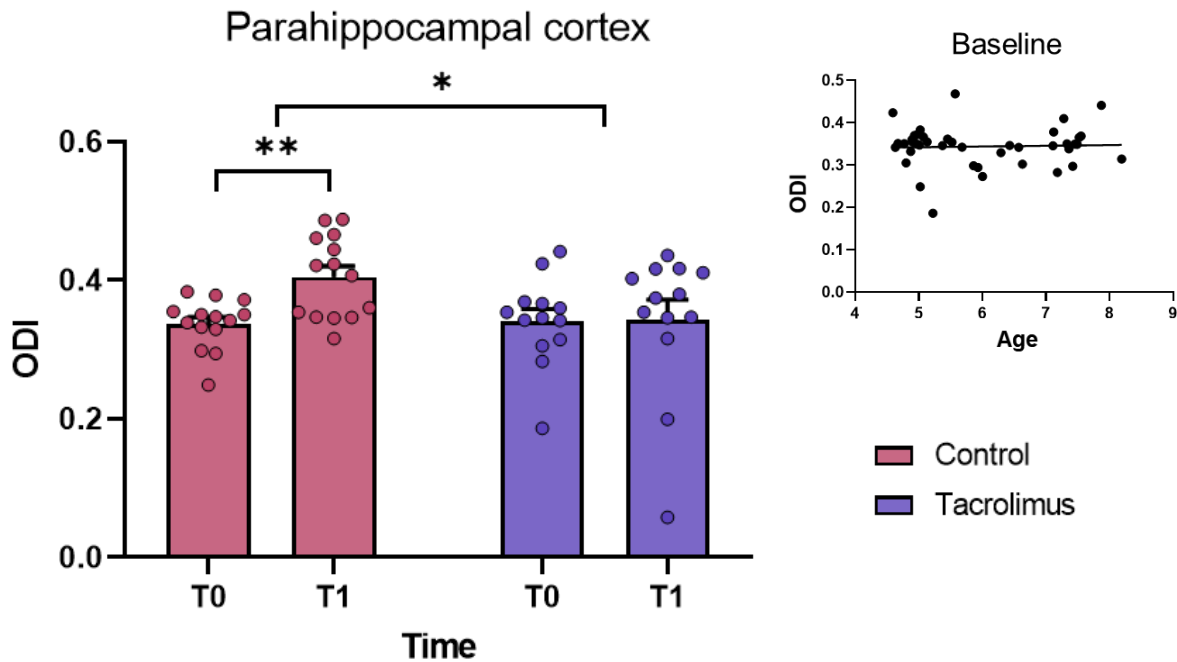
Figure 4.4: Though there was no correlation between age and parahippocampal ODI at baseline, the ODI of the parahippocampal gyrus increased in the control dogs after one year (t = 3.197, p = 0.007), but not in the dogs treated with tacrolimus (t = 0.082, p = 0.995), with a significant interaction between intervention and time (F = 4.660, p = 0.040, ANOVA). Error bars show standard error of the mean.

4.3.3 Tacrolimus protects against structural changes in the prefrontal cortex.

We next turned to changes outside of the hippocampal region. One of the first regions to be affected in the aging canine brain is the prefrontal cortex (PFC). MRI studies have

shown that the PFC starts reducing in volume at an earlier age (8-11 years) as compared to the hippocampus (Tapp et al., 2004). Cognitively, aging also leads to poorer performance on tasks associated with the PFC, like reversal learning and visuospatial memory (Head et al., 1998b; Studzinski et al., 2006; Tapp et al., 2003). While it is unclear if the prefrontal cortex is an early region affected by age-related neuroinflammation, it is one of the first areas in the canine brain to develop plaques (Bosch et al., 2012; Wieshmann et al., 1999). Formation of these plaques has consistently been reflected in diffusion MRI studies as a reduction of fractional anisotropy (Kealey et al., 2004; Tievsky et al., 1999; Wieshmann et al., 1999). It is not very surprising that we found no significant relationship between age and prefrontal NDI or ODI at baseline (NDI: R^2 = 0.001, p = 0.806; ODI: R^2 = 0.006, p = 0.608); and these metrics did not significantly change in either group over the year. However, despite the lack of a significant relationship between age and prefrontal FA at baseline (R^2 = 0.015, p = 0.440), it decreased in the control dogs after a year (t = 5.042, p < 0.001). This observation is directly analogous to the negative correlation between age and FA consistently observed in humans (Bennett et al., 2010; Kantarci et al., 2013). Interestingly, prefrontal FA did not decrease in the dogs treated with tacrolimus for a year (t = 1.890, p = 0.135), suggesting that the drug may be preventing age-associated structural deterioration in the prefrontal cortex (Figure 4.5). The lack of a cross-sectional relationship with age at baseline might be attributed to individual differences and the dogs not being old enough to exhibit clear differences.

We also segmented the PFC into white matter and gray matter regions as described in section 3.1. We found that the ratio of gray matter to white matter voxels was, on average,

60.55 : 1; showing that an overwhelming majority of the signal was driven by gray matter. Removal of the white matter voxels from the regions of interest when averaging across the parametric maps did not significantly change the results. No other studied metric showed an effect of time or intervention in these regions. All effects reported were bilateral. Our male/female distribution did not permit us to test for sex differences.
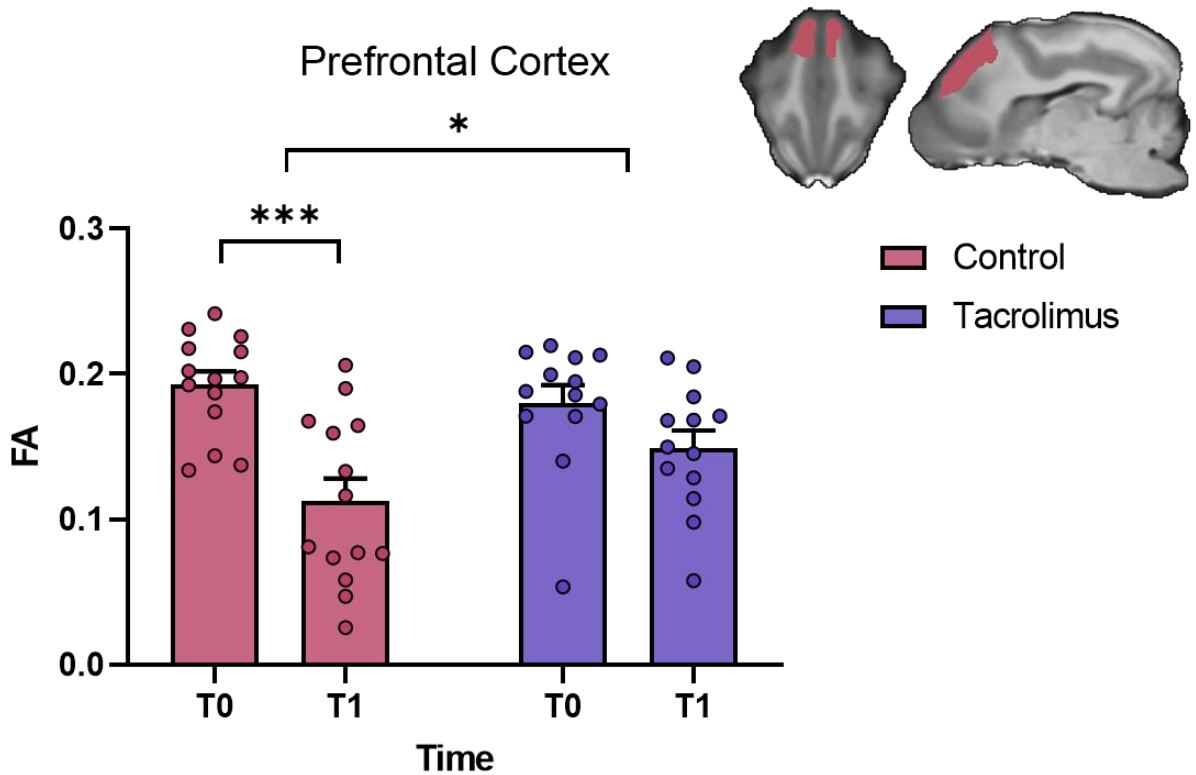

Figure 4.5: After one year, FA significantly reduced in the prefrontal cortex of the control dogs (t = 5.042, p < 0.0001), but not in the dogs treated with tacrolimus (t = 1.890, p = 0.135). The interaction between intervention and time was also significant (F = 4.568, p = 0.042, ANOVA). Error bars show standard error of the mean.

4.3.4 Whole brain exploratory analysis revealed disorganized decreases in white matter of the control dogs, but not of the dogs treated with tacrolimus.

Following these *a priori* regional analyses, we conducted a whole brain exploratory analysis to determine whether these changes were unique to these areas or whether they were found elsewhere as well. Voxel-wise comparisons were performed in a pairwise manner for each dog in both groups using AFNI's 3dttest++. We used the -clustsim option to determine the minimum cluster threshold to ensure an FDR corrected p-value of at least 0.05, with an alpha of 0.05. We observed a disorganized, but large-scale, decrease in FA in many white matter regions (Figure 4.6; 59207 voxels survived thresholding) in only the control dogs. This was not unexpected as the loss of white matter integrity is a classic hallmark of aging (Bennett et al., 2010; Madden et al., 2012; Vernooij et al., 2008). The dogs treated with tacrolimus did not show this same decrease (no voxels survived thresholding) further suggesting that the drug may be protecting against even sporadic neurodegeneration. However, these results should be interpreted cautiously as we found no significant interaction between intervention and time at our chosen thresholds i.e., no voxels survived thresholding when comparing the difference image in time (T0 – T1) between the two groups.

Interestingly, no other diffusion metric studied exhibited reliable differences over time in either group, suggesting a very specific age-related decrease in the control dogs in only the *a priori* regions, and a distinct protection against this effect by the drug. This finding bolsters our theory that NDI and ODI are sensitive to specific microstructural changes

associated with age and may be early predictors of MTL pathology in these specific regions.
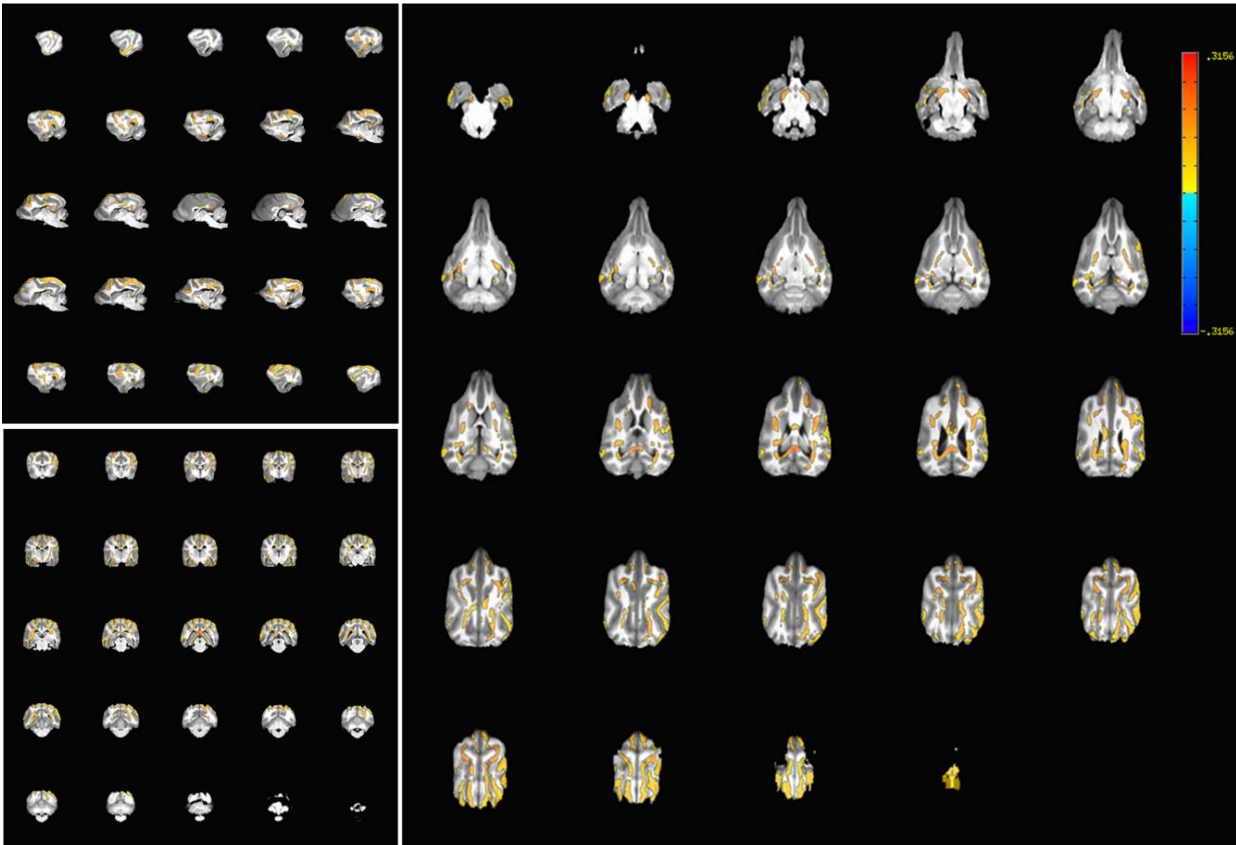
Figure 4.6: Difference in T0-T1 in FA of the control dogs. We found significant decreases in white matter FA after one year in control dogs, but not in the tacrolimus dogs. Colored regions show regions where the FA at T0 was significantly different from the FA at T1 for control dogs (Red - Yellow: T0>T1; Teal - Blue: T0<T1). Dogs treated with tacrolimus are not pictured here as there were no significant voxels of difference when comparing the two time points.

4.3.5 Limited cognitive changes were observed over time.

We also assessed the effect of age on baseline cognition as well as the interaction between intervention and cognition after a year. We observed no significant relationship between age and discrimination learning (R^2 = 0.014, p = 0.442) or reversal learning (R^2 = 0.017, p = 0.393). However, age had a negative effect on Spatial Accuracy [20s] (R^2 = 0.172, p =

0.007) and Spatial Accuracy [70s] (R^2 = 0.109, p = 0.036); but not with Spatial Accuracy [110s] (R^2 = 0.045, p = 0.186). After 1 year of intervention, there was no significant difference in either group with respect to discrimination learning (Control: p = 0.821; Tacrolimus: p = 0.628) or spatial accuracy (Control: p = 0.151, 0.796, 0.504; Tacrolimus: p = 0.999, 0.471, 0.625 for 20, 70 and 110s accuracy versions respectively). Performance on reversal learning trended towards a decrease in error scores (i.e., better function) over time in the control dogs (p = 0.057) but not in the dogs treated with tacrolimus (p = 0.112). After the removal of an outlier in the tacrolimus group, this effect of time was significant in both groups (Control: p = 0.041; Tacrolimus: p = 0.029). These data, in conjunction, suggest that while these dogs are not exhibiting major cognitive decline, continued treatment will allow for more opportunities to see improvements. To that end, continued treatment may also be able to reveal whether the structural protection that tacrolimus grants to the study group translates to cognitive benefits as well. None of the cognitive scores studied were significantly correlated with the diffusion metrics; possibly because the middle-aged dogs do not yet show significant decline but are already displaying signs of microstructural deterioration.

4.4. DISCUSSION

In this study, we used the drug tacrolimus to test the hypothesis that calcineurin inhibitors can prevent aging-related pathology, as measured by neuroimaging, in the middle-aged canine. We observed a positive correlation between hippocampal and parahippocampal NDI with age at baseline; a relationship that agreed with our observations in humans from previous studies (Radhakrishnan et al., 2020; Venkatesh et

al., 2020). Interestingly, one-year treatment with tacrolimus resulted in a decrease in both hippocampal and parahippocampal NDI, while the control dogs did not exhibit this effect. The drug also protected against an increase in parahippocampal ODI and a decrease in prefrontal FA, both consistently recognized as negative consequences of aging. We also showed that these changes precede most widespread volumetric changes and all cognitive changes and are specific to the *a priori* regions studied. These data, put together, suggest that i) calcineurin inhibitors may rescue negative microstructural outcomes associated with age and ii) advanced diffusion imaging measures may be valuable biomarkers for predicting aging-associated pathology well before other symptoms are present.

The overexpression of calcineurin helps drive neuroinflammation and astrogliosis, commonly observed in aging (Norris et al., 2005; Reese & Taglialatela, 2011; Rusnak & Mertz, 2000). Even though neuroinflammation is ultimately a systemic consequence of age, the dogs we studied are not old enough to exhibit these changes globally (Section 3.4). However, the hippocampus and nearby regions are thought to be some of the initial hotspots of such inflammation (Akiyama et al., 2000; Gavilán et al., 2007; Head, 2011; Verbitsky et al., 2004), which could potentially be captured in our middle-aged model. Older dogs display an increase in GFAP immunoreactivity and protein levels in the hippocampus and neighboring regions, as well as increased astrogliosis and astrocyte hypertrophy (Borràs et al., 1999; Hwang et al., 2008; Pugliese et al., 2006). While there are currently no effective methods to measure such inflammatory changes non-invasively, several mouse studies have demonstrated reliable positive correlations between both the

NDI and the ODI with immunoreactivity, astrocyte reactivity, and microglia count (Colgan et al., 2016; Grussu et al., 2017; Wang et al., 2019). Here, we showed that tacrolimus reduces hippocampal and parahippocampal NDI after just a year of treatment. Though neuropathological outcomes have not yet been obtained, increases in NDI in gray matter regions could be a consequence of inflammation, as microglial and astrocyte swelling cause the cells to expand, resulting in an increase in intracellular volume fraction, which is estimated by NDI (Colgan et al., 2016; Garcia-Hernandez et al., 2020). The hypothesis that tacrolimus may prevent neuroinflammation is further supported by our finding that it protects against an increase in parahippocampal ODI, which could be a marker for microglial density (Colgan et al., 2016; Garcia-Hernandez et al., 2020; Yi et al., 2019). Region-specific increases in microglial densities in the hippocampus and parahippocampal regions also precede plaque formation and are suppressed in mouse models of AD by inhibition of calcineurin signaling pathways (Furman et al., 2012; Sompol & Norris, 2018), again suggesting that tacrolimus administration in dogs may be protecting against aging-related pathological changes through calcineurin inhibition (Fakhoury, 2018; Marlatt et al., 2014). However, these theories must be handled cautiously, as we are yet to find adequate histological evidence for the neurobiological specificity of NODDI metrics.

We also found that tacrolimus protects against an age-associated decrease in prefrontal FA, suggesting that the drug may be capable of preventing, or at least delaying, the formation of amyloid plaques (Andrews-Hanna et al., 2007; Kantarci et al., 2017; Nasrabady et al., 2018), again, consistent with the effects of calcineurin inhibition in

rodent models (Hong et al., 2010). Moreover, the dogs showed no adverse effects on kidney function as a consequence of the drug, as measured by blood urea nitrogen (BUN), creatine, and phosphorous levels in the blood reducing concerns that tacrolimus might cause nephrotoxicity in this model.

Perhaps most striking is the fact that these effects are specific to the prefrontal and hippocampal regions in both groups of dogs. Other than the drug protecting against global neurodegeneration in white matter (reflected as a decrease in FA in the control dogs, but not those treated with tacrolimus), the diffusion metrics in no other brain regions, except those considered *a priori* aging hotspots, changed after a year. This specificity and the fact that these protections are displayed before cognitive decline is promising. These results strongly support the potential of tacrolimus to prevent age-related pathological decline and suggest that similar drugs could be used as middle-aged preventative care in humans. More research on the neurobiological mechanisms of calcineurin inhibitors would help indicate a more specific time frame in the human lifespan in which these drugs could be most effective in preventing neuropathology.

The results from this study also suggest a compelling case for using higher-order diffusion imaging measures. NDI, ODI, and even tensor metrics like FA computed on multi-shell data, all show potential to be early biomarkers for aging-related pathology. They may be sensitive to microstructural alterations preceding other measurable pathologies and capture these changes well before gross atrophy or cognitive decline is present. Acquisition of higher-order, multi-shell data allows for both forms of analyses, and the complexity and tissue-agnostic approach of NODDI (Zhang et al., 2012) makes it far more

applicable to the study of gray matter microstructure and longitudinal change that may result from AD-associated neuropathological changes (e.g., inflammation and astrogliosis).

This study provides novel outcomes that include 1) evidence for treatment benefits of tacrolimus on brain structure before cognitive decline; 2) support for a canine model that shows changes in NODDI metrics that can be detected both in both cross-sectional and longitudinal studies. However, this study is not without limitations. The advanced diffusion metrics, specifically NDI and ODI, have not been adequately histologically validated; and though some studies suggest that they might be sensitive to inflammation, these results must be interpreted cautiously. The male/female ratio prevents us from assessing sex differences, and these results may not be as significant in male beagles. However, all male dogs studied had diffusion metrics well within the range of their female counterparts, with no significant outliers. Moreover, dogs were middle-aged without signs of significant cognitive decline, posing a challenge to detect structure-behavior relationships. Unfortunately, both groups showed a significant decrease in hippocampal volume after one year- suggesting that the drug may not be able to protect against more macrostructural atrophy. The study will continue for another year and our hypothesis that structural brain changes occur before cognitive decline may be testable at the next time point. Also, future neuropathology outcome measures will help us determine if our speculations regarding FA and Aβ, and NDI and glial activation/inflammation are valid.

In summary, treatment with low doses of tacrolimus in the canine model of aging protects against age-associated structural changes, as shown by neuroimaging, and presents no

observable adverse effects. It is intriguing to consider that the structural neuroimaging outcomes noted here may precede cognitive decline in control dogs and may predict benefits in treated animals, which will be evaluated as the study continues.

References

Abdul, H.M., Sama, M.A., Furman, J.L., Mathis, D.M., Beckett, T.L., Weidner, A.M., Patel, E.S., Baig, I., Murphy, M.P., LeVine, H., Kraner, S.D., Norris, C.M., 2009. Cognitive decline in Alzheimer's disease is associated with selective changes in calcineurin/NFAT signaling. J. Neurosci. 29, 12957–12969. https://doi.org/10.1523/JNEUROSCI.1064-09.2009

Abe, O., Aoki, S., Hayashi, N., Yamada, H., Kunimatsu, A., Mori, H., Yoshikawa, T., Okubo, T., Ohtomo, K., 2002. Normal aging in the central nervous system: quantitative MR diffusion-tensor analysis. Neurobiology of Aging 23, 433–441. https://doi.org/10.1016/S0197-4580(01)00318-9

Andersson, J.L.R., Sotiropoulos, S.N., 2016. An integrated approach to correction for off-resonance effects and subject movement in diffusion MR imaging. NeuroImage 125, 1063–1078. https://doi.org/10.1016/j.neuroimage.2015.10.019

Andrews-Hanna, J.R., Snyder, A.Z., Vincent, J.L., Lustig, C., Head, D., Raichle, M.E., Buckner, R.L., 2007. Disruption of large-scale brain systems in advanced aging. Neuron 56, 924–935.

Basser, P.J., Mattiello, J., LeBihan, D., 1994. MR diffusion tensor spectroscopy and imaging. Biophysical Journal 66, 259–267. https://doi.org/10.1016/S0006-3495(94)80775-1

Bennett, I.J., Madden, D.J., Vaidya, C.J., Howard, D.V., Howard, J.J., 2010. Age-related differences in multiple measures of white matter integrity: A diffusion tensor imaging study of healthy aging. Hum Brain Mapp 31, 378–90. https://doi.org/10.1002/hbm.20872

Billiet, T., Vandenbulcke, M., Mädler, B., Peeters, R., Dhollander, T., Zhang, H., Deprez, S., Van den Bergh, B.R.H., Sunaert, S., Emsell, L., 2015. Age-related microstructural differences quantified using myelin water imaging and advanced diffusion MRI. Neurobiol. Aging 36, 2107–2121. https://doi.org/10.1016/j.neurobiolaging.2015.02.029

Borràs, D., Ferrer, I., Pumarola, M., 1999. Age-related Changes in the Brain of the Dog. Vet Pathol 36, 202–211. https://doi.org/10.1354/vp.36-3-202

Bosch, M.N., Pugliese, M., Gimeno-Bayón, J., Rodríguez, M.J., Mahy, N., 2012. Dogs with cognitive dysfunction syndrome: a natural model of Alzheimer's disease. Curr Alzheimer Res 9, 298–314. https://doi.org/10.2174/156720512800107546

Budde, M.D., Kim, J.H., Liang, H.-F., Schmidt, R.E., Russell, J.H., Cross, A.H., Song, S.-K., 2007. Toward accurate diagnosis of white matter pathology using diffusion tensor imaging. Magnetic Resonance in Medicine 57, 688–695. https://doi.org/10.1002/mrm.21200

Christie, L.-A., Studzinski, C.M., Araujo, J.A., Leung, C.S.K., Ikeda-Douglas, C.J., Head, E., Cotman, C.W., Milgram, N.W., 2005. A comparison of egocentric and allocentric age-dependent spatial learning in the beagle dog. Progress in Neuro-Psychopharmacology and Biological Psychiatry, canine model of cognitive aging: further developments and practical applications 29, 361–369. https://doi.org/10.1016/j.pnpbp.2004.12.002

Chua, T.C., Wen, W., Slavin, M.J., Sachdev, P.S., 2008. Diffusion tensor imaging in mild cognitive impairment and Alzheimer's disease: a review. Curr.Opin.Neurol. 21, 83–92.

Colgan, N., Siow, B., O'Callaghan, J.M., Harrison, I.F., Wells, J.A., Holmes, H.E., Ismail, O., Richardson, S., Alexander, D.C., Collins, E.C., Fisher, E.M., Johnson, R., Schwarz, A.J., Ahmed, Z., O'Neill, M.J., Murray, T.K., Zhang, H., Lythgoe, M.F., 2016. Application of neurite orientation dispersion and density imaging (NODDI) to a tau pathology model of Alzheimer's disease. NeuroImage 125, 739–744. https://doi.org/10.1016/j.neuroimage.2015.10.043

Cox, R.W., 1996. AFNI: software for analysis and visualization of functional magnetic resonance neuroimages. Comput Biomed Res 29, 162–173.

Czeibert, K., Andics, A., Petneházy, Ö., Kubinyi, E., 2019. A detailed canine brain label map for neuroimaging analysis. Biologia Futura 70, 112–120. https://doi.org/10.1556/019.70.2019.14

Dalgaard, L., 2015. Comparison of minipig, dog, monkey and human drug metabolism and disposition. Journal of Pharmacological and Toxicological Methods 74, 80–92. https://doi.org/10.1016/j.vascn.2014.12.005

Datta, R., Lee, J., Duda, J., Avants, B.B., Vite, C.H., Tseng, B., Gee, J.C., Aguirre, G.D., Aguirre, G.K., 2012. A Digital Atlas of the Dog Brain. PLOS ONE 7, e52140. https://doi.org/10.1371/journal.pone.0052140

Dos Santos Picanco, L.C., Ozela, P.F., de Fatima de Brito, M., Pinheiro, A.A., Padilha, E.C., Braga, F.S., de Paula da Silva, C.H.T., Dos Santos, C.B.R., Rosa, J.M.C., da Silva Hage-Melim, L.I., 2018. Alzheimer's Disease: A Review from the Pathophysiology to Diagnosis, New Perspectives for Pharmacological Treatment. Curr. Med. Chem. 25, 3141–3159. https://doi.org/10.2174/0929867323666161213101126

Ezekiel, F., Chao, L., Kornak, J., Du, A.-T., Cardenas, V., Truran, D., Jagust, W., Chui, H., Miller, B., Yaffe, K., Schuff, N., Weiner, M., 2004. Comparisons between global and focal brain atrophy rates in normal aging and Alzheimer disease: Boundary Shift Integral versus tracing of the entorhinal cortex and hippocampus. Alzheimer Dis Assoc Disord 18, 196–201.

Fakhoury, M., 2018. Microglia and Astrocytes in Alzheimer's Disease: Implications for Therapy. Curr Neuropharmacol 16, 508–518. https://doi.org/10.2174/1570159X15666170720095240

Forestier, A., Douki, T., De Rosa, V., Béal, D., Rachidi, W., 2015. Combination of Aβ Secretion and Oxidative Stress in an Alzheimer-Like Cell Line Leads to the Over-Expression of the Nucleotide Excision Repair Proteins DDB2 and XPC. Int J Mol Sci 16, 17422–17444. https://doi.org/10.3390/ijms160817422

Forman, S.D., Cohen, J.D., Fitzgerald, M., Eddy, W.F., Mintun, M.A., Noll, D.C., 1995. Improved assessment of significant activation in functional magnetic resonance imaging (fMRI): use of a cluster-size threshold. Magn Reson Med 33, 636–647. https://doi.org/10.1002/mrm.1910330508

Furman, J.L., Sama, D.M., Gant, J.C., Beckett, T.L., Murphy, M.P., Bachstetter, A.D., Van Eldik, L.J., Norris, C.M., 2012. Targeting Astrocytes Ameliorates Neurologic Changes in a Mouse Model of Alzheimer's Disease. J Neurosci 32, 16129–16140. https://doi.org/10.1523/JNEUROSCI.2323-12.2012

Garcia-Hernandez, R., Carpena, A.T., Drakesmith, M., Koller, K., Jones, D.K., Canals, S., Santis, S.D., 2020. Imaging Microglia and Astrocytes non-invasively using Diffusion MRI (preprint). Neuroscience. https://doi.org/10.1101/2020.02.07.938910

Grieve, S.M., Williams, L.M., Paul, R.H., Clark, C.R., Gordon, E., 2007. Cognitive aging, executive function, and fractional anisotropy: a diffusion tensor MR imaging study. AJNR Am J Neuroradiol 28, 226–235.

Grussu, F., Schneider, T., Tur, C., Yates, R.L., Tachrount, M., Ianuş, A., Yiannakas, M.C., Newcombe, J., Zhang, H., Alexander, D.C., DeLuca, G.C., Gandini Wheeler-Kingshott, C.A.M., 2017. Neurite dispersion: a new marker of multiple sclerosis spinal cord pathology? Annals of Clinical and Translational Neurology 4, 663–679. https://doi.org/10.1002/acn3.445

Hardy, J.A., Higgins, G.A., 1992. Alzheimer's disease: the amyloid cascade hypothesis. Science 256, 184–186.

Harms, R.L., Fritz, F.J., Tobisch, A., Goebel, R., Roebroeck, A., 2017. Robust and fast nonlinear optimization of diffusion MRI microstructure models. NeuroImage 155, 82–96. https://doi.org/10.1016/j.neuroimage.2017.04.064

Head, E., 2011. Neurobiology of the aging dog. Age (Dordr) 33, 485–496. https://doi.org/10.1007/s11357-010-9183-3

Head, E., Callahan, H., Muggenburg, B.A., Cotman, C.W., Milgram, N.W., 1998a. Visual-discrimination learning ability and beta-amyloid accumulation in the dog. Neurobiol Aging 19, 415–425. https://doi.org/10.1016/s0197-4580(98)00084-0

Head, E., Callahan, H., Muggenburg, B.A., Cotman, C.W., Milgram, N.W., 1998b. Visual-discrimination learning ability and beta-amyloid accumulation in the dog. Neurobiol Aging 19, 415–425. https://doi.org/10.1016/s0197-4580(98)00084-0

Head, E., Pop, V., Vasilevko, V., Hill, M., Saing, T., Sarsoza, F., Nistor, M., Christie, L.-A., Milton, S., Glabe, C., Barrett, E., Cribbs, D., 2008. A Two-Year Study with Fibrillar β-Amyloid (Aβ) Immunization in Aged Canines: Effects on Cognitive Function and Brain Aβ. J. Neurosci. 28, 3555–3566. https://doi.org/10.1523/JNEUROSCI.0208-08.2008

Hendrie, H.C., Hake, A., Lane, K., Purnell, C., Unverzagt, F., Smith-Gamble, V., Murrell, J., Ogunniyi, A., Baiyewu, O., Callahan, C., Saykin, A., Taylor, S., Hall, K., Gao, S., 2015. Statin Use, Incident Dementia and Alzheimer Disease in Elderly African Americans. Ethn Dis 25, 345–354. https://doi.org/10.18865/ed.25.3.345

Hoffman, J.M., Creevy, K.E., Franks, A., O'Neill, D.G., Promislow, D.E.L., 2018. The companion dog as a model for human aging and mortality. Aging Cell 17, e12737. https://doi.org/10.1111/acel.12737

Holm, S., 1979. A Simple Sequentially Rejective Multiple Test Procedure. Scandinavian Journal of Statistics 6, 65–70.

Holtzman, D.M., John, C.M., Goate, A., 2011. Alzheimer's Disease: The Challenge of the Second Century. Sci Transl Med 3, 77sr1. https://doi.org/10.1126/scitranslmed.3002369

Hong, H.-S., Hwang, J.-Y., Son, S.-M., Kim, Y.-H., Moon, M., Inhee, M.-J., 2010. FK506 reduces amyloid plaque burden and induces MMP-9 in AβPP/PS1 double transgenic mice. J Alzheimers Dis 22, 97–105. https://doi.org/10.3233/JAD-2010-100261

Hsu, J.-L., Leemans, A., Bai, C.-H., Lee, C.-H., Tsai, Y.-F., Chiu, H.-C., Chen, W.-H., 2008. Gender differences and age-related white matter changes of the human brain: a diffusion tensor imaging study. Neuroimage 39, 566–577. https://doi.org/10.1016/j.neuroimage.2007.09.017

Hudry, E., Wu, H.-Y., Arbel-Ornath, M., Hashimoto, T., Matsouaka, R., Fan, Z., Spires-Jones, T.L., Betensky, R.A., Bacskai, B.J., Hyman, B.T., 2012. Inhibition of the NFAT pathway

alleviates amyloid β neurotoxicity in a mouse model of Alzheimer's disease. J Neurosci 32, 3176–3192. https://doi.org/10.1523/JNEUROSCI.6439-11.2012

Hwang, I.K., Choi, J.H., Li, H., Yoo, K.-Y., Kim, D.W., Lee, C.H., Yi, S.S., Seong, J.K., Lee, I.S., Yoon, Y.S., Won, M.-H., 2008. Changes in glial fibrillary acidic protein immunoreactivity in the dentate gyrus and hippocampus proper of adult and aged dogs. J Vet Med Sci 70, 965–969. https://doi.org/10.1292/jvms.70.965

Inouye, K., Pedrazzani, E.S., Pavarini, S.C.I., 2010. [Alzheimer's disease influence on the perception of quality of life from the elderly people]. Rev Esc Enferm USP 44, 1093–1099. https://doi.org/10.1590/s0080-62342010000400034

Jenkinson, M., Beckmann, C.F., Behrens, T.E.J., Woolrich, M.W., Smith, S.M., 2012. FSL. Neuroimage 62, 782–790. https://doi.org/10.1016/j.neuroimage.2011.09.015

Jones, E., Oliphant, T., Peterson, P., 2001. SciPy: Open Source Scientific Tools for Python [WWW Document]. SciPy.org. URL https://www.scipy.org (accessed 8.12.19).

Kantarci, K., Murray, M.E., Schwarz, C.G., Reid, R., Przybelski, S.A., Lesnick, T., Zuk, S.M., Raman, M.R., Senjem, M.L., Gunter, J.L., Boeve, B.F., Knopman, D.S., Parisi, J.E., Petersen, R.C., Jack, C.R., Dickson, D., 2017. White Matter Integrity on DTI and the Pathologic Staging of Alzheimer's Disease. Neurobiol Aging 56, 172–179. https://doi.org/10.1016/j.neurobiolaging.2017.04.024

Kantarci, K., Weigand, S.D., Przybelski, S.A., Preboske, G.M., Pankratz, V.S., Vemuri, P., Senjem, M.L., Murphy, M.C., Gunter, J.L., Machulda, M.M., Ivnik, R.J., Roberts, R.O., Boeve, B.F., Rocca, W.A., Knopman, D.S., Petersen, R.C., Jack, C.J., 2013. MRI and MRS predictors of mild cognitive impairment in a population-based sample. Neurology 81, 126–33. https://doi.org/10.1212/WNL.0b013e31829a3329

Kealey, S.M., Kim, Y., Provenzale, J.M., 2004. Redefinition of Multiple Sclerosis Plaque Size Using Diffusion Tensor MRI. American Journal of Roentgenology 183, 497–503. https://doi.org/10.2214/ajr.183.2.1830497

Kellner, E., Dhital, B., Kiselev, V.G., Reisert, M., 2016. Gibbs-ringing artifact removal based on local subvoxel-shifts: Gibbs-Ringing Artifact Removal. Magnetic Resonance in Medicine 76, 1574–1581. https://doi.org/10.1002/mrm.26054

Kumar, A., Singh, N., 2017. Calcineurin inhibitors improve memory loss and neuropathological changes in mouse model of dementia. Pharmacology Biochemistry and Behavior 153, 147–159. https://doi.org/10.1016/j.pbb.2016.12.018

Kumar, M., Duda, J., Yoon, S., Bagel, J., O'Donnell, P., Vite, C., Pickup, S., Gee, J., Wolfe, J., Poptani, H., 2016. Diffusion Tensor Imaging for Assessing Brain Gray and White Matter Abnormalities in a Feline Model of a-Mannosidosis. Journal of Neuropathology and Experimental Neurology 75, 1–9. https://doi.org/10.1093/jnen/nlv007

Liu, F., Grundke-Iqbal, I., Iqbal, K., Oda, Y., Tomizawa, K., Gong, C.-X., 2005. Truncation and activation of calcineurin A by calpain I in Alzheimer disease brain. J Biol Chem 280, 37755–37762. https://doi.org/10.1074/jbc.M507475200

Liu, J., Liu, Z., Zhang, Y., Yin, F., 2015. A novel antagonistic role of natural compound icariin on neurotoxicity of amyloid β peptide. Indian J Med Res 142, 190–195. https://doi.org/10.4103/0971-5916.164254

Madden, D.J., Bennett, I.J., Burzynska, A., Potter, G.G., Chen, N.K., Song, A.W., 2012. Diffusion tensor imaging of cerebral white matter integrity in cognitive aging. Biochim Biophys Acta 1822, 386–400. https://doi.org/10.1016/j.bbadis.2011.08.003

Malleret, G., Haditsch, U., Genoux, D., Jones, M.W., Bliss, T.V., Vanhoose, A.M., Weitlauf, C., Kandel, E.R., Winder, D.G., Mansuy, I.M., 2001. Inducible and reversible enhancement of learning, memory, and long-term potentiation by genetic inhibition of calcineurin. Cell 104, 675–686. https://doi.org/10.1016/s0092-8674(01)00264-1

Mansuy, I.M., 2003. Calcineurin in memory and bidirectional plasticity. Biochem. Biophys. Res. Commun. 311, 1195–1208. https://doi.org/10.1016/j.bbrc.2003.10.046

Margarit, C., Rimola, A., Gonzalez-Pinto, I., Cuervas-Mons, V., Edo, A., Andreu, H., Moreno-Gonzalez, E., Calleja, J.L., 1998. Efficacy and safety of oral low-dose tacrolimus treatment in liver transplantation. Transpl Int 11 Suppl 1, S260-266. https://doi.org/10.1007/s001470050474

Marlatt, M.W., Bauer, J., Aronica, E., van Haastert, E.S., Hoozemans, J.J.M., Joels, M., Lucassen, P.J., 2014. Proliferation in the Alzheimer Hippocampus Is due to Microglia, Not Astroglia, and Occurs at Sites of Amyloid Deposition. Neural Plast 2014. https://doi.org/10.1155/2014/693851

Milgram, N.W., 2003. Cognitive Experience and Its Effect on Age-Dependent Cognitive Decline in Beagle Dogs. Neurochem Res 28, 1677–1682. https://doi.org/10.1023/A:1026009005108

Milgram, N.W., Adams, B., Callahan, H., Head, E., Mackay, B., Thirlwell, C., Cotman, C.W., 1999. Landmark Discrimination Learning in the Dog. Learn Mem 6, 54–61.

Milgram, N.W., Zicker, S.C., Head, E., Muggenburg, B.A., Murphey, H., Ikeda-Douglas, C.J., Cotman, C.W., 2002. Dietary enrichment counteracts age-associated cognitive dysfunction in canines. Neurobiol Aging 23, 737–745. https://doi.org/10.1016/s0197-4580(02)00020-9

Mohmmad Abdul, H., Baig, I., Levine, H., Guttmann, R.P., Norris, C.M., 2011. Proteolysis of calcineurin is increased in human hippocampus during mild cognitive impairment and is stimulated by oligomeric Abeta in primary cell culture. Aging Cell 10, 103–113. https://doi.org/10.1111/j.1474-9726.2010.00645.x

Mole, J.P., Fasano, F., Evans, J., Sims, R., Kidd, E., Aggleton, J.P., Metzler-Baddeley, C., 2020. APOE-ε4-related differences in left thalamic microstructure in cognitively healthy adults. Scientific Reports 10, 19787. https://doi.org/10.1038/s41598-020-75992-9

Nasrabady, S.E., Rizvi, B., Goldman, J.E., Brickman, A.M., 2018. White matter changes in Alzheimer's disease: a focus on myelin and oligodendrocytes. Acta Neuropathol Commun 6. https://doi.org/10.1186/s40478-018-0515-3

Nazeri, A., Chakravarty, M.M., Rotenberg, D.J., Rajji, T.K., Rathi, Y., Michailovich, O.V., Voineskos, A.N., 2015. Functional consequences of neurite orientation dispersion and density in humans across the adult lifespan. J. Neurosci. 35, 1753–1762. https://doi.org/10.1523/JNEUROSCI.3979-14.2015

Nitzsche, B., Boltze, J., Ludewig, E., Flegel, T., Schmidt, M.J., Seeger, J., Barthel, H., Brooks, O.W., Gounis, M.J., Stoffel, M.H., Schulze, S., 2019. A stereotaxic breed-averaged, symmetric T2w canine brain atlas including detailed morphological and volumetrical data sets. Neuroimage 187, 93–103. https://doi.org/10.1016/j.neuroimage.2018.01.066

Norris, C.M., Kadish, I., Blalock, E.M., Chen, K.-C., Thibault, V., Porter, N.M., Landfield, P.W., Kraner, S.D., 2005. Calcineurin Triggers Reactive/Inflammatory Processes in Astrocytes and Is Upregulated in Aging and Alzheimer's Models. J Neurosci 25, 4649–4658. https://doi.org/10.1523/JNEUROSCI.0365-05.2005

Pahnke, J., Walker, L.C., Scheffler, K., Krohn, M., 2009. Alzheimer's disease and blood–brain barrier function—Why have anti-β-amyloid therapies failed to prevent dementia progression?

Neuroscience & Biobehavioral Reviews 33, 1099–1108. https://doi.org/10.1016/j.neubiorev.2009.05.006

Patronek, G.J., Waters, D.J., Glickman, L.T., 1997. Comparative Longevity of Pet Dogs and Humans: Implications for Gerontology Research. J Gerontol A Biol Sci Med Sci 52A, B171–B178. https://doi.org/10.1093/gerona/52A.3.B171

Perl, D.P., 2010. Neuropathology of Alzheimer's Disease. Mt Sinai J Med 77, 32–42. https://doi.org/10.1002/msj.20157

Prpar Mihevc, S., Majdič, G., 2019. Canine Cognitive Dysfunction and Alzheimer's Disease – Two Facets of the Same Disease? Front Neurosci 13. https://doi.org/10.3389/fnins.2019.00604

Pugliese, M., Geloso, M.C., Carrasco, J.L., Mascort, J., Michetti, F., Mahy, N., 2006. Canine cognitive deficit correlates with diffuse plaque maturation and S100β (−) astrocytosis but not with insulin cerebrospinal fluid level. Acta Neuropathol 111, 519. https://doi.org/10.1007/s00401-006-0052-1

Radhakrishnan, H., Stark, S.M., Stark, C.E.L., 2020. Microstructural Alterations in Hippocampal Subfields Mediate Age-Related Memory Decline in Humans. Front. Aging Neurosci. 12, 94. https://doi.org/10.3389/fnagi.2020.00094

Raffelt, D., Tournier, J.-D., Rose, S., Ridgway, G.R., Henderson, R., Crozier, S., Salvado, O., Connelly, A., 2012. Apparent Fibre Density: a novel measure for the analysis of diffusion-weighted magnetic resonance images. Neuroimage 59, 3976–3994. https://doi.org/10.1016/j.neuroimage.2011.10.045

Reese, L.C., Taglialatela, G., 2011. A Role for Calcineurin in Alzheimer's Disease. Curr Neuropharmacol 9, 685–692. https://doi.org/10.2174/157015911798376316

Reese, L.C., Zhang, W., Dineley, K.T., Kayed, R., Taglialatela, G., 2008. SELECTIVE INDUCTION OF CALCINEURIN ACTIVITY AND SIGNALING BY OLIGOMERIC AMYLOID BETA. Aging Cell 7, 824–835. https://doi.org/10.1111/j.1474-9726.2008.00434.x

Reitz, C., Mayeux, R., 2014. Alzheimer disease: epidemiology, diagnostic criteria, risk factors and biomarkers. Biochem Pharmacol 88, 640–651. https://doi.org/10.1016/j.bcp.2013.12.024

Rojanathammanee, L., Floden, A.M., Manocha, G.D., Combs, C.K., 2015. Attenuation of microglial activation in a mouse model of Alzheimer's disease via NFAT inhibition. J Neuroinflammation 12, 42. https://doi.org/10.1186/s12974-015-0255-2

Rozkalne, A., Hyman, B.T., Spires-Jones, T.L., 2011. Calcineurin inhibition with FK506 ameliorates dendritic spine density deficits in plaque-bearing Alzheimer model mice. Neurobiol Dis 41, 650–654. https://doi.org/10.1016/j.nbd.2010.11.014

Rusnak, F., Mertz, P., 2000. Calcineurin: form and function. Physiol. Rev. 80, 1483–1521. https://doi.org/10.1152/physrev.2000.80.4.1483

Sarasa, M., Pesini, P., 2009. Natural Non-Trasgenic Animal Models for Research in Alzheimer's Disease. Curr Alzheimer Res 6, 171–178. https://doi.org/10.2174/156720509787602834

Shimada, A., Kuwamura, M., Awakura, T., Umemura, T., Itakura, C., 1992. An immunohistochemical and ultrastructural study on age-related astrocytic gliosis in the central nervous system of dogs. J Vet Med Sci 54, 29–36. https://doi.org/10.1292/jvms.54.29

Sompol, P., Furman, J.L., Pleiss, M.M., Kraner, S.D., Artiushin, I.A., Batten, S.R., Quintero, J.E., Simmerman, L.A., Beckett, T.L., Lovell, M.A., Murphy, M.P., Gerhardt, G.A., Norris, C.M., 2017. Calcineurin/NFAT Signaling in Activated Astrocytes Drives Network Hyperexcitability in Aβ-Bearing Mice. J Neurosci 37, 6132–6148. https://doi.org/10.1523/JNEUROSCI.0877-17.2017

Sompol, P., Norris, C.M., 2018. Ca2+, Astrocyte Activation and Calcineurin/NFAT Signaling in Age-Related Neurodegenerative Diseases. Front. Aging Neurosci. 10. https://doi.org/10.3389/fnagi.2018.00199

Song, S.-K., Sun, S.-W., Ju, W.-K., Lin, S.-J., Cross, A.H., Neufeld, A.H., 2003. Diffusion tensor imaging detects and differentiates axon and myelin degeneration in mouse optic nerve after retinal ischemia. Neuroimage 20, 1714–1722.

Stancu, I.-C., Vasconcelos, B., Terwel, D., Dewachter, I., 2014. Models of β-amyloid induced Tau-pathology: the long and "folded" road to understand the mechanism. Mol Neurodegener 9, 51. https://doi.org/10.1186/1750-1326-9-51

Studzinski, C., Christie, L., Araujo, J., Burnham, W., Head, E., Cotman, C., Milgram, N., 2006. Visuospatial function in the beagle dog: An early marker of cognitive decline in a model of human aging and dementia. Neurobiology of Learning and Memory 86, 197–204. https://doi.org/10.1016/j.nlm.2006.02.005

Su, M.-Y., Tapp, P.D., Vu, L., Chen, Y.-F., Chu, Y., Muggenburg, B., Chiou, J.-Y., Chen, C., Wang, J., Bracco, C., Head, E., 2005. A longitudinal study of brain morphometrics using serial magnetic resonance imaging analysis in a canine model of aging. Prog

Neuropsychopharmacol Biol Psychiatry 29, 389–397. https://doi.org/10.1016/j.pnpbp.2004.12.005

Taglialatela, G., Hogan, D., Zhang, W.-R., Dineley, K.T., 2009. Intermediate- and Long-Term Recognition Memory Deficits in Tg2576 Mice Are Reversed with Acute Calcineurin Inhibition. Behav Brain Res 200, 95–99. https://doi.org/10.1016/j.bbr.2008.12.034

Taglialatela, G., Rastellini, C., Cicalese, L., n.d. Reduced Incidence of Dementia in Solid Organ Transplant Patients Treated with Calcineurin Inhibitors. J Alzheimers Dis 47, 329–333. https://doi.org/10.3233/JAD-150065

Tapp, P.D., Head, K., Head, E., Milgram, N.W., Muggenburg, B.A., Su, M.-Y., 2006. Application of an automated voxel-based morphometry technique to assess regional gray and white matter brain atrophy in a canine model of aging. Neuroimage 29, 234–244. https://doi.org/10.1016/j.neuroimage.2005.07.043

Tapp, P.D., Siwak, C.T., Estrada, J., Head, E., Muggenburg, B.A., Cotman, C.W., Milgram, N.W., 2003. Size and reversal learning in the beagle dog as a measure of executive function and inhibitory control in aging. Learn Mem 10, 64–73. https://doi.org/10.1101/lm.54403

Tapp, P.D., Siwak, C.T., Gao, F.Q., Chiou, J.-Y., Black, S.E., Head, E., Muggenburg, B.A., Cotman, C.W., Milgram, N.W., Su, M.-Y., 2004. Frontal lobe volume, function, and beta-amyloid pathology in a canine model of aging. J Neurosci 24, 8205–8213. https://doi.org/10.1523/JNEUROSCI.1339-04.2004

Thal, D.R., Rüb, U., Orantes, M., Braak, H., 2002. Phases of A beta-deposition in the human brain and its relevance for the development of AD. Neurology 58, 1791–1800. https://doi.org/10.1212/wnl.58.12.1791

Tievsky, A.L., Ptak, T., Farkas, J., 1999. Investigation of Apparent Diffusion Coefficient and Diffusion Tensor Anisotropy in Acute and Chronic Multiple Sclerosis Lesions. American Journal of Neuroradiology 20, 1491–1499.

Tournier, J.-D., Calamante, F., Connelly, A., 2012. MRtrix: Diffusion tractography in crossing fiber regions. International Journal of Imaging Systems and Technology 22, 53–66. https://doi.org/10.1002/ima.22005

Tustison, N.J., Avants, B.B., Cook, P.A., Yuanjie Zheng, Egan, A., Yushkevich, P.A., Gee, J.C., 2010. N4ITK: Improved N3 Bias Correction. IEEE Transactions on Medical Imaging 29, 1310–1320. https://doi.org/10.1109/TMI.2010.2046908

Venkatesh, A., Stark, S.M., Stark, C.E.L., Bennett, I.J., 2020. Age- and memory- related differences in hippocampal gray matter integrity are better captured by NODDI compared to single-tensor diffusion imaging. Neurobiol Aging 96, 12–21. https://doi.org/10.1016/j.neurobiolaging.2020.08.004

Veraart, J., Fieremans, E., Novikov, D.S., 2016. Diffusion MRI noise mapping using random matrix theory: Diffusion MRI Noise Mapping. Magnetic Resonance in Medicine 76, 1582–1593. https://doi.org/10.1002/mrm.26059

Vernooij, M.W., de Groot, M., van der Lugt, A., Ikram, M.A., Krestin, G.P., Hofman, A., Niessen, W.J., Breteler, M.M.B., 2008. White matter atrophy and lesion formation explain the loss of structural integrity of white matter in aging. NeuroImage 43, 470–477. https://doi.org/10.1016/j.neuroimage.2008.07.052

Wang, N., Zhang, J., Cofer, G., Qi, Y., Anderson, R.J., White, L.E., Allan Johnson, G., 2019. Neurite orientation dispersion and density imaging of mouse brain microstructure. Brain Struct Funct 224, 1797–1813. https://doi.org/10.1007/s00429-019-01877-x

Wieshmann, U.C., Clark, C.A., Symms, M.R., Franconi, F., Barker, G.J., Shorvon, S.D., 1999. Reduced anisotropy of water diffusion in structural cerebral abnormalities demonstrated with diffusion tensor imaging. Magnetic Resonance Imaging 17, 1269–1274. https://doi.org/10.1016/S0730-725X(99)00082-X

Wu, H.-Y., Hudry, E., Hashimoto, T., Kuchibhotla, K., Rozkalne, A., Fan, Z., Spires-Jones, T., Xie, H., Arbel-Ornath, M., Grosskreutz, C.L., Bacskai, B.J., Hyman, B.T., 2010. Amyloid β Induces the Morphological Neurodegenerative Triad of Spine Loss, Dendritic Simplification, and Neuritic Dystrophies through Calcineurin Activation. J Neurosci 30, 2636–2649. https://doi.org/10.1523/JNEUROSCI.4456-09.2010

Yi, S.Y., Barnett, B.R., Torres-Velázquez, M., Zhang, Y., Hurley, S.A., Rowley, P.A., Hernando, D., Yu, J.-P.J., 2019. Detecting Microglial Density With Quantitative Multi-Compartment Diffusion MRI. Front. Neurosci. 13, 81. https://doi.org/10.3389/fnins.2019.00081

Zhang, H., Schneider, T., Wheeler-Kingshott, C.A., Alexander, D.C., 2012. NODDI: practical in vivo neurite orientation dispersion and density imaging of the human brain. Neuroimage 61, 1000–1016. https://doi.org/10.1016/j.neuroimage.2012.03.072

CHAPTER 5:

A pipeline to predict cell densities from diffusion metrics

The last few chapters have shown that diffusion metrics can capture important microstructural changes associated with pathology and cognition. These discoveries suggest the massive potential of DWI to non-invasively detect explicit neurobiological properties, beyond what is possible with the resolution of conventional neuroimaging. However, there is very little known about what neurobiological properties these metrics, especially those derived from NODDI, correspond to. While these diffusion metrics do not promise any inherent cell type specificity, different brain cells and even cell states have varying morphologies, which could influence the diffusion signal in many ways. This relationship is currently not well-characterized. Understanding the possible cytoarchitectural signatures of these measures would enable them to estimate different cell counts, potentially resulting in a very powerful clinical diagnostic tool. Here, using advanced diffusion imaging in the mouse brain, we demonstrate that different regions have unique relationships between cell counts and diffusion metrics. We then take advantage of this exclusivity, and introduce a framework to create region-specific models, which can be used to predict densities of different cell populations- including neurons and glia.

5.1 INTRODUCTION

While advances in immunohistochemistry and microscopy have been extremely valuable in capturing microstructural properties of the brain at cellular resolution, these techniques are not very feasible in human studies, and cannot be used *in vivo* and non-invasively. In the previous few chapters, we have established that modern diffusion analysis techniques may be well-equipped to non-invasively detect various aging and cognition-related microstructural properties in gray matter. However, perhaps because of the recency of these technological developments and the challenges of conducting such experiments, diffusion metrics suffer from inadequate validation and a severe lack of understanding of the specific neurobiological properties these metrics might be correlated to. Moreover, the sensitivity of these diffusion metrics is yet to be taken advantage of in a predictive capacity. Examining specific structural properties across scales of measurement would not only assist in delineating changes particular to certain disease and senescence states but could also enable the identification of valid noninvasive biomarkers specific to these states.

As diffusion imaging has evolved, the need for validating and re-examining these diffusion models has only become more pressing. Newer models hold the potential for higher accuracy and specificity. However, just as older diffusion techniques could only reliably predict white matter microstructure, most attempts to find histological correlations with diffusion metrics have primarily focused on white matter. Moreover, despite a growing number of potentially more advanced and powerful models, the diffusion tensor has remained the focus for most of these correlation studies [Table 5.1].

Model	Region of interest	Observations
Ex vivo wild type mice (Chang et al., 2016)	Corpus callosum, fimbria, fornix	FA: Positively correlated with myelin density
Ex vivo Rats with retinal ischemia (Rojas-Vite et al., 2019)	Optic nerve and chiasm	FA: positively correlated with axon density, volume fraction, and myelin volume fraction. Negatively correlated with axon diameter and myelin thickness.
Ex vivo Human with multiple sclerosis (Mottershead et al., 2003; Schmierer et al., 2007)	Whole-brain white matter, spinal cord white matter	FA: positively correlated with myelin density and axon count. MD: negatively correlated with myelin density and axon count.
Ex vivo Human with Alzheimer's Disease (Gouw et al., 2008)	Whole-brain white matter	FA: Positive correlated with axonal density
Ex vivo Elderly human (Back et al., 2011)	Prefrontal cortex white matter	FA: Negatively correlated with free radical injury and oligodendrocyte lineage marker. MD: Positively correlated with free radical injury, oligodendrocyte lineage marker, and myelin damage

In vivo human with temporal lobe epilepsy (Concha et al., 2010)	Fornix	FA: Positively correlated with total axon membrane circumference

Table 5.1: Analysis of studies correlating tensor metrics with cellular properties.

While studies in Table 5.1 have been very useful in understanding standard tensor metrics like fractional anisotropy and mean diffusivity, very few such studies have been conducted to correlate axonal structure measures obtained from histology with more advanced diffusion metrics. Even fewer have attempted to study this in gray matter, even though these more recent diffusion metrics may be effective at examining gray matter microstructure.

Moreover, the nomenclature of these diffusion metrics, like NDI which stands for "neurite density index", are often both misleading and vague. NDI simply attempts to measure intracellular volume fraction, and the brain has more cells than just neurons. Glial cells contribute significantly to diffusion metrics, but this is often overlooked to simplify the model. Recently, it was shown that another NODDI metric, the ODI, is positively correlated with microglial density (Yi et al., 2019), demonstrating the potential of these modern diffusion models to probabilistically estimate cell type-specific counts. Perhaps, even more interestingly, the different inflammatory states of astrocytes and microglia were found to be reflected in certain biophysical model-based diffusion metrics (Garcia-Hernandez et al., 2020, p.).

3D-BOND (3D Bridging of Optically-clear histology with Neuroimaging Data) is one of the only pipelines developed for registering medical images with 3D histology, with a

focus on bridging the gap between low-resolution MRI and cellular-resolution microscopy (Stolp et al., 2018). This study not only showed that axonal content was correlated with apparent fiber density (AFD), mean diffusivity (MD), and radial diffusivity (RD) in a 3D space, but it also demonstrated that metrics like MD and RD were associated with cell density. Even more specifically, FA was observed to be positively correlated with astrocyte density, suggesting that diffusion metrics had the potential to garner information beyond just white matter integrity. However, this study still relied on traditional tensor metrics and not higher-order NODDI metrics. Moreover, such studies often depend on simple linear regression models when comparing diffusion metrics with cellular properties, while it is likely that more mathematically complex models may better represent these relationships. Furthermore, these studies tend to overlook the highly complex spatial dynamics of the brain: different regions may present very different relationships between these metrics, and this is often ignored to generate potentially less accurate but general brain models.

In this chapter, we outline a pipeline to not only further understand the cytoarchitectural basis for the diffusion metrics discussed in this thesis, but also provide a framework to non-invasively predict cell counts using them. We first demonstrate that a single model is not capable of capturing the morphological complexity of the whole brain, and different regions have different diffusion metric/cell count relationships. Next, using the CA1 region of the hippocampus as a test case, we successfully develop an algorithm that can separately predict the counts of different cell types.

5.2 METHODS

5.2.1 Animals

All animal procedures were conducted in accordance with the guidelines set forth by the National Institutes of Health (NIH) and the University of California, Irvine Institutional Animal Care and Use Committee. All mice were age and sex-matched and group-housed on a 12h/12h light/dark cycle with food and water ad libitum. Six B6CBAF1/J mice (Jackson Laboratory, stock number 100011) were perfused at P120 with ice-cold 1x PBS. Brains were in 4% PFA for 48 hours and then stored in 1X PBS until MRI scanning.

5.2.2 MR Image Acquisition

The brains were scanned in skull *ex vivo* using an Avance III HD spectrometer manufactured by Bruker Bio-Spin operating at a field strength of 17.6 T (750 MHz) with an 89mm bore.

T1w: A Fast Low Angle Shot (FLASH) scan was acquired with the following parameters: echo time (TE)/repetition time (TR) = 20/160 ms, flip angle = 30°, and in 0.07mm isotropic resolution.

DWI: Coronal diffusion-weighted echo-planar images were acquired with b = 1000 s/mm^2 (20 directions) and b = 3000 s/mm^2 (52 directions) with the following parameters: TE/TR = 5/28 s, FOV = 212 x 182 mm, pulse duration – 4ms, pulse spacing = 12 ms and in 0.125 mm isotropic resolution. Two images with no diffusion weighting (b = 0) were also collected.

5.2.3 Diffusion preprocessing

All preprocessing steps employed MRtrix3 (Tournier et al., 2012) (www.mrtrix.org) commands or used MRtrix3 scripts that linked external software packages. Physiological noise arising from thermal motion of water molecules in the brain was first removed (Veraart et al., 2016), followed by removal of Gibbs ringing artifacts (Kellner et al., 2016), eddy current correction (Andersson & Sotiropoulos, 2016), and bias field correction (Tustison et al., 2014). The image intensity was then normalized across subjects in the log-domain (Raffelt et al., 2012). Images with no diffusion weighting (b=0) were extracted and averaged to aid with structural registration.

5.2.4 Structural preprocessing

Each participant's structural image was nonlinearly co-registered to the average of their respective preprocessed b0 images (ANTS v2.3.4) (Tustison et al., 2010), so that the structural and diffusion images were in the same space for the rest of the analyses. Registration was manually checked to ensure accuracy. These images were then nonlinearly co-registered to the Allen Reference Atlas (Lein et al., 2007).

5.2.5 Deriving diffusion metrics

We calculated traditional tensor metrics using MRtrix3 with data from all shells. A weighted least squares (WLS) approach was first used to fit the diffusion tensor to the log signal, using weights based on empirical signal intensities (Basser et al., 1994). We repeated the weighted least squares with weights determined by the signal predictions from the previous step (Veraart et al., 2013). We then generated maps of the following tensor-derived parameters: the mean apparent diffusion coefficient (ADC, sometimes also referred to as Mean Diffusivity or MD), fractional anisotropy (FA), axial diffusivity

(AD, same as principal eigen value) and radial diffusivity (RD, equal to mean of the two non-principal eigen values) (Westin, 1997).

Higher-order multi-compartment metrics were derived using the *ex vivo* Neurite Orientation Dispersion and Density Imaging (NODDI) (Zhang et al., 2012) model in the Microstructure Diffusion Toolbox (Harms et al., 2017). The intrinsic diffusivity was set to $1.7 \, \mu m^2 \, ms^{-1}$. Note that even though the NODDI model typically generates three primary metrics: NDI, ODI and FISO, our analysis for this chapter is limited to the NDI and the ODI. The FISO is a free water measure, typically proportional to the amount of CSF in a voxel, and such a measure is meaningless in perfused tissue.

5.2.6 Deriving cell counts

Typical cell counts from each voxel were obtained from the Markram atlas (Erö et al., 2018). The atlas uses a variety of whole-brain image datasets, including Nissl-staining for cells and genetic marker stains to distinguish glia from neurons, as well as subtype staining for both glia (astrocytes, microglia, and oligodendrocytes) and neurons (excitatory and inhibitory). For validation, these estimates were compared against values in the literature not used in the reconstruction of the cell densities. A unique property of this atlas is that it is not limited to generating a single expected value at each location. Rather, it integrates data from the literature to be able to reflect local variation based on age, sex and other individual variability. Using this atlas to generate cell counts was preferred over empirically determining them not only because it eliminated most of the experimental noise and error, but also because this atlas promised more robust estimates

as they were combined from multiple sources. A limitation of the atlas is that it does not take into account the individual differences in cell counts of the mice scanned.

5.2.7 Voxel-wise correlations

To perform voxel-wise correlations, region-specific masks were generated using the Allen Brain Atlas, and the masks were eroded by a factor of 3 to account for any partial volume effects. To deal with any registration artifacts and individual differences in cellularity, these masks were then re-gridded from 0.125 mm resolution to 3.75mm resolution isotropic (each new voxel was a composite of 30x30x30 voxels), and each voxel was assigned a unique value (Figure 5.1). This regridding factor of 30 voxels was determined empirically: ensuring a large enough set of data points for each region, while also maintaining the variance. AFNI's *3dROIstats* was then used to generate voxel-wise averages of the diffusion metrics and the cell counts. Correlation matrices for each mouse were generated by determining the Pearson correlation for each pair. The concatenated correlation was determined by calculating the Fisher Z score of all subjects' Pearson R values and performing a one-sample t-test for each diffusion metric/cell count pair. All statistics and modeling were performed using Python and GraphPad Prism.

5.2.8 Extra Trees Prediction Pipeline

We developed a prediction pipeline to individually estimate various cell densities (Dependent variables [6]: all cells, all neurons, all glia, oligodendrocytes, astrocytes, microglia) from our diffusion metrics alone (independent variables [5]: AD, ADC, FA, RD NDI, ODI). The data from the six mice were divided into training and testing data using a 6-fold Leave One Out cross-validation approach, which selected 5 mice for training and

1 mouse for testing and this was repeated 6 times for 6 non-overlap validation data sets. The model performance metrics were determined by averaging the predicted variables over the 6 trials.

We have already established that these diffusion metrics are highly correlated to each other (Chapter 3). Since high collinearity between the independent parameters is undesirable for most prediction algorithms, the input data was first recreated by compressing the diffusion metrics into a reduced dimensional space using a Keras autoencoder (*Keras: The Python Deep Learning API*, n.d.), with the Adam optimization algorithm, optimized for mean squared error. Autoencoder performed better than principal component analysis, perhaps due to the relatively small size of the data set.

We then built our extra trees regression model. Model parameters were determined for each region using a grid search with a five-fold cross validation. The parameters were optimized for Pearson R rather than the slope of the fit as we were aiming for stronger relative predictability over absolute predictive power. Random decision trees were then trained on bootstrapped subsamples of the dataset over 1000 iterations. To verify that nothing about the subsampling was driving any of the observed effects, we performed 1000 random samplings of 70% of our data, and the resulting slopes were entirely consistent with our regression-based confidence intervals. To generate the probability distribution of our performance metrics (Pearson correlation and p value), the training and testing data were randomly subsampled at 80% over 1000 iterations for each trial prior to fitting the model (Figure 5.1).
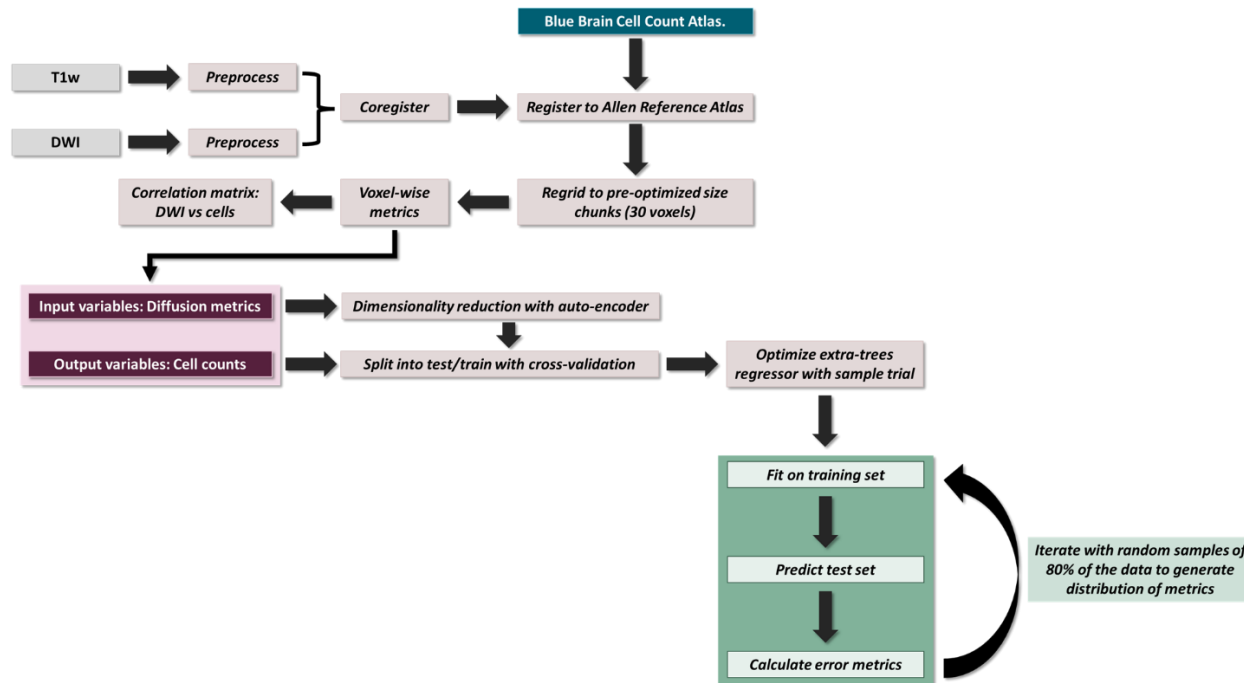
Figure 5.1: Overview of pipeline

5.3 RESULTS

5.3.1 Whole brain diffusion metrics have limited relationships with cell densities.

Our first question was whether the diffusion metrics and various cell counts in the whole brain had significant observable relationships. We downsampled the image to larger voxel-sizes to account for individual differences and any registration artifacts (Figure 5.2a). Voxel-wise metrics were generated for each mouse by averaging the measures for each downsampled voxel. We then calculated the Pearson correlation coefficient for each diffusion metric/cell count pair, with each mouse as a separate replicate. These correlation metrics were then converted into Z-scores, and a one sample t-test was performed with the Z-scores of each diffusion metric/cell count pair. To account for

multiple comparisons, we applied the Holm-Sidak correction to all p values, and only corrected p values < 0.05 were considered significant. We found that the oligodendrocyte counts were negatively correlated with the AD, ADC, and RD and positively correlated with the FA and NDI. The FA was also positively correlated with total glia and astrocyte count, and the RD was negatively correlated with counts of all cells except microglia (Figure 5.2b).
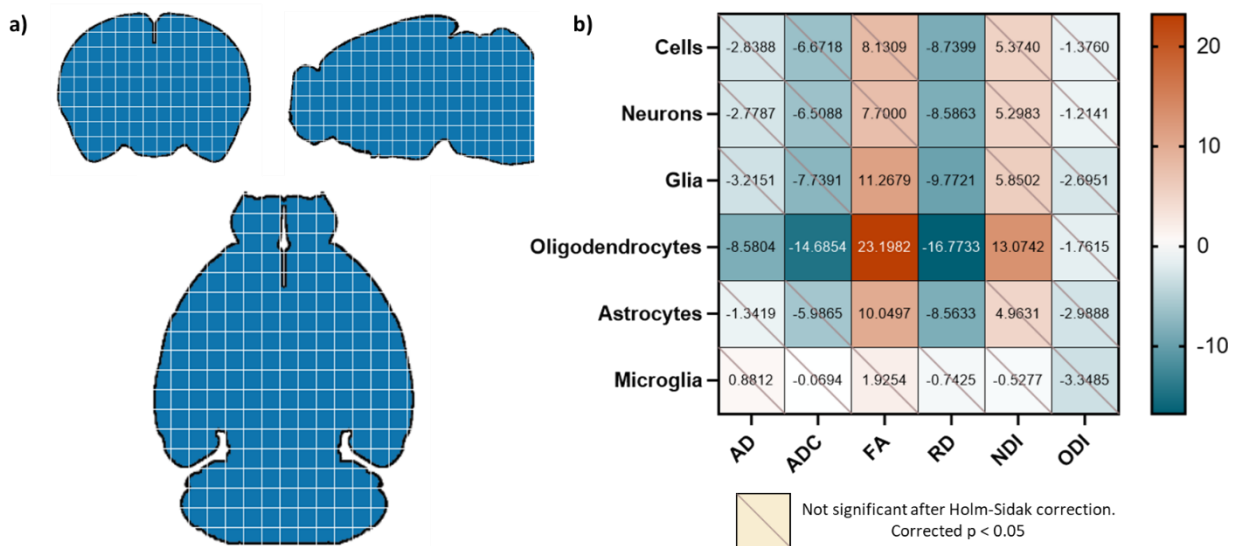

Figure 5.2: a) The whole brain was regridded into 30x30x30 voxels, and data points were generated by averaging the diffusion metrics and cell counts in each of these voxels for each mouse. b) Oligodendrocyte counts were highly correlated with all diffusion metrics except the ODI. FA was positively correlated with glia and astrocytes as well; and RD was negatively correlated with all cell types except microglia. Values in the correlation matrix represent the t-value from a one-sample t-test of the Z-score of the Pearson correlation coefficient of each subject's pair.

5.3.2 Whole brain predictor models fail for all cell types except oligodendrocytes.

We then asked if these diffusion metric/cell count relationships were consistent enough to generate a successful prediction model for the different cell types. Since we were aiming

for strong *relative* predictability, we determined model fit performance by linearly plotting the atlas counts against the predicted counts for each cell type. The stronger the Pearson correlation, the better the model was considered to be. Despite extensive optimization, we found that the model only performed well when predicting oligodendrocyte counts (Figure 5.3), perhaps because this cell type had the strongest relationships with the most diffusion metrics. For cells, neurons, and glia, despite the scores appearing high, it was evident that the model from whole-brain data could only perform well on a small subset of the voxels, and that there was very high variance in the cell counts themselves. We speculate that this distribution was influenced by the fact that the brain is made of diverse morphologies, and while our algorithm is capable of learning a set of rules for a subset of the data, a single model might not have the capacity to learn the disparate relationships between cell counts and diffusion metrics that this diversity entails.
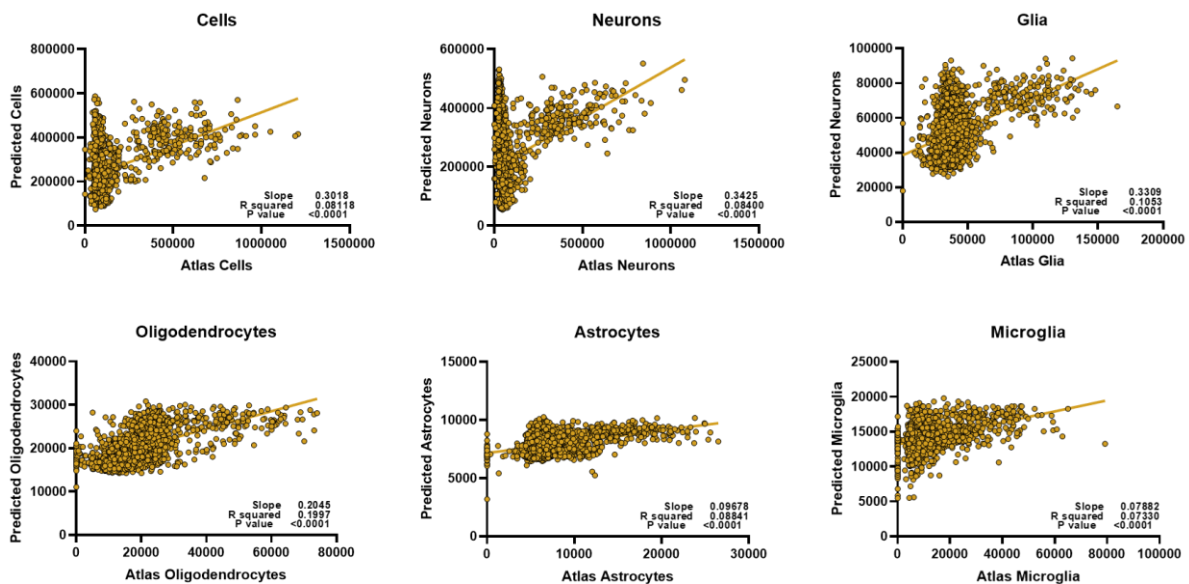
Figure 5.3: Despite extensive optimization, whole brain voxel-wise relationships cannot be exploited to develop meaningful prediction models for most cell types. We could only successfully estimate oligodendrocyte counts for the whole brain.

5.3.3 Diffusion metrics have unique relationships with different cell counts in a region-specific fashion.

Although the complexity of the relationships between DWI and cell types may preclude a single model from predicting cell type density across the whole brain, it is still quite possible that this can be effective when the scope is limited to smaller regions. To further examine whether the varied cytoarchitecture of the brain influenced the nature of diffusion-metric cell count relationships, we reevaluated the correlation matrices for three representative regions of different tissue compositions: primary motor cortex (cortical gray matter), CA1 of the hippocampus (subcortical gray matter), and the corpus callosum (white matter). Indeed, each of these regions had unique relationships between cell counts and the diffusion metrics (Figure 5.4), perhaps explaining why a common model would not be successful at predicting cell counts in these separate regions. We also observed that these relationships were distinct even to the level of subregions: the hippocampal correlation matrix was slightly different compared to that of just the CA1 with fewer statistically significant relationships, suggesting that the subfields had enough variance in their morphologies to warrant separate models. Moreover, even within a given "tissue composition", the correlation matrices did not remain consistent: the primary motor area had very different significant relationships compared to the supplementary somatosensory area, despite them both being cortical regions.
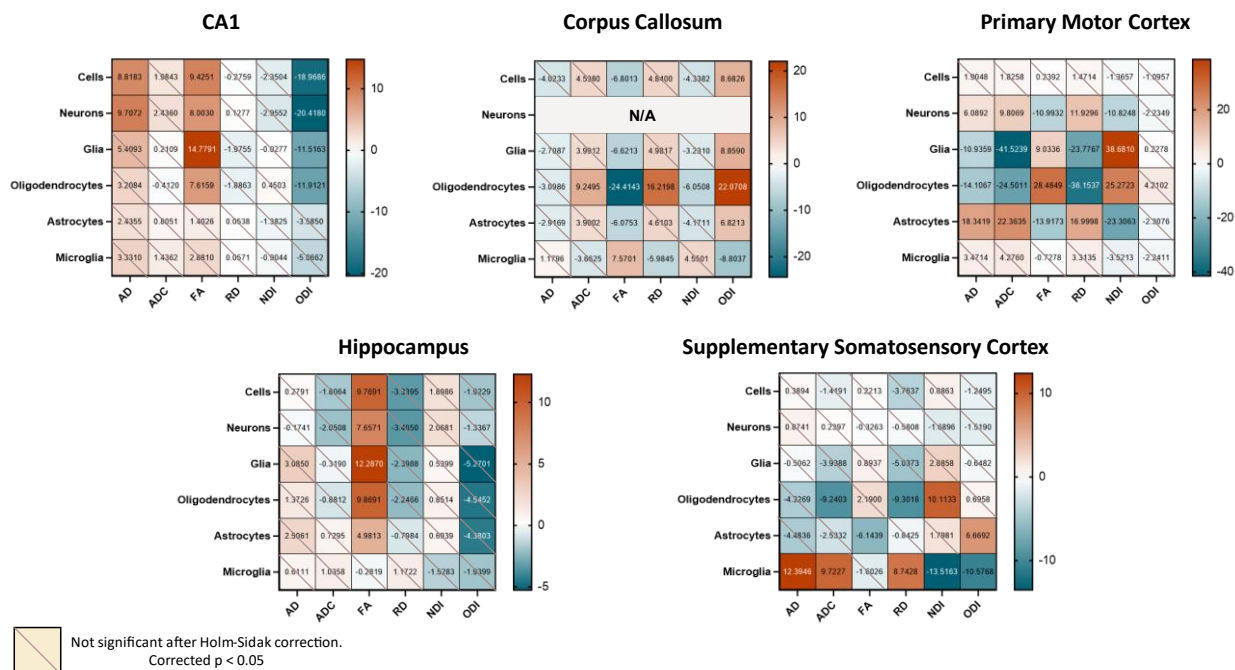
Figure 5.4: When examining different regions, we find unique region-specific relationships between diffusion metrics and cell types. Values in the correlation matrix represent the t-value from a one-sample t-test of the Z-score of the Pearson correlation coefficient of each subject's pair.

5.3.4 Localized, regional models show DWI can predict cell type density: CA1 as a test case.

We then asked if these stronger, region-specific relationships could be exploited to build unique models that could predict cell counts from the diffusion metrics alone. The results in section 3.3 warrant the construction of a separate predictor model for every structurally associated set of regions. Defining the exact regions that should be modelled together is beyond the scope of this chapter but will be worked on prior to publication.

As a proof of concept that it is possible to derive a regressor that can predict cell counts from diffusion metrics alone, however, we limit the remaining model generation to just the CA1 (as the rest of this thesis has primarily focused on the hippocampus, and the CA1 takes up the most area in the hippocampus). We recreated our extra trees regressor using

a subset of just the CA1 data, optimized for the Pearson correlation between the atlas and predicted counts. We find that constructing our model this way results in successful prediction of cells, neurons, glia and oligodendrocytes, but not that of astrocytes or microglia (Figure 5.5).
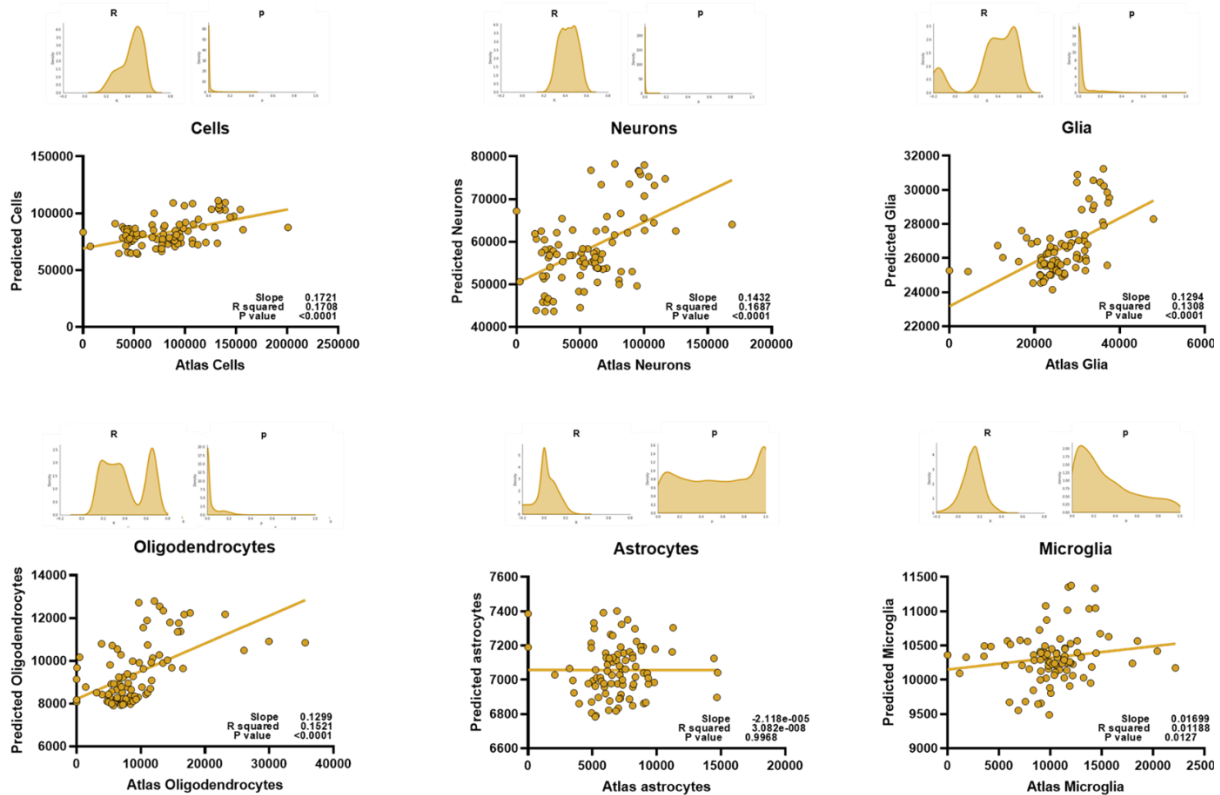

Figure 5.5: The region-specific relationships can be exploited to create models that can successfully predict certain major cell types, but not glial subtypes like astrocytes and microglia. To prevent bias, the y-values on the linear regressions are from an average of the predicted values of each mouse for a given voxel, on a random trial. The histograms represent the distributions of R and p of the model when testing and training 1000 samplings of 80% of the data, cross-validated on all mice.

5.4 DISCUSSION

In this chapter, we laid out a framework for using the diffusion metrics discussed in this thesis to predict neurobiological properties of the brain, specifically cell counts. We first

asked whether there were any clear voxel-wise relationships between the diffusion metrics and these various cell counts when looking at the brain as a single entity. We found that the most significant relationships were between the diffusion metrics and glial cell counts, especially those of oligodendrocytes! We also found that the tensor metrics FA and RD were highly correlated with many cell counts. However, except for oligodendrocytes, the diffusion metrics were not differentially correlated with any of the cell types. In turn, our extra trees regression algorithm was only successfully able to predict counts of the oligodendrocytes from the diffusion metrics, but not of any of the other cell types. When looking at the distribution of voxel-wise counts in the major cell categories i.e., overall cell, neuron, and glia count, we found that part of the failure of the model could be caused by the cell counts themselves falling into discrete groups. We hypothesized that this was because the brain is cytoarchitecturally very complex, and it is unlikely that diffusion metrics in different parts of the brain were capturing identical microstructural properties. To further test this hypothesis, we re-evaluated the voxel-wise relationships between diffusion metrics and cell counts in separate regions representing different tissue compositions: Primary Motor Cortex (cortical gray matter), Field CA1 (subcortical gray matter) and the Corpus Callosum (white matter). We discovered that the voxel-wise diffusion metrics in these sample regions had unique relationships with their cell densities, suggesting that these metrics were indeed capturing different properties in different regions.

We next asked if modeling these regions individually would benefit our algorithm's predictive capacity, using the CA1 of the hippocampus as a test case. Interestingly, we

158

found that region-specific models could successfully predict all cell types studied, except for microglia and astrocytes! This is perhaps because astrocytes and microglia are slightly closer in soma size and shape to each other as compared to the other cells studied and our diffusion measures do not have the resolution to tell these cells apart. Moreover, these are some of the most dynamic cell types of the brain, and it has been shown that state-based morphologies could significantly influence the diffusion signal (Garcia-Hernandez et al., 2020). More studies examining the differences in the diffusion signal following acute inflammation or increase in reactivity in these cell types could refine the predictive power of our model.

The region-specific success of our model is not particularly surprising: adjacent voxels are more likely to have similar associations between diffusion metrics and cell counts. However, we have yet to establish what properties exactly constitute a "region". We found that simply splitting the brain into gray/white or cortical/subcortical regions was not enough to build a successful model. We theorize that these regions must be large enough to possess adequate variance across all metrics (we did not find significant relationships between diffusion metrics and cell counts within individual layers of the primary motor cortex), but conservative enough such that a model is not expected to learn disparate patterns of relationships (aggregating across hippocampal subfields resulted in an unreliable correlation matrix, Figure 5.4). The next step would be to determine the exact morphological properties that should define the boundaries of a "region" that warrants a discrete model.

One could argue that the success of our model lies solely in the computational power of the extra trees prediction algorithm we utilize, or that our model might be behaving as a mere look-up table and not relying on distinct relationships between the diffusion metrics and the cell counts. However, if such were the case, a single model would have been able to predict whole brain cell counts and, as we show in Figure 5.3, this is not true. Moreover, the failure of the model to fit certain glial subtypes, while disappointing, demonstrates that our model is truly attempting to learn relationships between the diffusion metrics and the cell counts, and is not just fitting noise. Moreover, only the cell types that are strongly correlated with the diffusion metrics (Figures 5.2 and 5.4) are successfully estimated by our model, further demonstrating that it is relying on real associations between the metrics and the counts.

It should also be noted that the model works on the same cell types when training on one hemisphere and testing on the other hemisphere of individual mice. Moreover, the successful results were consistent across all mice, and were consistent even in random samplings of the training and testing data, demonstrating that the prediction was not just dependent on specific mice or sets of voxels. As a sanity check, we also confirmed that a model trained in a region and tested in a different region was not successful, and performed at chance, further demonstrating our model was not capable of fitting any sporadic pattern and that there were discernible region-specific relationships between the cell counts and diffusion metrics.

It is important to note that the cell counts reported in this study are derived from an atlas. Though these counts are robust and reliable estimates and less prone to experimental

error, using atlas counts overlooks potential individual differences of the mice studied. While we do not expect differences in counts so large that they could be detected by diffusion measures, it is possible that a small part of the error from our prediction model might be arising from not being able to measure the exact cell counts of these individual mice.

Throughout the results in this chapter, the relationship between oligodendrocytes and the diffusion metrics is curious: these cell types are the only ones that can be predicted with the whole brain data. The results in the other cells suggest that the model is not capable of generalizing patterns within the entire brain, given its cytoarchitectural complexity, but why is this not the case with the oligodendrocytes? Even if the relationships between oligodendrocytes and diffusion metrics was consistent across the whole brain, why is the cluster-like prediction structure of the other cells (Figure 5.3) not influencing oligodendrocyte prediction? One hypothesis is that this pertains to the relationships between the cell counts themselves. Not only are the cell types *highly correlated with each other* in the whole brain, the relationship between oligodendrocytes and neurons (and even total cells) forms a similar cluster-like pattern (Figure 5.6a).
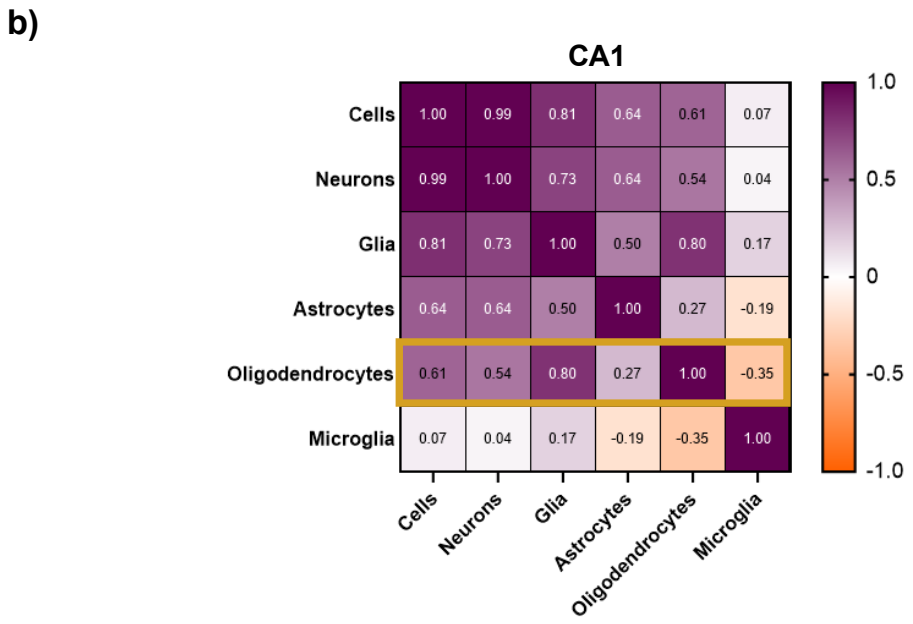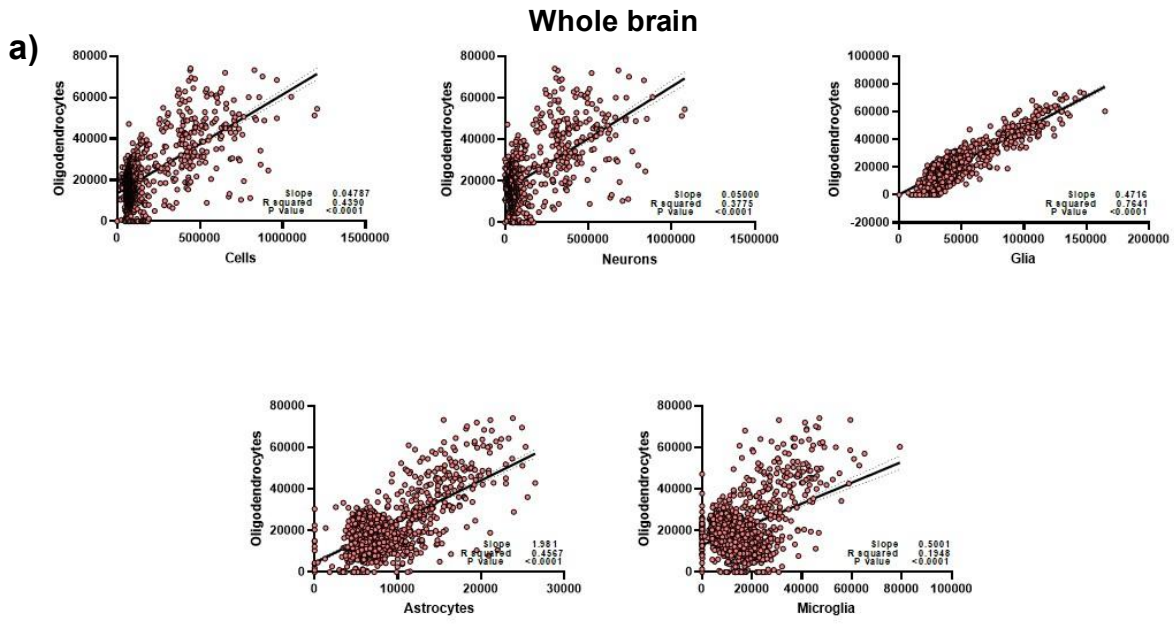
Figure 5.6: a) Oligodendrocyte counts are highly correlated to other cell counts in the whole brain. **b)** CA1 oligodendrocyte counts are only strongly correlated to counts of Cells, Neurons and total glia. Values in the matrix represent Pearson R coefficients.

Further examination shows that this interconnectedness is only true for certain cell types when examining individual regions like the CA1. One central observation is that the cell counts that are most correlated with oligodendrocyte counts in the CA1 are also the cell counts that the model predicts best (Figure 5.5 and Figure 5.6b). These might suggest that the model is primarily relying on changes in diffusion driven by oligodendrocytes to not only predict their counts, but also to predict the other cell types (given the correlation, the count of oligodendrocytes is a reasonable proxy for the count of neurons, glia, and astrocytes). While a compelling and simple hypothesis, there are aspects that do not fit into this story. Notably, our model performs best in the total cells and neuron counts instead of the oligodendrocytes. If oligodendrocytes' diffusion properties served as a proxy for neurons, this would not be the case. This phenomenon also does not extend to other regions like the corpus callosum, where the prediction of our model does not correlate with the relationship between the cell type of interest and oligodendrocytes. Moreover, it is highly unlikely that all of the other diffusion results presented in this thesis were completely driven by oligodendrocyte counts. To resolve this issue, in our future work, we will consider the relationship between the cell counts themselves when selecting areas of interest and when defining the "boundaries" of a region. Central to this will be to determine whether our model can still predict cell counts in regions whose oligodendrocytes do not correlate with the other cell counts at all. Future imaging studies, causally manipulating counts of these cells and breaking patterns between these cell counts, could help further pinpoint the exact drivers of these diffusion metrics.

Nevertheless, these results demonstrate that diffusion metrics in gray matter are selectively sensitive to different cell counts. Collectively, we have laid the foundation for a pipeline that could non-invasively detect cell counts in a region-specific manner. This chapter further establishes that diffusion metrics can be used to examine gray matter cytoarchitecture. Currently, clinical MRI resolution is nowhere close to reaching the resolution of histology, but pipelines like the one proposed in this chapter may help bridge this gap.

References

Andersson, J. L. R., & Sotiropoulos, S. N. (2016). An integrated approach to correction for off-resonance effects and subject movement in diffusion MR imaging. *NeuroImage*, *125*, 1063–1078. https://doi.org/10.1016/j.neuroimage.2015.10.019

Back, S. A., Kroenke, C. D., Sherman, L. S., Lawrence, G., Gong, X., Taber, E. N., Sonnen, J. A., Larson, E. B., & Montine, T. J. (2011). White matter lesions defined by diffusion tensor imaging in older adults. *Annals of Neurology*, *70*(3), 465–476. https://doi.org/10.1002/ana.22484

Basser, P. J., Mattiello, J., & Lebihan, D. (1994). Estimation of the Effective Self-Diffusion Tensor from the NMR Spin Echo. *Journal of Magnetic Resonance, Series B*, *103*(3), 247–254. https://doi.org/10.1006/jmrb.1994.1037

Chang, E. H., Argyelan, M., Aggarwal, M., Chandon, T.-S. S., Karlsgodt, K. H., Mori, S., & Malhotra, A. K. (2016). Diffusion tensor imaging measures of white matter compared to myelin basic protein immunofluorescence in tissue cleared intact brains. *Data in Brief*, *10*, 438–443. https://doi.org/10.1016/j.dib.2016.12.018

Concha, L., Livy, D. J., Beaulieu, C., Wheatley, B. M., & Gross, D. W. (2010). In Vivo Diffusion Tensor Imaging and Histopathology of the Fimbria-Fornix in Temporal Lobe Epilepsy. *Journal of Neuroscience*, *30*(3), 996–1002. https://doi.org/10.1523/JNEUROSCI.1619-09.2010

Erö, C., Gewaltig, M.-O., Keller, D., & Markram, H. (2018). A Cell Atlas for the Mouse Brain. *Frontiers in Neuroinformatics*, *12*. https://doi.org/10.3389/fninf.2018.00084

Garcia-Hernandez, R., Carpena, A. T., Drakesmith, M., Koller, K., Jones, D. K., Canals, S., & Santis, S. D. (2020). *Imaging Microglia and Astrocytes non-invasively using Diffusion MRI* [Preprint]. Neuroscience. https://doi.org/10.1101/2020.02.07.938910

Gouw, A. A., Seewann, A., Vrenken, H., van der Flier, W. M., Rozemuller, J. M., Barkhof, F., Scheltens, P., & Geurts, J. J. G. (2008). Heterogeneity of white matter hyperintensities in Alzheimer's disease: Post-mortem quantitative MRI and neuropathology. *Brain*, *131*(12), 3286–3298. https://doi.org/10.1093/brain/awn265

Harms, R. L., Fritz, F. J., Tobisch, A., Goebel, R., & Roebroeck, A. (2017). Robust and fast nonlinear optimization of diffusion MRI microstructure models. *NeuroImage*, *155*, 82–96. https://doi.org/10.1016/j.neuroimage.2017.04.064

Kellner, E., Dhital, B., Kiselev, V. G., & Reisert, M. (2016). Gibbs-ringing artifact removal based on local subvoxel-shifts: Gibbs-Ringing Artifact Removal. *Magnetic Resonance in Medicine*, *76*(5), 1574–1581. https://doi.org/10.1002/mrm.26054

Keras: The Python deep learning API. (n.d.). Retrieved November 27, 2021, from https://keras.io/

Lein, E. S., Hawrylycz, M. J., Ao, N., Ayres, M., Bensinger, A., Bernard, A., Boe, A. F., Boguski, M. S., Brockway, K. S., Byrnes, E. J., Chen, L., Chen, L., Chen, T.-M., Chi Chin, M., Chong, J., Crook, B. E., Czaplinska, A., Dang, C. N., Datta, S., … Jones, A. R. (2007). Genome-wide atlas of gene expression in the adult mouse brain. *Nature*, *445*(7124), 168–176. https://doi.org/10.1038/nature05453

Mottershead, J. P., Schmierer, K., Clemence, M., Thornton, J. S., Scaravilli, F., Barker, G. J., Tofts, P. S., Newcombe, J., Cuzner, M. L., Ordidge, R. J., McDonald, W. I., & Miller, D. H. (2003). High field MRI correlates of myelin content and axonal density in multiple sclerosis: A post-mortem study of the spinal cord. *Journal of Neurology*, *250*(11), 1293–1301. Scopus. https://doi.org/10.1007/s00415-003-0192-3

Raffelt, D., Tournier, J.-D., Rose, S., Ridgway, G. R., Henderson, R., Crozier, S., Salvado, O., & Connelly, A. (2012). Apparent Fibre Density: A novel measure for the analysis of diffusion-weighted magnetic resonance images. *NeuroImage*, *59*(4), 3976–3994. https://doi.org/10.1016/j.neuroimage.2011.10.045

Rojas-Vite, G., Coronado-Leija, R., Narvaez-Delgado, O., Ramírez-Manzanares, A., Marroquín, J. L., Noguez-Imm, R., Aranda, M. L., Scherrer, B., Larriva-Sahd, J., & Concha, L. (2019). Histological validation of per-bundle water diffusion metrics within a region of fiber crossing following axonal degeneration. *NeuroImage*, *201*, 116013. https://doi.org/10.1016/j.neuroimage.2019.116013

Schmierer, K., Wheeler-Kingshott, C. A. M., Boulby, P. A., Scaravilli, F., Altmann, D. R., Barker, G. J., Tofts, P. S., & Miller, D. H. (2007). Diffusion tensor imaging of post mortem multiple sclerosis brain. *NeuroImage*, *35*(2), 467–477. https://doi.org/10.1016/j.neuroimage.2006.12.010

Stolp, H. B., Ball, G., So, P.-W., Tournier, J.-D., Jones, M., Thornton, C., & Edwards, A. D. (2018). Voxel-wise comparisons of cellular microstructure and diffusion-MRI in mouse hippocampus using 3D Bridging of Optically-clear histology with Neuroimaging Data (3D-BOND). *Scientific Reports*, *8*(1). https://doi.org/10.1038/s41598-018-22295-9

Tournier, J.-D., Calamante, F., & Connelly, A. (2012). MRtrix: Diffusion tractography in crossing fiber regions. *International Journal of Imaging Systems and Technology*, *22*(1), 53–66. https://doi.org/10.1002/ima.22005

Tustison, N. J., Avants, B. B., Cook, P. A., Yuanjie Zheng, Egan, A., Yushkevich, P. A., & Gee, J. C. (2010). N4ITK: Improved N3 Bias Correction. *IEEE Transactions on Medical Imaging*, *29*(6), 1310–1320. https://doi.org/10.1109/TMI.2010.2046908

Tustison, N. J., Cook, P. A., Klein, A., Song, G., Das, S. R., Duda, J. T., Kandel, B. M., van Strien, N., Stone, J. R., Gee, J. C., & Avants, B. B. (2014). Large-scale evaluation of ANTs and FreeSurfer cortical thickness measurements. *Neuroimage*, *99*, 166–179. https://doi.org/10.1016/j.neuroimage.2014.05.044

Veraart, J., Fieremans, E., & Novikov, D. S. (2016). Diffusion MRI noise mapping using random matrix theory: Diffusion MRI Noise Mapping. *Magnetic Resonance in Medicine*, *76*(5), 1582–1593. https://doi.org/10.1002/mrm.26059

Veraart, J., Sijbers, J., Sunaert, S., Leemans, A., & Jeurissen, B. (2013). Weighted linear least squares estimation of diffusion MRI parameters: Strengths, limitations, and pitfalls. *NeuroImage*, *81*, 335–346. https://doi.org/10.1016/j.neuroimage.2013.05.028

Westin. (1997). Geometrical diffusion measures for MRI from tensor basis analysis. *Proc. ISMRM'97*. https://ci.nii.ac.jp/naid/10021111885/

Yi, S. Y., Barnett, B. R., Torres-Velázquez, M., Zhang, Y., Hurley, S. A., Rowley, P. A., Hernando, D., & Yu, J.-P. J. (2019). Detecting Microglial Density With Quantitative Multi-Compartment Diffusion MRI. *Frontiers in Neuroscience*, *13*. https://doi.org/10.3389/fnins.2019.00081

Zhang, H., Schneider, T., Wheeler-Kingshott, C. A., & Alexander, D. C. (2012). NODDI: Practical in vivo neurite orientation dispersion and density imaging of the human brain. *NeuroImage*, *61*(4), 1000–1016. https://doi.org/10.1016/j.neuroimage.2012.03.072

CHAPTER 6:

DISCUSSION

I can't give you brains, but I can give you a diploma.

-The Wizard of Oz, to the Scarecrow.

The work presented in this thesis collectively demonstrate that recent advances have transformed diffusion-weighted MRI into a powerful tool to study gray matter microstructure, specifically in the context of cognitive aging. While we have discussed the implications of individual studies in their respective chapters, we shall summarize our results in this chapter. We have identified diffusion metrics in the hippocampus that can serve as novel biomarkers associated with age-related cognitive decline and have constructed a pipeline that can predict properties at a cellular resolution from these diffusion metrics alone. The major findings of this thesis can be summarized as follows:

1. Diffusion MRI is sensitive to aging-related changes in hippocampal subfield microstructure. (Chapters 2 and 3)

2. Diffusion MRI can detect neurobiological properties in hippocampal gray matter explicitly tied not only to aging-related cognitive decline, but also to individual differences in cognition. (Chapters 2 and 3)

3. Diffusion imaging can be used as a powerful non-invasive tool to monitor the success of interventions and clinical trials designed to protect against aging-associated microstructural deterioration, even in gray matter. (Chapter 4)

168

4. Despite its low resolution, diffusion metrics can be linked to certain cellular properties that can be estimated using creative computational methods. (Chapter 5)

Novelty of this research

These findings have resulted in many novel contributions. Chapter 2, which was published in *Frontiers in Aging Neuroscience* in 2020, was the first paper to demonstrate that the NODDI metric NDI was increased in the hippocampus of older adults in a subfield-specific manner, and that this increase specifically in DG/CA3 could be mediating aging-related cognitive decline in verbal memory. These results were further corroborated in Chapter 3, attesting to the robustness and reliability of NODDI metrics. Moreover, this chapter- which is now under review at *Neuroimage,* had the first set of results to indicate that combining NODDI and tensor measures across all hippocampal subfields could strongly predict both age and cognition on multiple scales better than either set of measures alone, and much better than more traditional gray matter structural metrics like volume. Moreover, this was true for predicting cognition even within just the older subpopulation, suggesting that these diffusion metrics were also sensitive to individual differences in cognition. These results together provide a strong framework for using multi-shelled diffusion metrics to examine the structural mechanisms of aging, specifically in gray matter. However, the results in these two chapters were from cross-sectional studies comparing older adults to younger adults, whose brains could be dramatically different from one another. In Chapter 4, we not only replicated relationships between diffusion metrics and age in an entirely different species, the

beagle; we also demonstrated that these metrics were sensitive to even subtle longitudinal changes in gray matter microstructure over the span of just a year! Further, we demonstrated for the first time that our methods could evaluate the ability of the calcineurin-inhibiting drug tacrolimus to protect against these changes! Finally, in Chapter 5, we established a pipeline to essentially perform virtual histology with just multi-shelled diffusion imaging, by creating a model that could non-invasively estimate cell counts in a region-specific manner.

Revisiting major results

Even in healthy aging, the brain undergoes major cytoarchitectural changes that precede gross atrophy and cognitive decline. This thesis uses this universal phenomenon to test the sensitivity and reliability of advanced diffusion imaging in non-invasively examining gray matter cytoarchitectural properties. By doing so, this work also presents a framework to extend this method to other domains. Researchers studying the microstructural mechanisms of both healthy developmental stages, as well as various neuropsychiatric illnesses, could massively benefit from implementing multi-shelled diffusion imaging in their protocols. In such studies, however, it is important to identify the "domain of validity" where both the assumptions and interpretations of these diffusion metrics are accurate (Lampinen et al., 2019), as diffusion indices tend to be very context-specific. Seemingly similar changes in diffusion metrics may have different anatomical implications across pathologies, age groups, and even across brain regions. For example, we report consistent and reproducible increases in hippocampal NDI with age. However,

the NDI of other regions, especially white matter, have been shown to decrease with age with similar associated cognitive decline (Merluzzi et al., 2016). Moreover, conditions like schizophrenia and bipolar disorder present decreased levels of hippocampal NDI, with potentially very different neurobiological implications (Nazeri et al., 2017). More research examining gray matter microstructure using these methods across the whole brain, in both the healthy lifespan and disease, can help in developing powerful signatures for both developmental milestones as well as neurological illnesses. This is another reason to advocate for the inclusion of multi-shell diffusion sequences in large-scale data collection efforts.

As shown in Chapter 5, each region's diffusion metrics is uniquely related to various cell counts, and these relationships cannot be generalized to the whole brain. While we were able to successfully build a model that could predict most cell counts in the CA1, we are yet to build such a model across the whole brain. We have demonstrated that region-specific models are the solution, but the boundaries of what constitute a "region" in this context remains ill-defined. As a next step, we aim to define this boundary by first examining the success of fitting label-based regions with models optimized by their neighbors, and empirically determine the extent to which a single model can be generalized. Next, we will include the defined region and its subsequent optimized parameters as independent variables in our dataset to build a spatially intuitive model that could simultaneously predict cell counts for the whole brain. These empirically determined set of boundaries could also then be extended to other interpretations of these diffusion metrics, like when examining relationships with age and behavior.

This non-specificity also leads to another major limitation of diffusion imaging: different patterns of cytoarchitecture could result in the exact same value for certain diffusion metrics but might not result in the exact same value for *all* diffusion metrics. Most prior work attempting to tie implicit neurobiological properties with diffusion imaging have tended to look at these relationships separately within each metric. However, as alluded to in Chapters 3 and 5, treating these varied diffusion metrics as a unique "signature" for each voxel can generate more specific models that can predict both behavior and microarchitecture more successfully. However, even with such a method, extreme caution must be taken when speculating on the neurobiological implications of these diffusion metrics.

The issue of domain-specificity is further emphasized in a recent pilot study we conducted comparing the diffusion signals from wild type mice (B6CBAF1/J) and mice with a CSF1R enhancer region deleted (*fmr*-intronic regulatory element or FIRE). The deletion of this region results in these mice having no microglia at all (Rojo et al., 2019). We hypothesized that this radical difference from the wild type mice would be likely reflected in their diffusion metrics as well. Surprisingly, we found that these mice had almost identical diffusion profiles throughout the brain compared to the wild type mice. Histology on these brains revealed that the absence of microglia might be compensated for by another cell type, perhaps similar in morphology, and that our methods are currently incapable of telling the difference between these cell types (Figure 6.1).
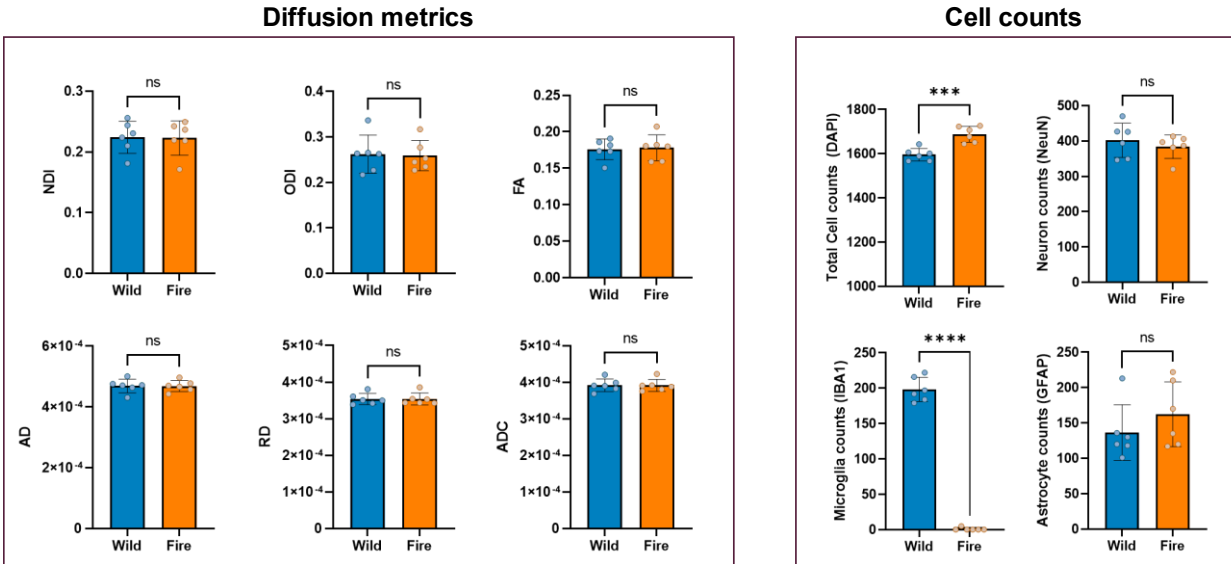
Figure 6.1: We observe no significant difference between the fire mice and wild type mice in all diffusion metrics. However, despite having no microglia, the fire mice have a significantly larger total cell count, compared to the wild type. The graphs here are from the dentate gyrus, but this was true for other brain regions studied as well (thalamus, cortex).

This is also evident in the performance of our model generated in Chapter 5: despite optimization, the slopes of the lines between atlas cell counts and predicted cell counts never get close to 1, and the intercepts never get close to 0. Our model still incorrectly predicts a significant number of cells in voxels where there are none, perhaps because the diffusion metrics cannot completely separate the contribution of different cell types to the signal. Despite the absolute cell counts suffering, however, our model still proves to be valuable as it can be represented by a linear regression and performs well when relative predictability is the determining factor of success.

This ability of these diffusion metrics to tell the relative difference between cell counts can serve it well in both identifying biomarkers and in intervention studies. For example, in Chapter 4, diffusion metrics were able to differentiate between dogs treated with a

calcineurin inhibiting drug and control dogs. However, this study also suffers from the non-specificity of diffusion metrics: while we observe a clear reversal of aging-related changes in diffusion metrics after treatment, we cannot say with certainty that this demonstrates a genuine reversal of aging-related changes cytoarchitecturally, or if this drug might be resulting in a completely different set of neurobiological events that contribute to a similar diffusion profile but might not be beneficial. More studies correlating histological data as well other data like blood and CSF biomarkers, along with understanding what these changes do to cognition, can help make diffusion imaging a reliable tool to evaluate the success of such intervention studies.

In conclusion, we have demonstrated that diffusion imaging is a powerful to study gray matter microstructure non-invasively. However, these results also raise questions on the specificity of these measures, and the extent to which these observations can be generalized. Better tools for validation, and a deliberate effort to generate large-scale publicly available datasets with multi-shelled data could not only help answer some of these questions, but also convince clinicians about the validity of this technique and be integrated in hospitals for diagnostic and other clinical applications.

References

Lampinen, B., Szczepankiewicz, F., Novén, M., van Westen, D., Hansson, O., Englund, E., Mårtensson, J., Westin, C.-F., & Nilsson, M. (2019). Searching for the neurite density with diffusion MRI: Challenges for biophysical modeling. *Human Brain Mapping*, *40*(8), 2529–2545. https://doi.org/10.1002/hbm.24542

Merluzzi, A. P., Dean, D. C., Adluru, N., Suryawanshi, G. S., Okonkwo, O. C., Oh, J. M., Hermann, B. P., Sager, M. A., Asthana, S., Zhang, H., Johnson, S. C., Alexander, A. L., & Bendlin, B. B. (2016). Age-dependent differences in brain tissue microstructure assessed with neurite orientation dispersion and density imaging. *Neurobiology of Aging*, *43*, 79–88. https://doi.org/10.1016/j.neurobiolaging.2016.03.026

Nazeri, A., Mulsant, B. H., Rajji, T. K., Levesque, M. L., Pipitone, J., Stefanik, L., Shahab, S., Roostaei, T., Wheeler, A. L., Chavez, S., & Voineskos, A. N. (2017). Gray Matter Neuritic Microstructure Deficits in Schizophrenia and Bipolar Disorder. *Biological Psychiatry*, *82*(10), 726–736. https://doi.org/10.1016/j.biopsych.2016.12.005

Rojo, R., Raper, A., Ozdemir, D. D., Lefevre, L., Grabert, K., Wollscheid-Lengeling, E., Bradford, B., Caruso, M., Gazova, I., Sánchez, A., Lisowski, Z. M., Alves, J., Molina-Gonzalez, I., Davtyan, H., Lodge, R. J., Glover, J. D., Wallace, R., Munro, D. A. D., David, E., … Pridans, C. (2019). Deletion of a Csf1r enhancer selectively impacts CSF1R expression and development of tissue macrophage populations. *Nature Communications*, *10*(1), 3215. https://doi.org/10.1038/s41467-019-11053-8